1-3-9 Consolidation of survey results

From the results of Phase I and II, it is concluded that the Veraguas area is made up of the following rocks.

Cerro Veraguas and Sierra Overa: Andesite volcanics of the Cretaceous Aeropuerto formation and porphyry intrusive rocks that have undergone hydrothermal alteration.

"Pampa District", the plain to the east of the Cerro Veraguas: Quartz diorite

The plain to the south of the Cerro Veraguas: Andesite volcanics and volcanic sandstone of the Paleogene Chile-Alemania formation.

Below are listed the special features of rocks for each area.

1. Cerro Veraguas and Sierra Overa District

(1) Andesitic volcanics of the Aeropuerto formation

These rocks form the basement of the area, and are comprised of porphyritic to aphanitic andesite lava, pseudobrecciated lava, tuff and lapilli tuff.

The rocks have undergone silicification, kaolinization, serification and chloritization so that the primary texture is indistinct.

(2) Porphyry intrusive rocks

These rocks comprise diorite to andesite porphyry intruding the andesitic volcanics in dyke or stock form. The rocks have a fine to medium grained in granular and/or porphyritic texture, in some places have sub-volcanic texture like tuff or pseudobrecciated lava, the boundariesr with andesitic volcanics being indistinct. The primary minerals such as plagioclase and hornblend have altered into secondary quartz, kaolin,sericite, biotite, chlorite, potassium feldspar and albite.

(3) Alteration

Both of the rocks described above have undergone strong hydrothermal alteration, and form the mass of the Cerro Veraguas and the Sierra Overa. ENAMI (1987) has divided the alteration into four zones, from the top down; intensely silicified, quartz-sericitized, siliceous-argillized and chloritized zones.

Intensely silicified, quartz-sericitized zones: These zones cover the ridge of the Cerro Veraguas and Sierra Overa to a depth of 50 to 200m. The border between the two is indistinct. The zones are an aggregate of fine massive secondary quartz, with sericite and kaolinite filling the spaces between the crystals; alunite and natroalunite films, and hematite dissemination and/or film are also observed.

Siliceous argillized zone: This zone occurs to a thickness of 100-300m beneath the intensely-silicified and quartz-sericitized zones, and is also markedly developed along the fault fracture zone. It is made up mainly of quartz, kaolinite, sericite and pyrophylite, and alunite, natroalunite, gypsum and anhydrite are observed. The zone is accompanied by hematite dissemination and film, while on the surface and along the fault a leached zone is formed, with strong concentrations of pulverized kaolinite clay, reddish hematite, jarosite and natrojarosite. As the zone goes deeper there is a shift into the chloritized

zone. Together with the appearance of chlorite, pyrite dissemination and film may be observed.

Chloritized zone: The primary mafic minerals have undergone chloritization; the texture of the original rocks remain. The altered minerals are, in addition to chlorite, secondary

quartz that has undergone corrosion, albite, potassium feldspar and sericite, biotite, gypsum and anhydrite. Pyritization is also marked in this zone. From the fact that the upper part of the chloritized zone shifts gradually into the siliceous-argillized zone, while in the lower part accompanies secondary quartz and potash feldspar, the zone may be divided from the top down into 4 zones, the combination of minerals corresponding to the phillic and potassic zones respectively of the alteration classification of porphyry copper minerals according to Lowell and Guilbert (1970):

Siliceous argillized-chloritized zone : phillic zone
Chlorite zone : phillic zone
Silicified-chloritized zone : phillic zone
Silicified-potash feldspar-chloritized zone : potassic zone

(4)Mineralization

As a result of this year's survey copper mineralizations have been encountered in the following areas.

a)Northwestern hillside of the Sierra Overa (MJCV-13)

In this district copper oxides disseminate in the aphanitic andesite below the leached zone that covers the surface. And in diorite porphyry copper oxides, native copper and chalcopyrite disseminate as follows:

Depth	Cu mineral	Cu ave.	max.	Auppm	Alteration
0- 11m	atacamite/brochanthite	0.55%	1.24%	0.20	siliceous argillized-chloritized
11- 70m	atacamite/brochanthite	0.24	1.12	0.14	chloritized
70- 78m	atacamite/brochanthite	0.34	0.40	0.21	chloritized
78-149m	Cu'·atacamite·azurite	0.23	0.86	0.13	chloritized
149-180m	Cu'·atacamite·azurite	0.18	0.52	0.13	silicified-chloiritized-potash feldspar
180-198m	atacamite·azurite	0.14	0.27	0.09	silicified-chloiritized-potash feldspar
198-250m	chalcopyrite	0.11	0.26	<0.04	silicified-chloiritized-potash feldspar
250-300m	chalcopyrite	0.10	0.55	<0.04	silicified-chloiritized-potash feldspar

The above shows that in the phillic zone between 0-149m there is a T.Cu grade of >0.2% and a Au grade of >0.1ppm, while in the potassic zone below 149m there is a tendency for the mineralization of both copper and gold to weaken.

Native copper occurs between 78-180m in disseminate and film form, but as the addition to potash feldspar and secondary quartz becomes stronger below 149m the amount of native copper lessens, becom-

ing infinitesimal below 180m. In addition to the copper minerals, hematite and magnetite disseminate throughout the hole, but in the places where native copper occurs hematite has not completely replaced the magnetite, and both iron minerals are invariably found together. The replacement of magnetite with hematite is more advanced in places where larger amounts of copper oxides occur.

b) Eastern foot of the Sierra Overa (MJCV-6)

Between 149-151m and 165-169m, around the borders between andesite and porphyry, chalcocite and covelline disseminate with chlorite. In the chloritized zone accompanying the addition to secondary quartz and potash feldspar below 318m, chalcopyrite disseminates with pyrite.

Depth	Cu mineral	T.Cu ave.	max.	Original rock	Alteration
149-151m	chalcocite·coveline	1.05%	1.38%	andesite	siliceous argillized-chloritized
165-169m	chalcocite·coveline	0.27%	0.34%	andesite	siliceous argillized-chloritized
318-339m	chalcopyrite	±0.1%		porphyry	silicified-chloiritized
339-400m	chalcopyrite	±0.1%		porphyry	silicified-chloiritized-potash feldspar

c) San Juan Mine, North side of the Sierra Overa (MJCV-9)

In the San Juan Mine, chalcanthite and atacamite disseminate within a siliceous argillized zone. Open pit mining was carried out on the scale of 50mx30m, at a depth of 10m below the surface.

The mine is closed now.

The hole, which shows marked siliceous argillization, comprises a leached zone with strong concentrations of pulverized reddish hematite, jarosite and natrojarosite. It has not been possible to encounter any continuity the deposits, but cu oxicides such as atacamite and chalcanthite have been found in the places listed below.

Depth	Cu mineral	T.Cu ave.	max.	Mopm	Original rock	Alteration	
30- 31m	atacamite	3.20%		35	unknown	siliceous argillized	jarosite,hematite rich
156-178m	chalcanthite	0.17%	0.24%	154	andesite	siliceous argillized	jarosite,hematite rich
182-196m	chalcanthite	0.14%	0.24%	123	andesite	siliceous argillized	jarosite,hematite rich
199-204m	chalcanthite	0.13%	0.14%	55	andesite	siliceous argillized	jarosite,hematite rich
226-248m	chalcanthite	0.12%	0.18%	69	andesite	siliceous argillized	jarosite,hematite rich

d) South-western foot of Cerro Veraguas (MJCV-10)

In and around the porphyry dykes between 59.0-90.2m, copper mineralization with a T.Cu grade of >0.2%, and molybdenum mineralization with a maximum of 780ppm have been encountered.

Depth	Cu mineral	T.Cu ave.	max.	Original rock	Alteration
59- 61m	chalcocite·coveline	0.28%	0.35%	andesite	siliceous argillized
68- 70m	chalcocite·coveline	0.20%	0.26%	porphyry	siliceous argillized-chloritized
82- 86m	chalcocite·coveline	0.23%	0.38%	porphyry	siliceous argillized-chloritized

e)Eastern foot of Cerro Veraguas (MJCV-11)

This area has formed a leached zone accompanying the NW-SE fracture. Between 265.2-266.85m chalcocite and covelline disseminate with calcite and quartz in porphyry under the leached zone.

Depth	Cu mineral	T.Cu ave.	max.	Original rock	Alteration
265-267m	chalcocite-covelline	0.76%	0.85%	porphyry	siliceous argillized-chloritized

2. Pampa District: the Plain east of the Cerro Veraguas (MJCV-12)

(1) Quartz diorite

Quartz diorite stock is distributed over a 2km x 2km area in the eastern part of the Veraguas area. The one or two kilometers between the Cerro Veraguas and the Pampa district are covered by alluviums and colluviums, and the border between the stock and the andesite volcanics of the Aeropuerto formation is not distinct.

(2) Alteration

The quartz diorite has undergone alteration: the augite and hornblende have been replaced by chlorite, and the plagioclase by epidote. In addition to these, secondary quartz, albite, potash feldspar, sericite, calcite, actinolite are observable throughout the hole.

(3) Mineralization

Specularitic hematite occurs in film, network and disseminate form, accompanying chlorite and epidote. Near the surface, to a depth of 53.0m, the hematite has been replaced by jarosite.

Between 0-131.0m and 178-182m chalcanthite, brockanthite and other copper oxides film along the fissures, in addition to which extremely small amounts of chalcocite and covelline are observable. Between 13-19m copper oxides occur with calcite and hematite, and the average T.Cu grade is 0.6%. Between 125-131m copper oxides disseminate and film accompanying hematite, and the average T.Cu grade is 1.02%. Between 131-178m chalcopyrite disseminates with pyrite and hematite. The average T.Cu grade is 0.31% between 131-148m, 0.1% between 148-178m.

3. Plain to the south of the Cerro Veraguas (MJCV-7)

(1)Andesite volcanics and volcanic sandstone of the Chile-Alemania formation (MJCV-7, 0-286.25m)

This formation is comprised of volcanic sandstone, andesitic pyroclastic rock and coarse grained vesicular andesitic lava displays a reddish-brown to reddish-purple coloration due to the hematite dissemination. The vesicles are filled with chlorite between 46.65-92.65m, and with chlorite, quartz and calcite between 207.55-286.25m. The phenocrysts of plagioclase have been replaced by albite.

(2) Andesitic volcanic rocks of the Aeropuerto formation (MJCV-7, 286.25-450m)

This formation is comprised of dacitic andesite that has undergone strong silicification, and fine grained andesite. The dacitic andesite displays a white coloration due to the strong silicification, and is made up of secondary quartz, as well as kaolin, deckite and gypsum. The fine grained andesite displays reddish-purple coloration due to the hematite dissemination. The rock shows very faint indications of chloritization, silicification and gypsum film.

(3) Mineralization

Hematite disseminates throughout the hole, but little or no sulfide minerals such as pyrite have been observed.

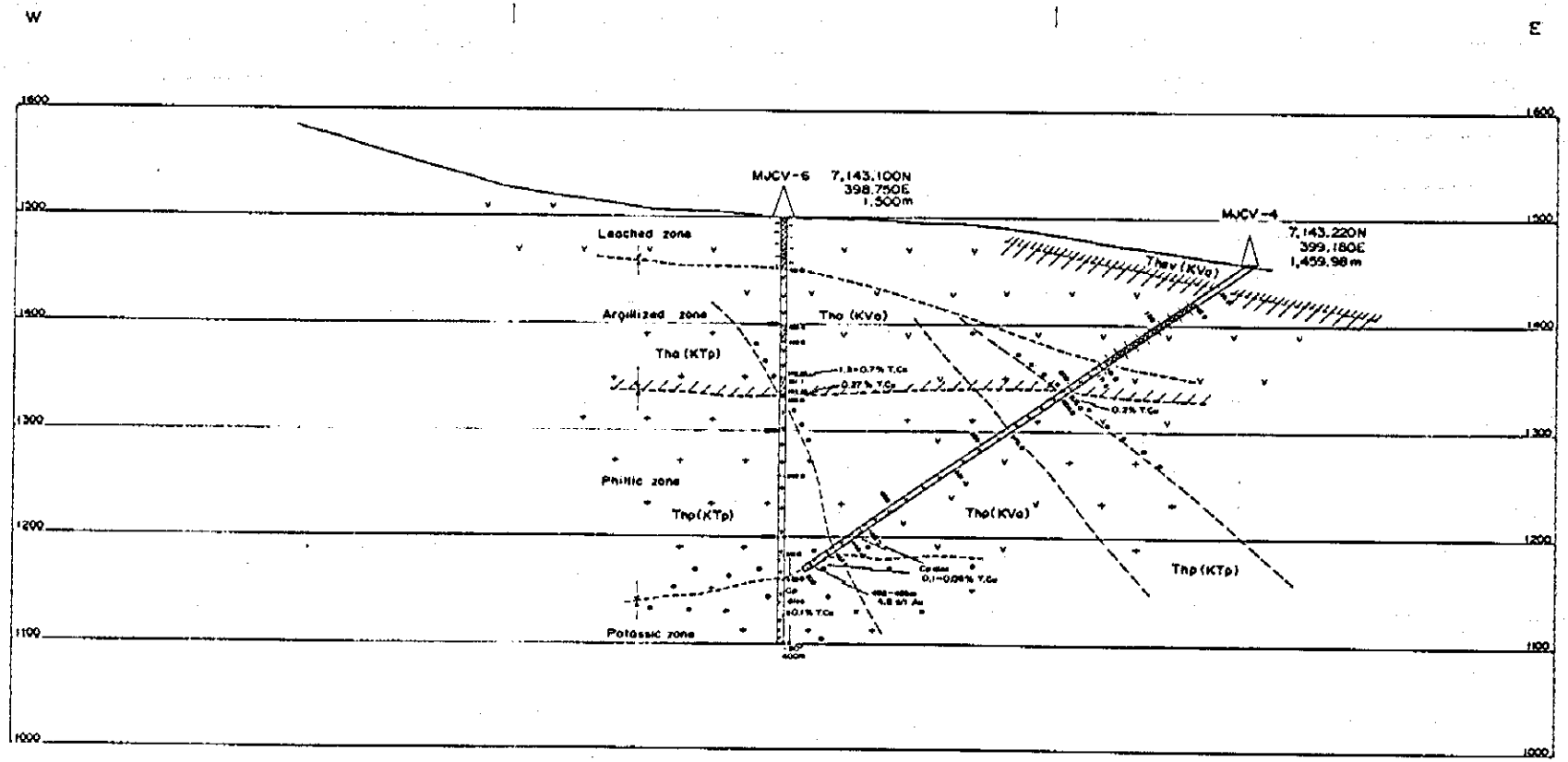

Legend

Aeropuerto formation
- KVa: Andesitic lava and autobrecciated lava
- KVa: Andesitic tuff and pyroclastics

Intrusive
- KTp: Diorite – andesitic porphyry

Hydrothermal Alteration zone
- Tha: (intensely silicified zone)
- Thsv: Quartz enriched zone
- Tho: Siliceous argillized zone
- Thp: Chloritized zone (Propylitized zone)

- Mineralization
- Limonite and Jarosite rich zone
- Fault (broken zone shown inferred fault)
- Fractured zone
- Geologic contact

Fig. II-1-2(1)

Geologic profile of the drill hole MJCV-6

(1:6,000)

Drilling Survey, Phase II

Yanacocha Project, JICA/MMAJ-ENAMI

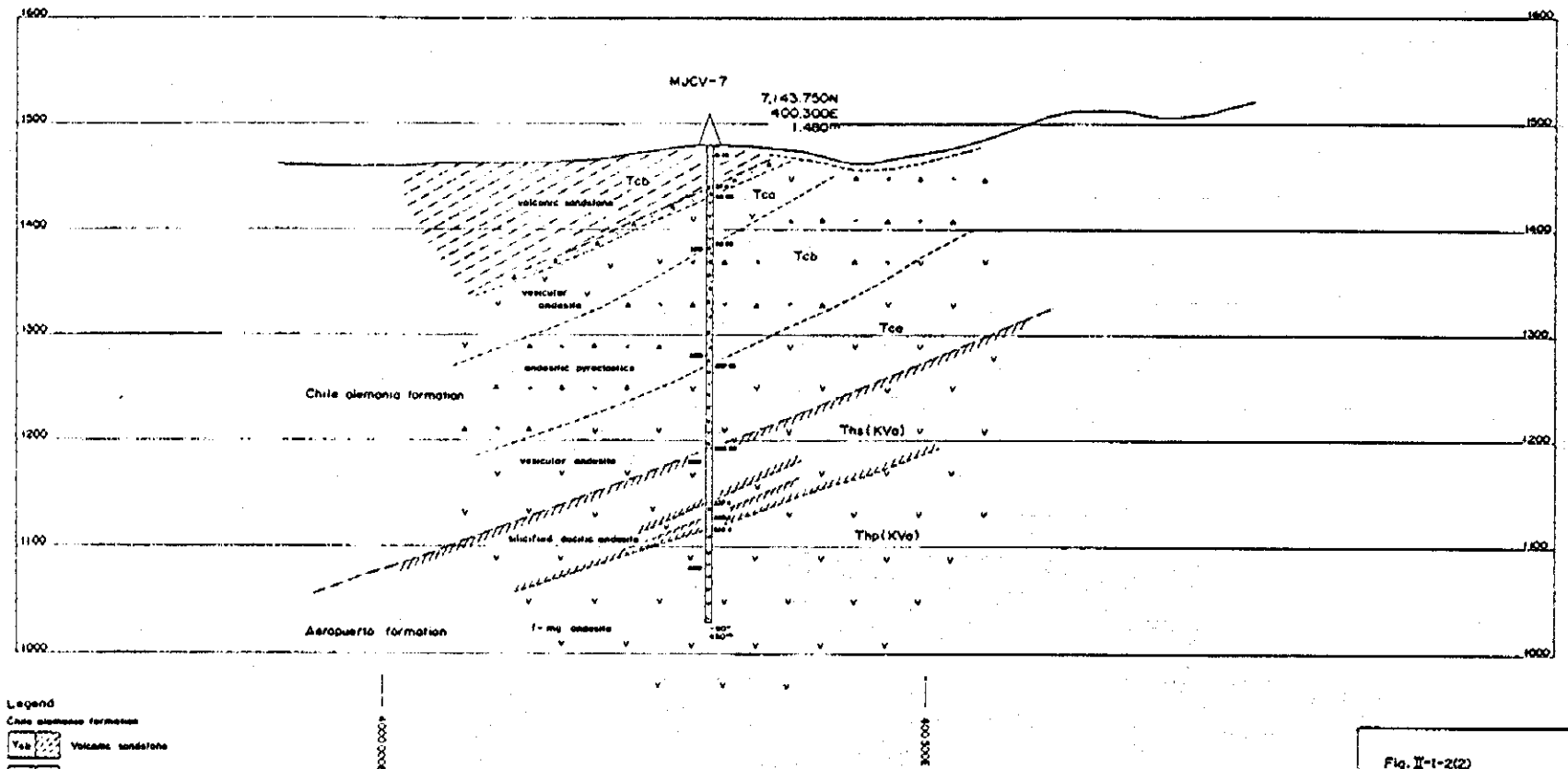

Fig. II-1-2(2)

Geologic profile of the drill hole MJCV-7

(1:6,000)

Drilling Survey, Phase II

Veraguas Project, JICA/MMAJ-ENAMI

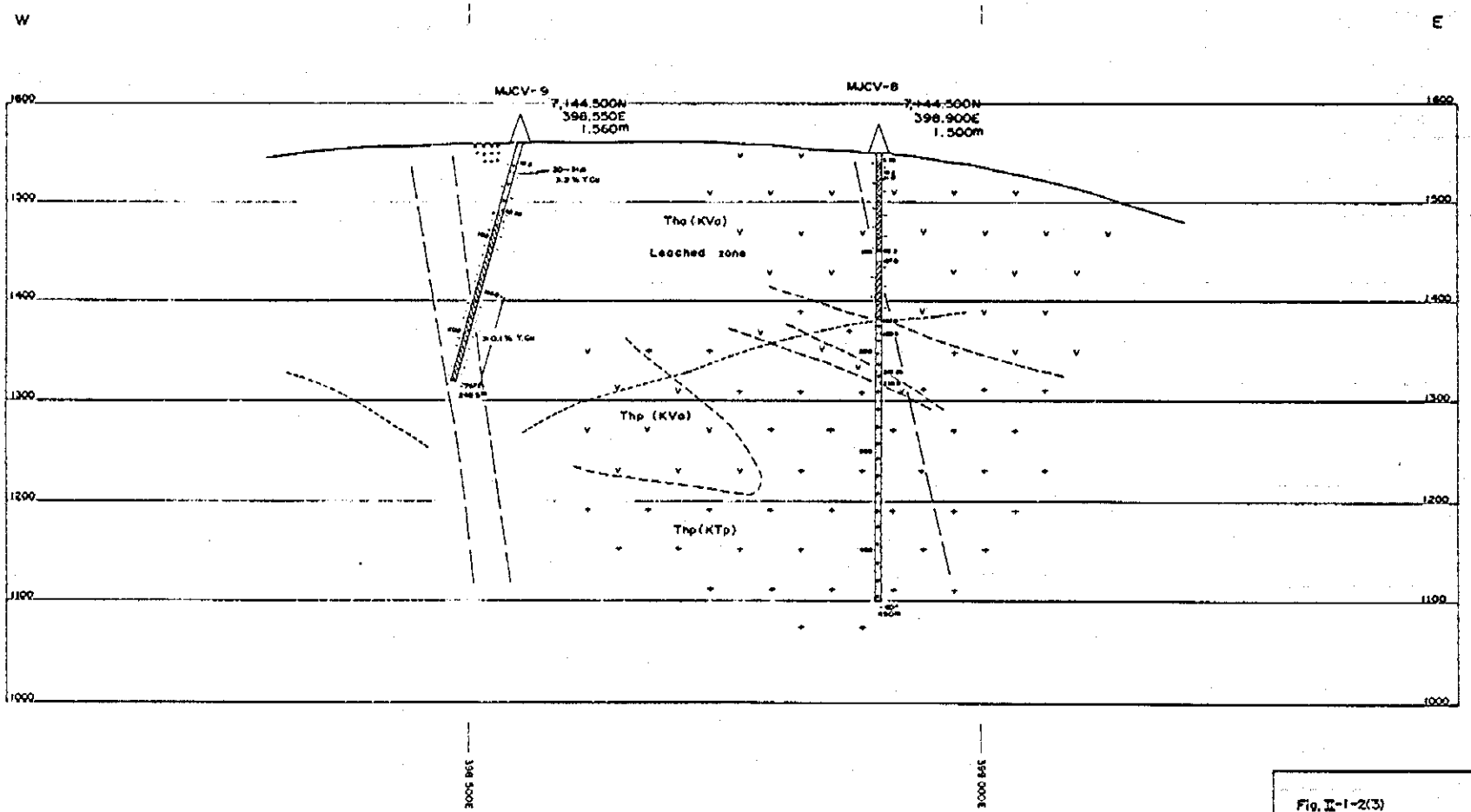

Legend

Aeropuerto formation

- KVa — Andesitic lava and autobrecciated lava
- KVa — Andesitic tuff and pyroclastics

Intrusion

- KTp — Diorite – andesite porphyry

Hydrothermal Alteration zone

- Tha — Intensely silicified zone
- Thsv — Quartz sericitized zone
- Tha — Siliceous argillized zone
- Thp — Chloritized zone (Propylitized zone)

- Mineralization
- Limonite and jarosite rich zone
- Fault (broken line shows inferred fault)
- Fractured zone
- Geologic contact

Fig. II-1-2(3)

Geologic profile of the drill hole MJCV-8&9

(1:6,000)

Drilling Survey, Phase II

Veraguas Project, JICA/MMAJ-ENAMI

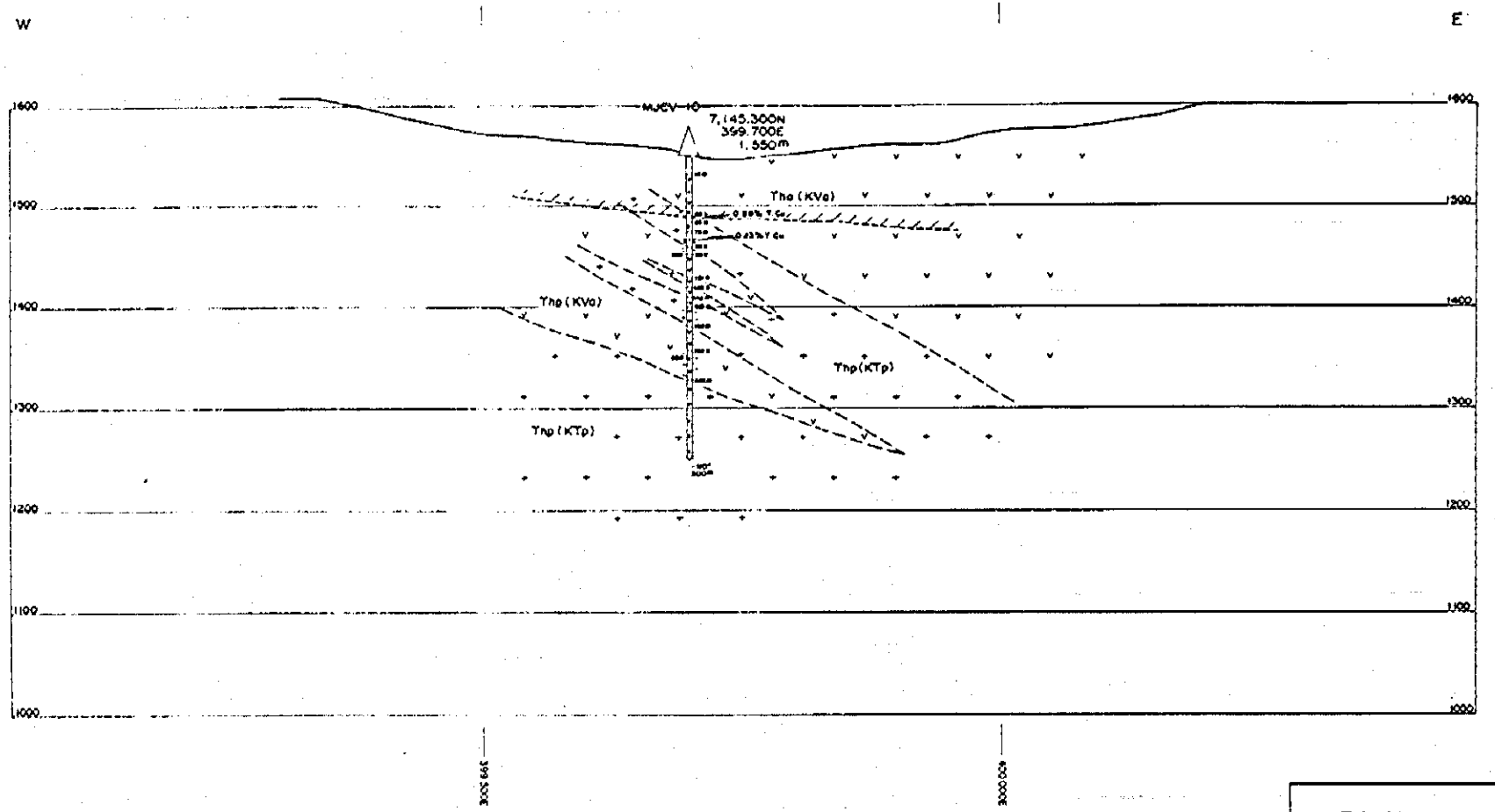

Legend

Adrapuerto formation

- KVa — Andesitic lava and autobrecciated lava
- KVa — Andesitic tuff and pyroclastics

Intrusion

- KTp — Quartz-andesite porphyry

Hydrothermal Alteration zone

- Tha — Intensely silicified zone
- Thsv — Quartz sericitized zone
- Tha — Siliceous argillized zone
- Thp — Chloritized zone (Propylitized zone)

- Mineralization
- Limonite and Jarosite rich zone
- Fault (broken line shows inferred fault)
- Fractured zone
- Geologic contact

Fig. II-1-2(4)

Geologic profile of the drill hole MJCV-10

(1:6,000)

Drilling Survey, Phase II

Veraguas Project, JICA/MMAJ-ENAMI

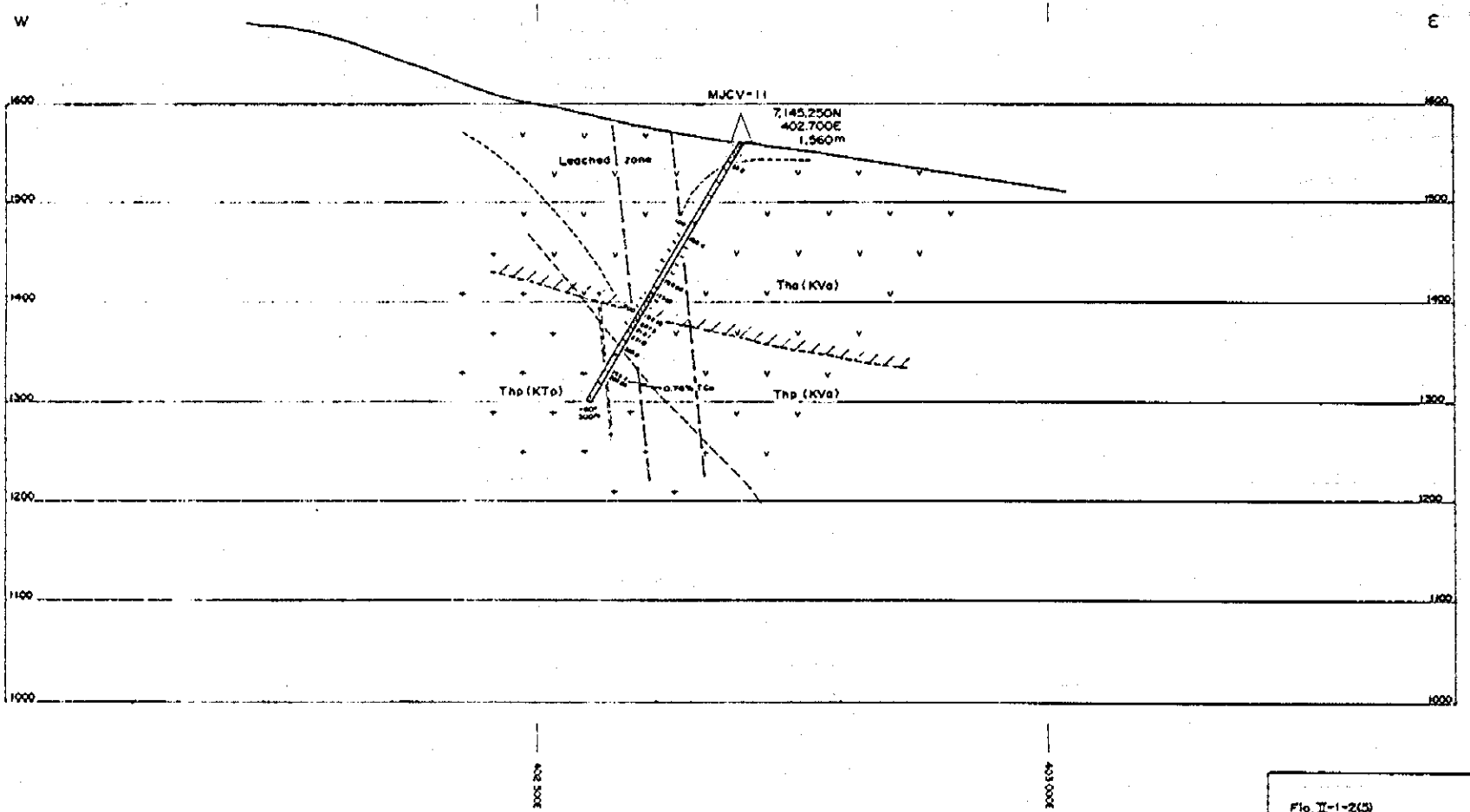

Legend

Aeropuerto formation

KVa — Andesitic lava and autobrecciated lava

KVa — Andesitic tuff and pyroclastics

Intrusive

KTp — Diorite – andesite porphyry

Hydrothermal Alteration zone

Tha — Intensely silicified zone

Thsr — Quartz sericitized zone

Tha — Smectite argillized zone

Thp — Chloritized zone (Propylitized zone)

Mineralization

Limonite and Jarosite rich zone

Fault (broken line shows inferred fault)

Fractured zone

Geologic contact

Fig. II-1-2(5)

Geologic profile of the drill hole MJCV-11

(1:6,000)

Drilling Survey, Phase II

Veraguas Project, JICA/MMAJ-ENAMI

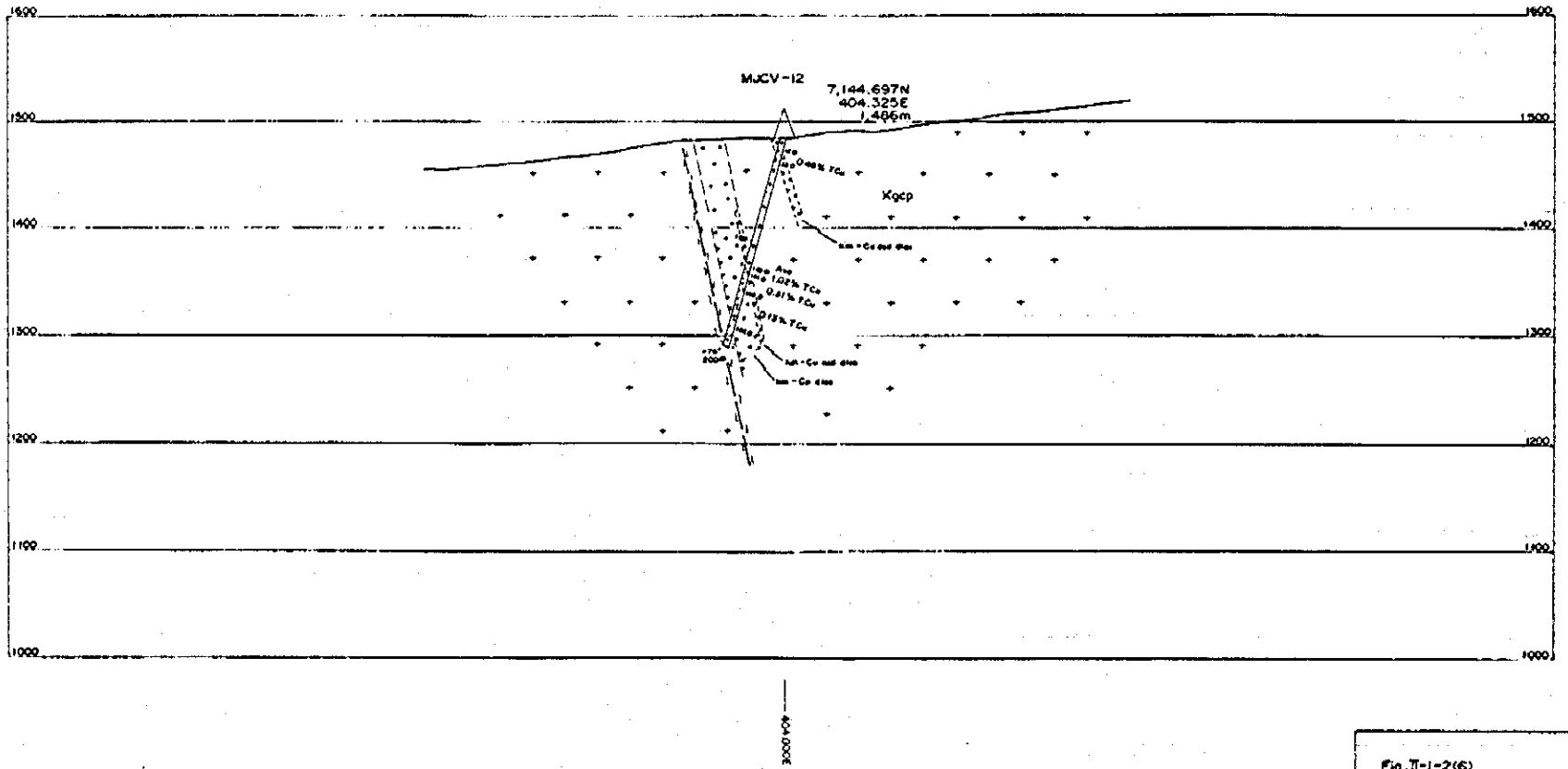

Legend

Aeropuerto formation

- KVa — Andesitic lava and autobrecciated lava
- KVa — Andesitic tuff and pyroclastics

Intrusion

- Kgcp — Quartz diorite

Hydrothermal Alteration zone

- Tha — Intensely silicified zone
- Thsv — Quartz sericitized zone
- Tha — Siliceous argillized zone
- Thp — Chloritized zone (Propylitized zone)

- Mineralization
- Limonite and Jarosite rich zone
- Fault (broken line shows inferred fault)
- Fractured zone
- Geologic contact

Fig. II-1-2(6)

Geologic profile of the drill hole MJCV-12

(1:6,000)

Drilling Survey, Phase II

Veraguas Project, JICA/MMAJ-ENAMI

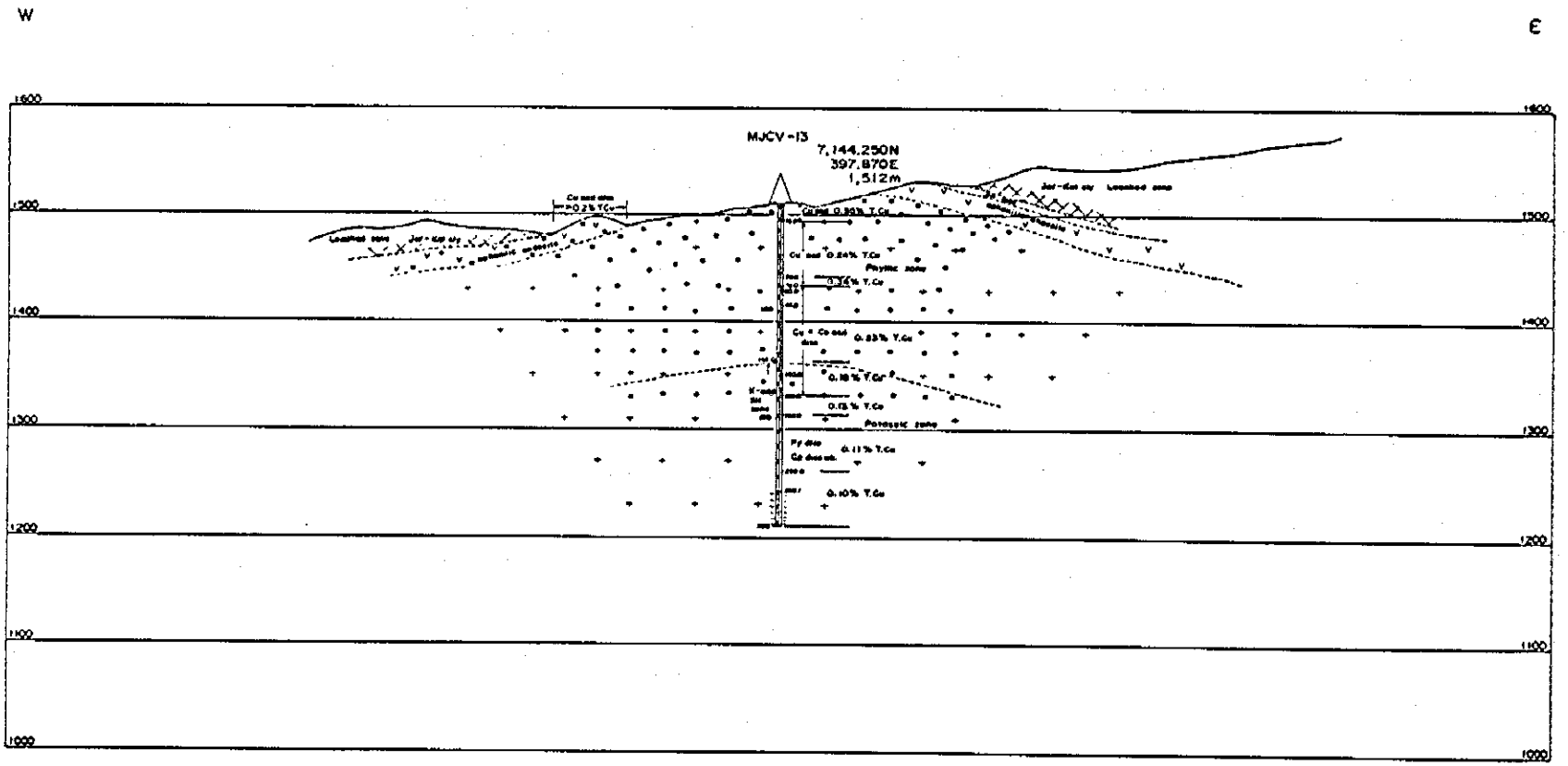

Legend

Aeroquerte formation

- KVa — Andesite lava and autobrecciated lava
- KVa — Andesite tuff and pyroclastics

Intrusion

- KTp — Diorite — andesite porphyry

Hydrothermal Alteration zone

- Tha — Intensely silicified zone
- Thsr — Quartz sericitized zone
- Ths — Siliceous argillized zone
- Thp — Chloritized zone (Propylitized zone)

- Mineralization
- Limonite and Jarosite rich zone
- Fault (broken line shows inferred fault)
- Fractured zone
- Geologic contact

Fig. II-1-2(7)

Geologic profile of the drill hole MJCV-13

(1:6,000)

Drilling Survey, Phase I

Veraguas Project, JICA/MMAJ-ENAMI

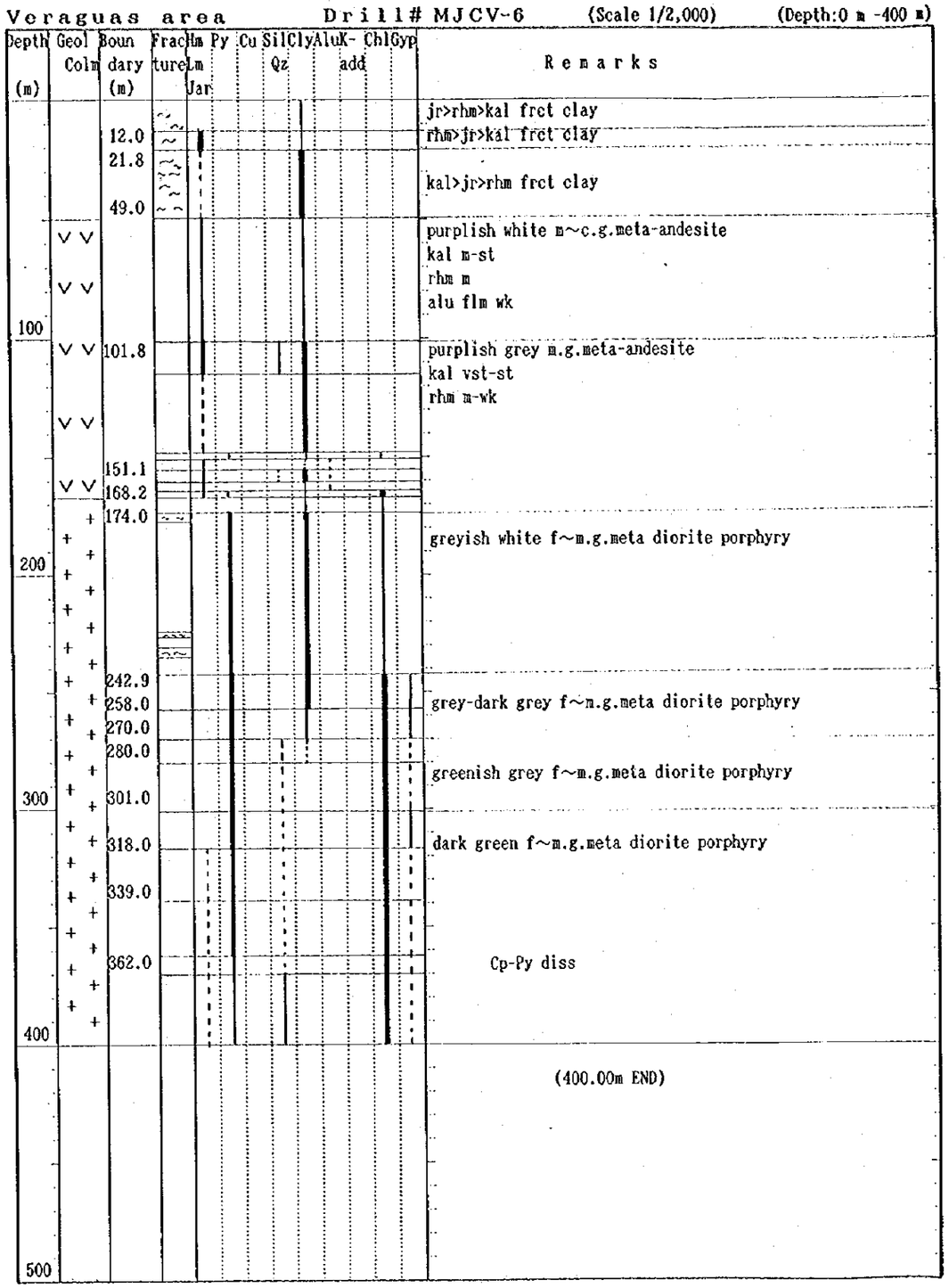

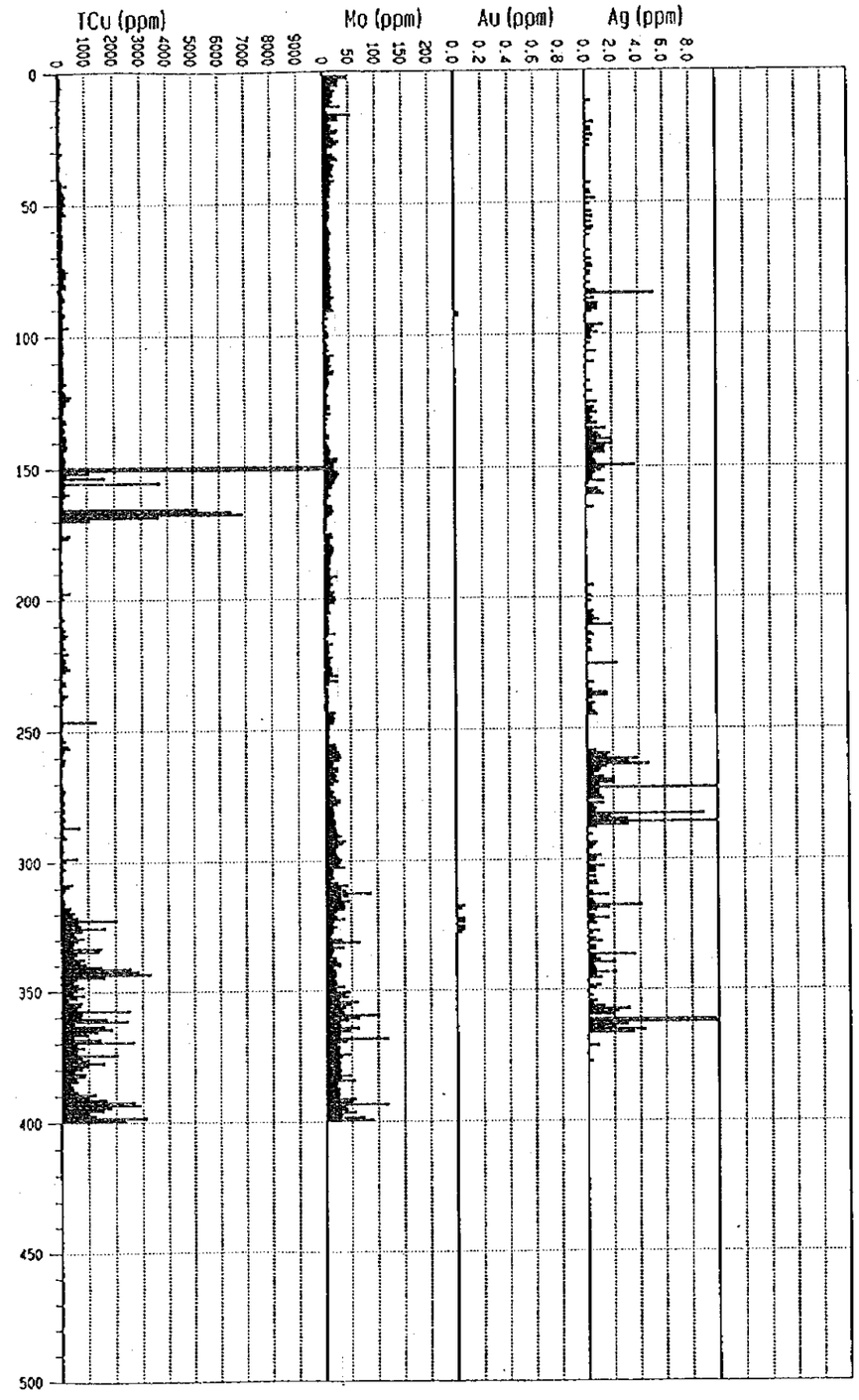

Fig.II-1-3(1) Synthetic column for MJCV-6 (1:2,000)

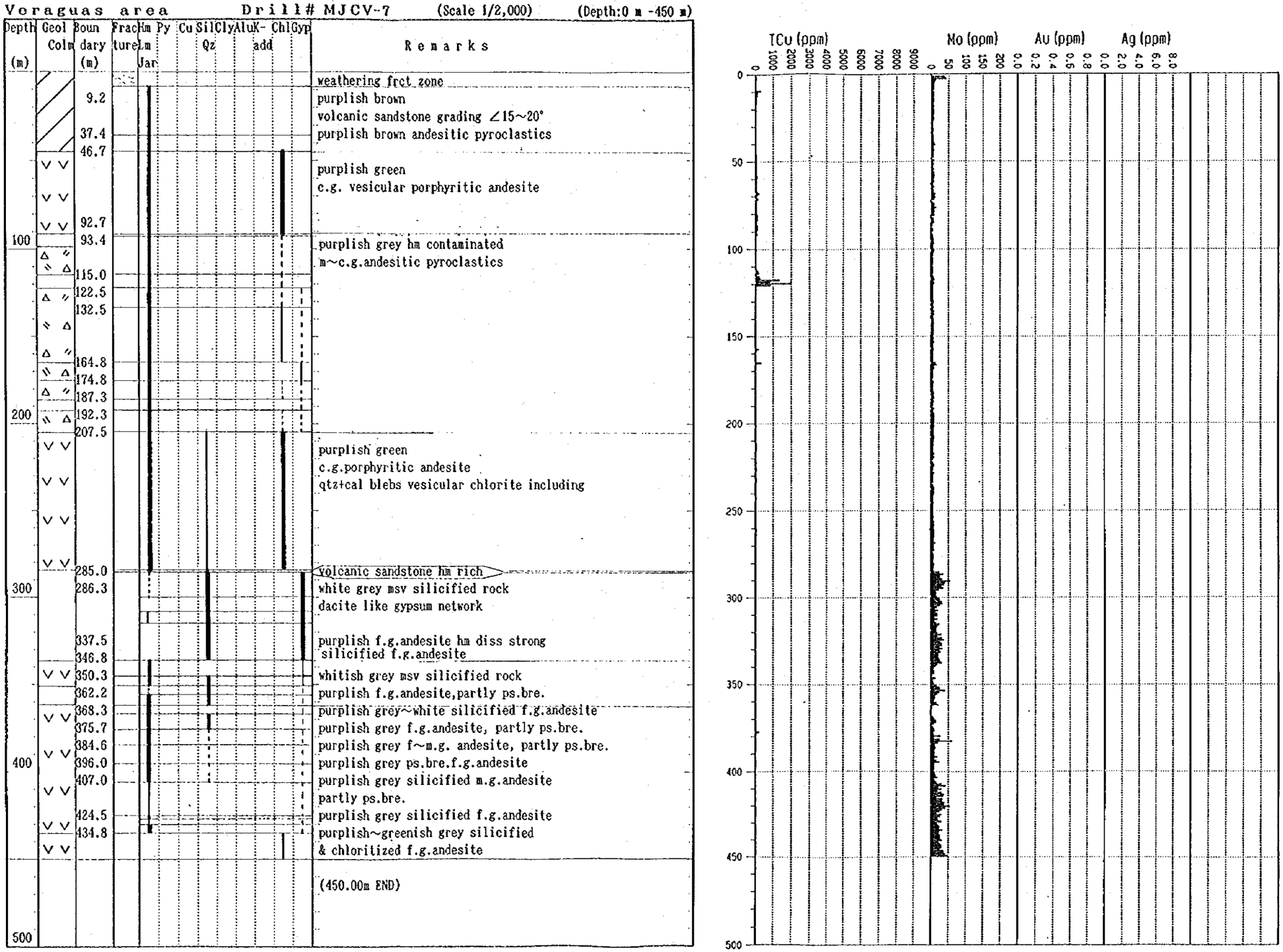

Fig.II−1−3(2) Synthetic column for MJCV−7 (1:2,000)

Veraguas area　　Drill#MJCV-8　　(Scale 1/2000)　　(Depth:0 m -450 m)

Depth (m)	Geol Colm	Boundary (m)	Fracture	Hm Lm	Py Jar	Cu	Sil Qz	Cly	Alu	K-add	Chl	Gyp	Remarks
		5.3											Grabel
		18.8											jar-rhm-kal clay frct
	V V	21.0											silicified zone
	V V	42.0											rhm>jar network kal>sil purplish grey f～m.g.partly ps.bre.meta-andesite
		51.0											jar-rhm-kal clay
	V V	62.7											rhm>jar diss～network kal>sil meta-andesite
	V V	62.7											jar-n.jar rich clay
	V V												r.hm>jar dis, netrwork kal>sil purplish ～reddish grey f～m.g.ps.bre.meta-andesite
100	V V	98.2											
		107.0											purplish grey～brownish grey jar>n jar rich kal clay
		147.4											
	V V												purplish white jar-kal f～m.g.ps.bre.meta-andesite
													frct jar-kal clay
	+												purplish～greenish grey m.g.ps.bre.meta-porphry
	+	180.5											greenish grey f～m.g.meta-diorite porphry
200	+												partly ps.bre.tex
	+	207.6											pale greenish grey f～m.g.ps.bre.meta-diorite porphry
	+	219.3											
	V V	230.9											greenish grey～greyish white m.g.meta-andesite
	+												bleached m.g.ps.bre.meta-diorite porphry
	+												
	+	266.0											greyish white bleached m.g.meta-diorite porphry partly ps.bre.tex
	+	280.0											greenish grey m.g.ps.bre.meta-diorite porphry
300	+												
	+	330.3											〃　py-hm diss cal flm gyp flm wk
	+	335.0											dark greenish grey f～m.g.ps.bre. meta-diorite porphry
	+	340.1											dark greenish grey f～m.g.ps.bre.meta -diorite porphry
	+	364.5											greenish grey f～m.g.ps.bre.meta-diorite porphry
	+												
400	+												
	+	403.0											dark greenish grey f.g.afanitic meta-diorite porphry
	+	408.9											greenish grey, partly bleached f.g.meta-diorite porphry
	+												f.g.meta-diorite porphry partly ps.bre. tex
	+												
													(450.00m END)
500													

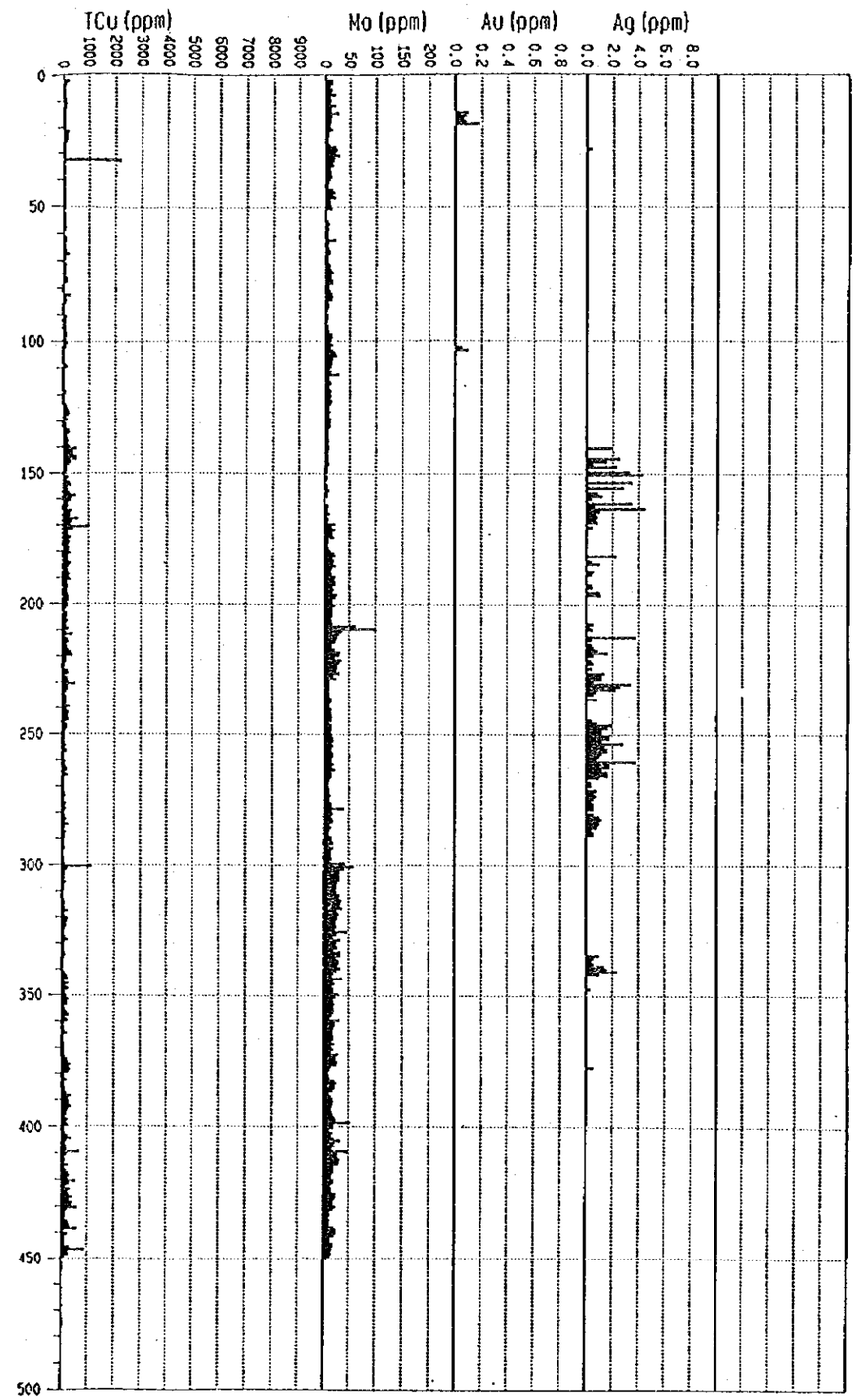

Fig.II-1-3(3) Synthetic column for MJCV-8 (1:2,000)

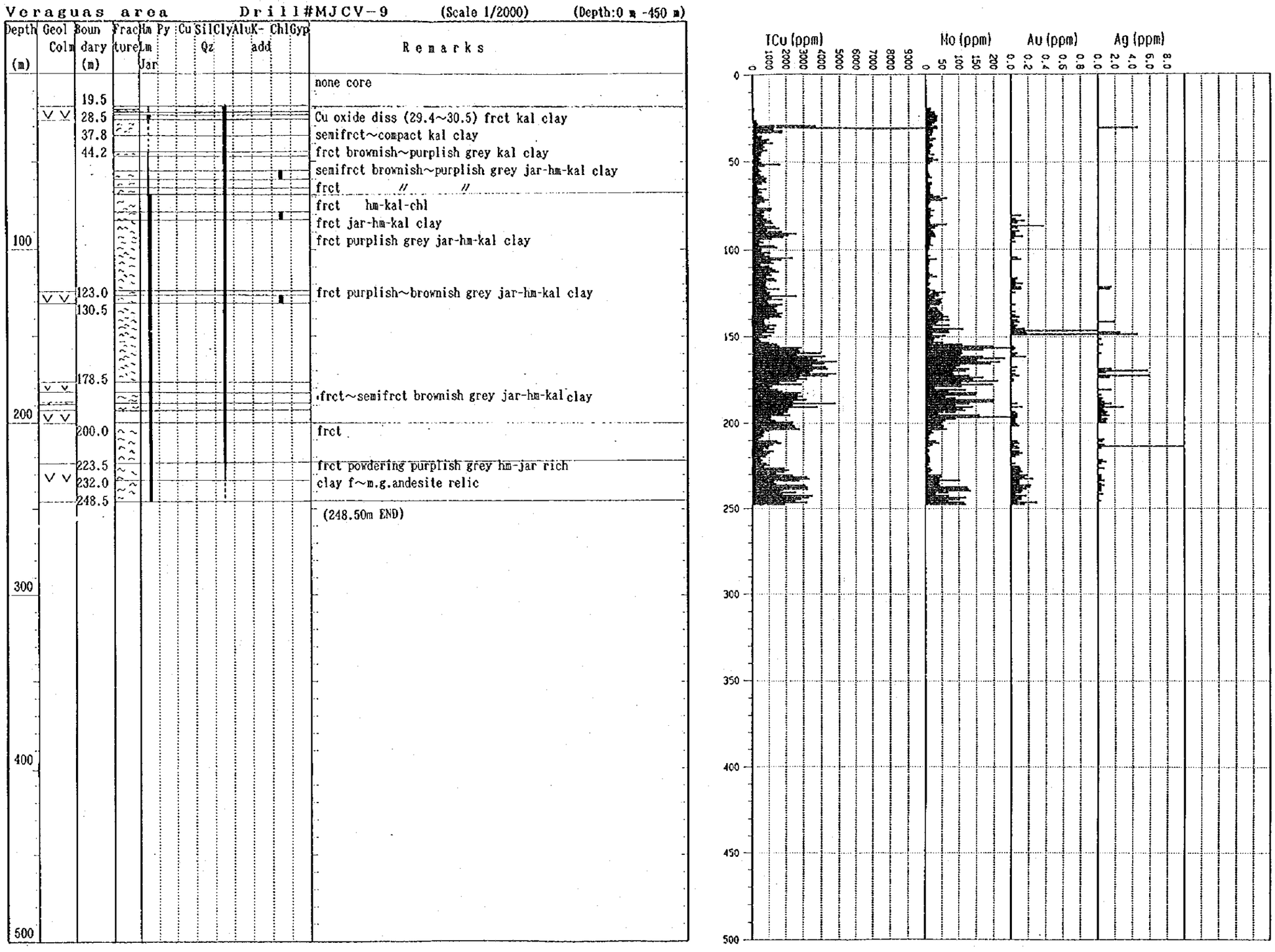

Fig.II-1-3(4) Synthetic column for MJCV-9 (1:2,000)

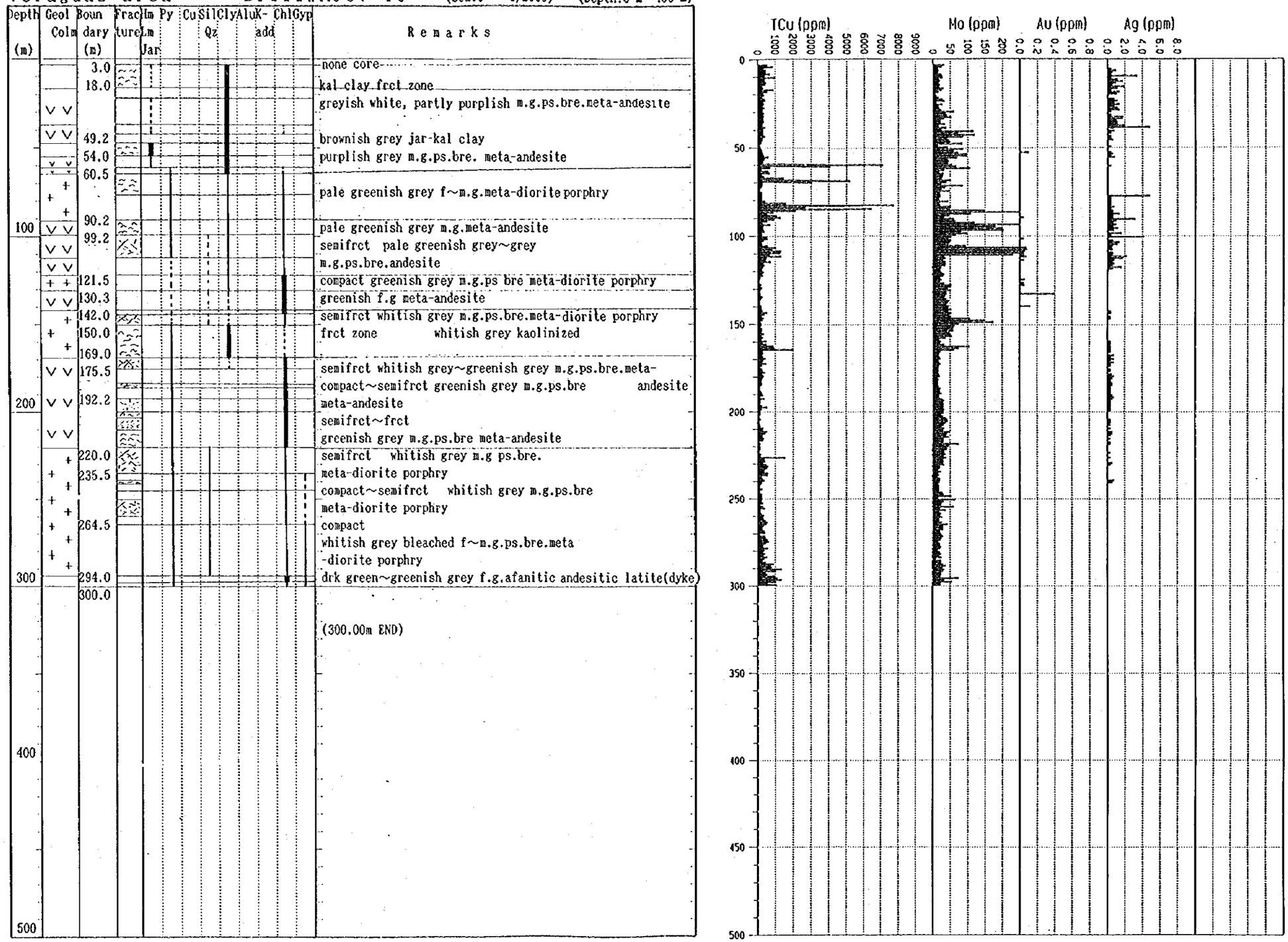

Fig.II-1-3(5) Synthetic column for MJCV-10(1:2,000)

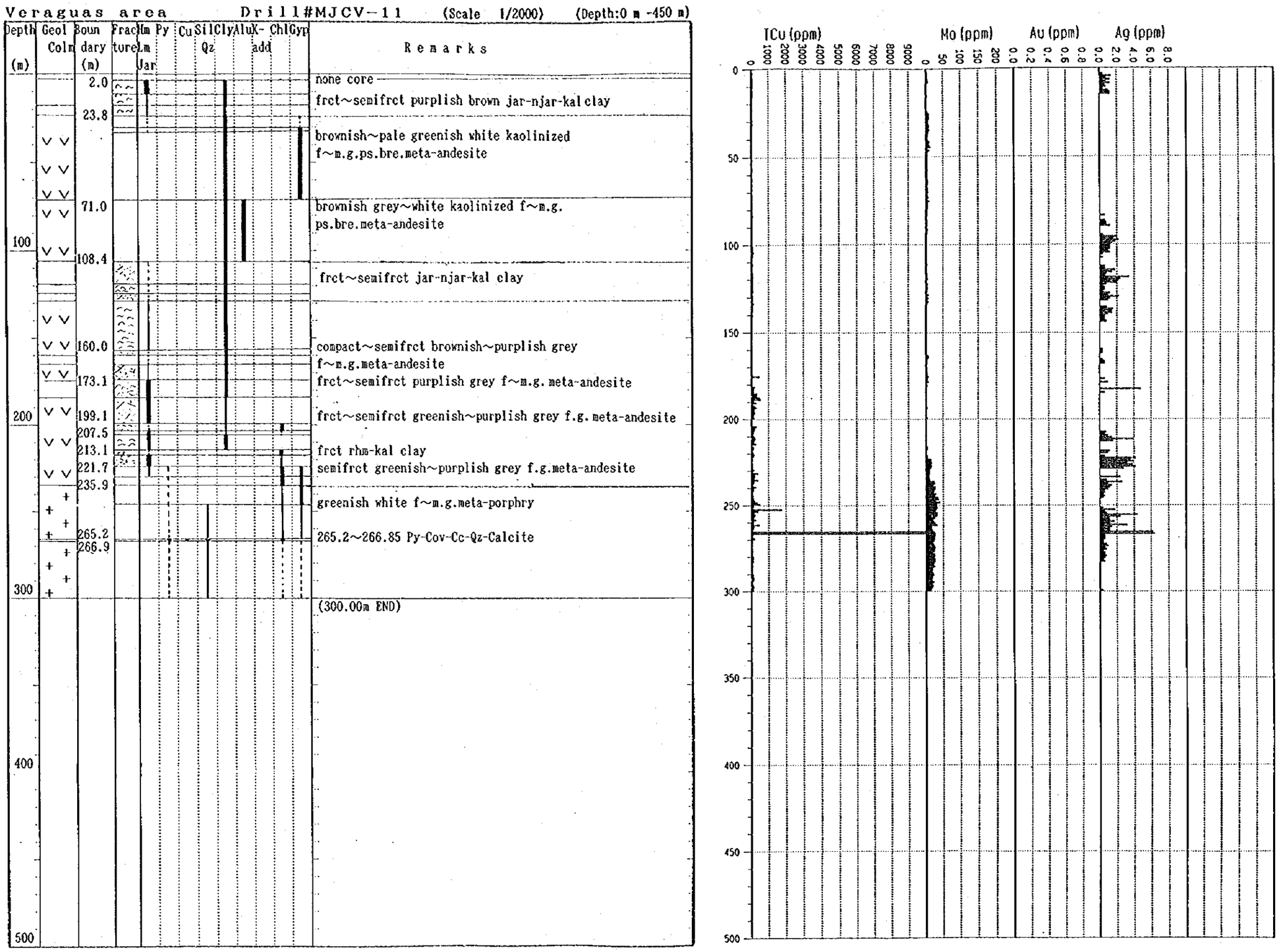

Fig.II-1-3(6) Synthetic column for MJCV-11(1:2,000)

Veraguas area　　Drill#MJCV-12　　(Scale 1/2000)　　(Depth:0 m -450 m)

Depth (m)	Geol Colm	Boundary (m)	Fracture	Hm Jar	Cu oxd	Cp	Py	Kal Cly	Chl	Epi	Gyp	Cal Qz	Sil	Remarks
		3.0												none core
		12.7												semifrct greenish white f.g.diorite
		17.5												calcite-Cu oxd network,metalic hm flm~network
														green f.g.diorite chl>epi Cu oxd in frct
														fracture metalic hm diss~flm
		53.9												greenish grey f.g.diorite jar-metalic hm diss~fine flm rich
		60.9												greenish grey chl~epi rich partly banded
														f~m.g.diorite
														88.8~89.95 frct Cu oxd diss rich
100		89.9												greenish chl>epi f~m.g.diorite, metalic hm diss m~wk
														Cu oxd wk~v.wk diss
		111.0												greenish chl>epi f.g.doirite,metalic hm diss wk Cu oxd nore
		124.3												metalic hm diss~flm rich Cu oxd diss~contani infront
		131.0												dark green f.g.diorite chl=epi rich
														Cp-Py diss with metalic hm flm
		172.0												dark green f.g.doirite chl>epi Cp-Py diss wk
		178.4												dark green f.g.diorite m.hm diss wk
200														frct
														(200.00m END)
300														
400														
500														

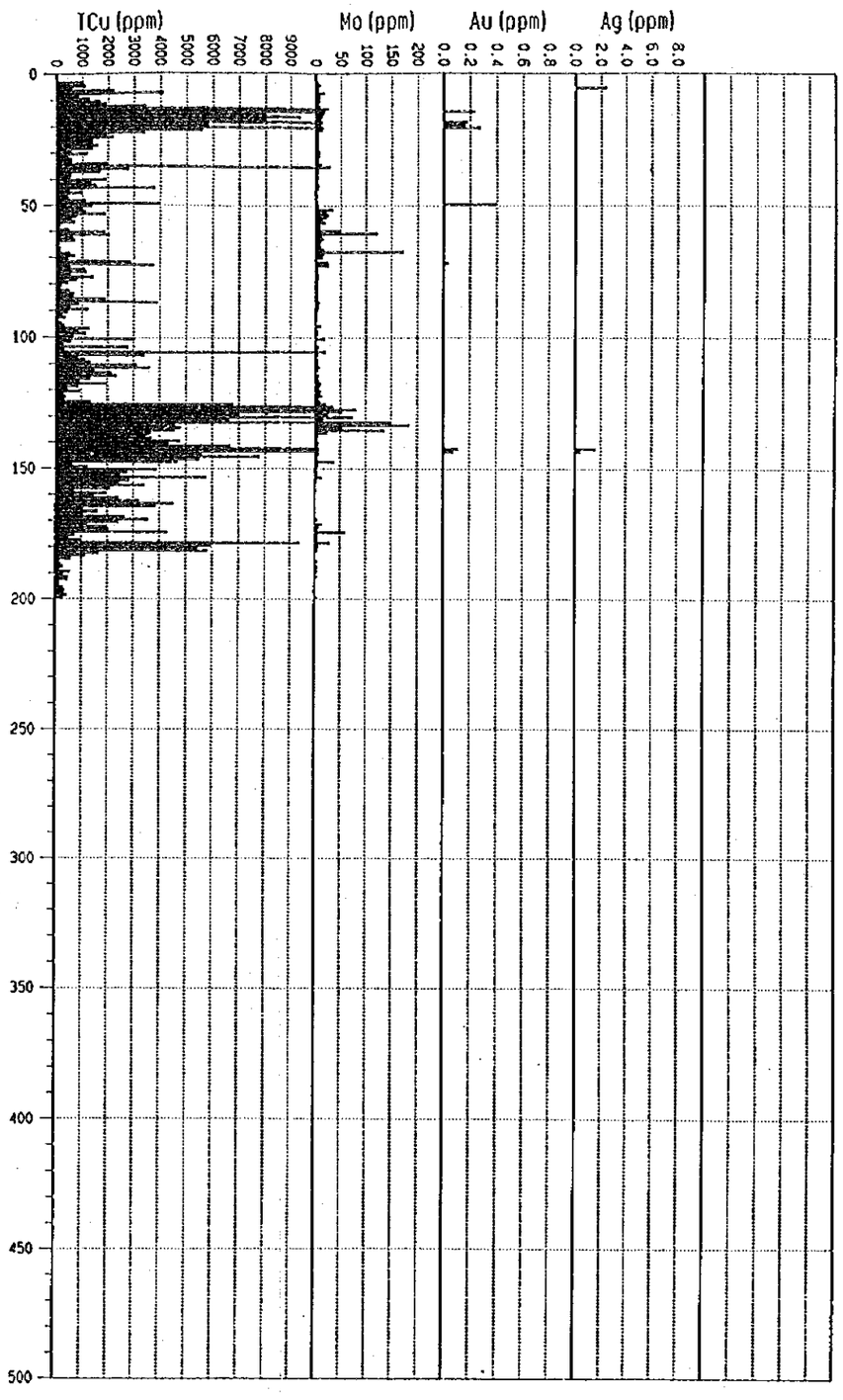

Fig.II-1-3(7) Synthetic column for MJCV-12(1:2,000)

Veraguas area　　Drill#MJCV-13　　(Scale 1/2000)　　(Depth:0 m -450 m)

Depth (m)	Geol Colm	Boun dary (m)	Frac ture	Im Cu oxd Jar	Cu sul	Py	Kal	Chl	Sil	X-Qz	Gyp add	Cal	Remarks
		1.5											purplish~brownish grey jar>kal gyp network
		16.9											Lixivited zone Cu oxd diss rich
		26.8											brownish green~dark green m.g.diorite porphry chl rich gyp
													brownish~greenish grey m.g.diorite porphr network st jar-
													chl>kal gyp-jar network limc rich
		50.0											greenish grey m.g.diorite porphry,weakly alteration
													Cu oxd diss wk in gyp flm jar chl gyp flm wk
		70.0											
		78.0											greenish f~m.g.diorite porphry gyp network rich metalic hmdiss
100													green f~m.g.diorite porphry gyp network rich
													native copper diss~fine film m~st
													Cu oxd diss in gyp network and frct
													metalic hm diss
		125.6											weakly sil-k-add alteration
		149.0											greenish~brownish grey f~m.g.diorite porphry
													.sil-k-add alteration,native copper
													diss~fine flm m~wk Cu oxd diss in frct
		180.0											brownish green jar-rhm rich
		185.6											greenish~brownish grey f~m.g.diorite porphry
200		198.5											metalic hm diss
		210.0											greenish grey f~m.g.diorite porphry
		221.0											Limonitized brownish sil-chl dacitic porphry
													.,pseudo brecciated tex.
													greenish grey f.g.diorite porphry
													Py-m hm-limo diss~flm Py>Cp diss
		268.1											
		274.0											v.frct zone (powdering)
													frct zone Py diss wk jar-chl-sil
300		290.2											greenish grey f.g.diorite porphry chl-sil
													(300.00m END)
400													
500													

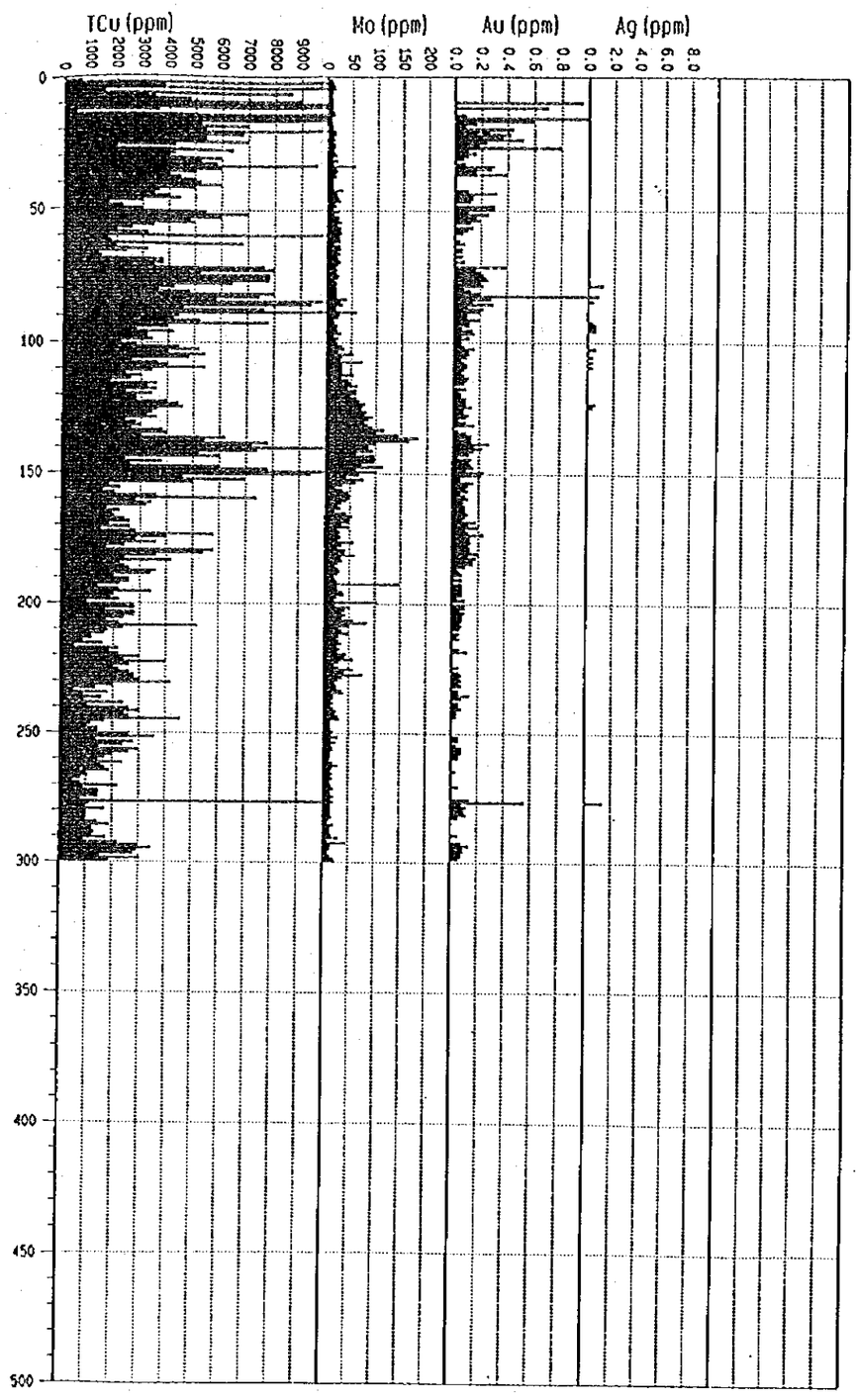

Fig II-1-3(8) Synthetic column for MJCV-13(1:2,000)

TableII−1−6 Results of the microscopic observation (Polished thin section)

Samples					Primary minerals						Original texture of igneous rock	Alteration Minerals																Opaque minerals												Remarks
No.	Drill Hole	Depth (m)	Original Rock	Alt. Zone	Qz	Pl	Px	Hb	Bt			degree of alt.	Qz	Ab	Kf	Bt	Se	Ch	Ep	Ah	Gp	Ca	Py	Po	Cu	Cp	Cv	Cc	Cu	Sp	Mt	Hm	Ge	
1	MVCV-6	149.6	Andesite									◆	◎	○			○						◎										·	Andesite?, Ka:○?
2	MVCV-6	250.0	Porphyry			△					porphyritic	◆	◎	◎			△						◎								△	△	△	Andesite?, Ka:○?, Mt→Py?
3	MVCV-6	260.7	Porphyry			·						◆	○	◎			○		△	△	◎		◎			·							·	Andesite?, Ka:△?
4	MVCV-6	295.2	And.pyro.		○	○					porphyritic	◆	○	◎			◎		○	△	○		◎										△	Tuff breccia?, Ka:○?
5	MVCV-6	320.0	Porphyry			◎					holocrystalline	◇	△	○			◎	◎		○	○	△	◎			○					·	△	△	dioritic, Qz-Ah veinlet
6	MVCV-6	335.8	Porphyry			○					porphyritic	◆	◎	◎			○	○		○		○	◎			◎					·		△	Mt→Py
7	MVCV-6	344.0	Porphyry			◎					porphyritic	◆	△	○			○	◎		△	○		◎			◎							○	Qz-Ah veinlet
8	MVCV-6	362.5	And.pyro.		◎	◎						◆	○	◎				◎		○	○	◎	◎			○					·		△	Tuff?
9	MVCV-6	369.5	Porphyry			·	·	?				◆	○	◎			?	◎		○	○	○	◎			◎							·	Am:○, Gp-Ah veinlet
10	MVCV-6	389.0	Porphyry			○		△			porphyritic	◆	◎	◎	○		○	◎	·	○	△	△	◎			○							△	And.pyro.?
11	MVCV-6	394.5	Porphyry			○						◆	○	◎	△		○	◎	△	○	○	○	○			○					○	△	△	Mo: ·
12	MVCV-7	55.0	Andesite			◎		○			porphyritic	◇	○				△	○				○										○		Ka:△?, Zo:△?
13	MVCV-7	140.0	And.pyro.			◎		○			porphyritic	◇	○		○			○				○										○	△	Porphyrite?, Rutile:△
14	MVCV-7	212.3	Andesite			◎					porphyritic	◇	○		○			○		△		◎									△	○	△	Sm:○, Zo:△?, Dolomite?→Ca
15	MVCV-7	450.0	And.pyro.		◎							◆	◎							◎	○										·	△	△	Tuff?, Sm:○, Zo:△
16	MVCV-8	215.6	Porphyry			○					porphyritic	◆	○	◎			○	○			△	·	◎									·	·	Sm:○
17	MVCV-8	276.1	Porphyry			◎					porphyritic	◆	△	◎			△	△		·		○	◎										·	Sm:△
18	MVCV-8	319.9	And.pyro.		◎	○						◆	○	◎			◎	○		△		◎	◎											Tuff?, Sm:△
19	MVCV-8	331.0	And.pyro.		◎	○						◆	○	◎	?		○	△	·	○	○	◎	◎										△	Tuff, Sm:△
20	MVCV-8	450.0	Porphyry			○			○		porphyritic	◆	○	◎			△	◎	△	○			◎			·								
21	MVCV-10	64.6	Andesite			○					porphyritic	◆	○	○			○						◎										·	Ka:○?, Se:○
22	MVCV-10	92.6	Andesite			○					porphyritic	◆	◎	○			○	?	△				◎			·			?	·	△	△	Se:△
23	MVCV-10	293.0	Porphyry									◆	◎	◎	○		○	○		△	○		◎			△								Porphyrite?
24	MVCV-11	205.1	Andesite			○	△				porphyritic	◇	△	◎			△	○	○												·	◎	△	
25	MVCV-11	232.0	Andesite		·	○					porphyritic	◆	○	◎			○	○	△				◎			△							△	Zo:○, Se:△, Rutile:△
26	MVCV-11	245.8	Porphyry			○					holocrystalline	◆	○	◎			◎			△			◎											Sm:△
27	MVCV-11	266.5	Porphyry			○						◆	◎	○			○			△	△	◎	◎				△	○						Porphyrite?
28	MVCV-11	300.0	Porphyry			◎						◆	○	○			○	?		△		△	◎			·								Zo:○, Sm:○
29	MVCV-12	48.0	Q.Diorite			○	·	◎			holocrystalline	◇	△	◎			△	○	△			○										○	△	Am:○, Px: · ?
30	MVCV-12	72.0	Q.Diorite		△	◎					holocrystalline	◇	△	○		○		◎				○		○								◎	○	fine grain
31	MVCV-12	141.0	Q.Diorite			○	○?				holocrystalline	◆	△	◎	○		·	◎	○			○	○		△	○							○		Se:△, secondary Px vein
32	MVCV-12	145.5	Q.Diorite			△	△				holocrystalline	◆	△	◎	△		○	◎	◎			○	△		△	○							◎	△	
33	MVCV-12	153.0	Q.Diorite			◎	△				holocrystalline	◇	○	○	△			◎	○			○	○		△	○							◎		Se:○, Qz vein
34	MVCV-13	12.0	Di-Porphyry			△						◆	◎	○	?		◎	△			◎			○	·							○	△	Porphyrite?, Mt→Ht(Maghemite?)
35	MVCV-13	39.5	Di-Porphyry			△				?		◆	◎	○	△	△	○	△							·							○	○	Porphyrite?, Mt→Ht?
36	MVCV-13	78.5	Di-Porphyry							?		◆	◎	△	○	○	△	△	·	△	○				·			△		○	○	△	Mt→Ht
37	MVCV-13	105.0	Di-Porphyry			◎				?		◆	◎	△	△	◎	△	△		△	○				·			△		○	○	△	Porphyrite?, Mt→Ht?
38	MVCV-13	142.1	Di-Porphyry	?	△				?		holocrystalline	◆	○	◎?		○	○	○			○				·			◎		◎	◎	○	dioritic, Cu? and Fe oxides?
39	MVCV-13	164.7	Di-Porphyry									◆	◎	○	○		○	○			○												
40	MVCV-13	194.7	Di-Porphyry			◎						◆	◎	○	○			○				○			·	○	·					○	○	Mt→Ht
41	MVCV-13	200.2	Di-Porphyry			△					holocrystalline	◆	◎	◎	△		○	◎	△			○						○		◎	○	○	△	dioritic
42	MVCV-13	209.0	Di-Porphyry			△					holocrystalline	◆	○	◎			△	◎			○					△	·	·				○	◎	dioritic, Am:△, Mt→Ht
43	MVCV-13	230.6	Di-Porphyry			△					holocrystalline	◆	○	◎	○		△	◎			○			○		○	△	○						○	dioritic, Mo:△, Py-Cc-Cv vein
44	MVCV-13	250.5	Di-Porphyry									◆	◎	◎	△	?	△	○	△	○	△	○	·			△	·	·		·	○	○	△	dioritic, Mt→Ht
																																		Porphyrite?, Mt→Ht

[abandance]
◎:abandant
○:common
△:minor
·:rare

[degree of alteration]
◆:completely altered
◇:partly altered
:fresh or not altered

[Mineral names]
Qz:quartz, Pl:plagioclase, Px:pyroxene, Hb:hornblende, Bt:biotite, Ab:albite, Kf:K-feldspar, Se:sericite, Ch:chlorite, Ep:epidote, Ah:anhydrite, Gp:gypsum, Ca:carbonate, Py:pyrite, Po:pyrrhotite, Cu':oxidized copper, Cp:chalcopyrite, Cv:covelline, Cc:chalcocite, Cu:native copper, Sp:sphalerite, Mt:magnetite, Hm:hematite, Ge:goethite, Mo:molybdenite, Am:amphibole group, Se:sphene, Ka:kaolinite, Sm:smectite, Zo:zeolite group, Bo:bornite

* Di-Porpyry:Diorite Porphyry
* And.pyro. :Andesitic pyroclastics
* Q.Diorite :Quartz

TableII-1-7 Results of the microscopic observation (Polished section)

Samples					Opaque minerals																
No.	Drill Hole	Depth (m)	Original Rock	Remarks	Py	Cu ox	Cp		Bo		Cv	Cc	Cu°	by point counter		Mt	Hm	Il	by point counter		
								ϕ		ϕ				wt%	ϕ					wt%	ϕ
1	MVCV-13	16.0	Di-Porp.				·	5-15μ					·	--	10- 25μ	○	◎	△		7.5	5-350μ
2	MVCV-13	78.4	Di-Porp.				·	10-20μ					△	2.4	5-300μ	○	◎	△		17.1	5-400μ
3	MVCV-13	95.9	Di-Porp.	gyp network			·	5-10μ	·	10μ			·	0.9	5-150μ	○	◎	△		11.2	5-400μ
4	MVCV-13	98.8	Di-Porp.	gyp network			·	<10μ	·	<10μ			△	0.9	5-100μ	○	◎	△		11.8	5-250μ
5	MVCV-13	123.9	Di-Porp.	gyp network									·	0.4	5-300μ	○	◎	△		11.1	10-350μ
6	MVCV-13	126.6	Di-Porp.	gyp network			·	5μ					△	1.7	5-250μ	△	○	·		9.7	5-350μ
7	MVCV-13	129.4	Di-Porp.				·	<10μ					·	0.4	5-100μ	○	◎	△		14.4	5-250μ
8	MVCV-13	134.1	Di-Porp.	gyp network			·	< 5μ					○	2.6	5-200μ	○	◎	△		19.0	5-300μ
9	MVCV-13	135.9	Di-Porp.	gyp network			·	<10μ	·	<10μ			△	1.3	5-200μ	△	○	·		7.1	5-250μ
10	MVCV-13	140.5	Di-Porp.	gyp network	· <10μ	· azurite	·	5-15μ	·	<10μ							◎	△		17.5	5-500μ
11	MVCV-13	143.0	Di-Porp.	gyp network	?		·	< 5μ					·	0.4	5-300μ	·	○			7.8	5-300μ
12	MVCV-13	147.0	Di-Porp.				·	5-10μ					○	3.5	5-250μ	·	◎	△		10.9	5-300μ
13	MVCV-13	152.0	Di-Porp.	qz film			·	5-10μ					△	1.2		·	◎	△		15.5	10-100μ
14	MVCV-13	159.5	Di-Porp.	gyp network	?	· atacamite	·	< 5μ			·	·	·	--	5-10μ	·	◎			15.5	5-300μ
15	MVCV-13	181.3	Di-Porp.			· azurite	△	<15μ	·	<10μ			·	--	< 5μ		○			6.8	5-150μ
16	MVCV-13	225.0	Di-Porp.	gyp network			·	< 5μ	·	< 5μ			·	0.5	5-150μ	·	◎			20.0	5-300μ

[abandance]
◎:abandant
○:common
△:minor
·:rare

* Di-Porp. : Diorite Porphyry

Py : pyrite
Cu ox : copper oxide
Cp : chalcopyrite
Bo : bornite
Cv : coveline
Cc : chalcocite
Cu° : native copper

Mt : magnetite
Hm : hematite
Il : ilmenite
gyp : gypsum
qz : quartz

TableII--1--8 Results of the powder X--ray diffraction (1)

Clasification		Abbr.	Mineral Name	Chemical Formulas	No.	1	2	3	4	5	6	7	8	9	10	11	12	13	14	15	16	17	18	19	20
					Drill hol Depth(m)	48.0	100.0	149.6	200.0	250.0	295.0	357.8	369.5	389.0	44.3	55.0	119.0	140.0	189.3	212.3	240.5	284.4	310.0	388.0	450.0
						NJCV-6									NJCV-7										
Cu	Sulphide	Tet	Tetrahedrite	$Cu_{12}Sb_4S_{13}$																					
		Cc	Chalcosine	Cu_2S						·			·												
		Djr	Djurleite	$Cu_{31}S_{16}$																					
		Ena	Enargite	Cu_3AsS_4																					
		Cv	Coveline	CuS																					
		Cp	Chalcopyrite	$CuFeS_2$						·			·	·											
	Metal	Cu*	Native copper	Cu																					
	Sulfate	Cln	Chalcanthite	$Cu(SO_4)\cdot 5H_2O$																					
		Ant	Antrelite	$Cu_3(SO_4)(OH)_4$																					
		Brc	Brochanthite	$Cu_4(SO_4)(OH)_6$																					
	Carbonate	Az	Azurite	$Cu_3(CO_3)_2(OH)_2$																					
		Mg	Malaquite	$Cu_2CO_3(OH)_2$																					
	Others	Atc	Atacamite	$Cu_2Cl(OH)_3$																					
		Lam	Lammerite	$Cu_3(AsO_4)_2$																					
		Clc	Clinoclase	$Cu_3(AsO_4)(OH)_3$																					
		Chn	Chnevixite	$Cu_2Fe_2(AsO_4)_2(OH)_2\cdot H_2O$																					
		Chr	Chrysocola	$Cu_2-xSi_2O_5(OH)_3/xH_2O$																					
Fe	Oxide & Hydrooxide	Ht	Hematite	Fe_2O_3		△									△	△		○	○	△	·			○	○
		Mgh	Maghemite	Fe_2O_3											·										
		Mt	Magnetite	Fe_3O_4											·										
		Akg	Akaganeite	FeO(OH)																					
		Frx	Feroxybyite	FeO(OH)																					
		Goe	Goethite	FeO(OH)																					
	Sulphide	Po	Pyrrhotite	Fe_7S_8																					
		Apy	Arsenopyrite	FeAsS																					
		Py	Pyrite	FeS_2				○	○	○	○	○	△	○						·					
	Sulfate	Jar	Jarosite	$(K)Fe_3(SO_4)_2(OH)_6$																					
		Na-Jar	Natrojarosite	$(K,Na)Fe_3(SO_4)_2(OH)_6$																·					·
		Btl	Butlerite	$Fe(SO_4)(OH)\cdot 2H_2O$																					
		Prb	Parabutlerite	$Fe(SO_4)(OH)\cdot 2H_2O$																					
		Cri	Kornelite	$Fe_2(SO_4)_3\cdot 7H_2O$																					
		Rzn	Rozenite	$Fe(SO_4)\cdot 4H_2O$																					
		Sdr	Siderotil	$Fe(SO_4)\cdot 5H_2O$																					
	Others	Scr	Scorodite	$Fe(AsO_4)\cdot 2H_2O$																					
		Fml	Ferrimolybdit	$Fe_2(MoO_4)_3\cdot nH_2O$																					
		Ptk	Pseudobrookite	$Fe_2(TiO_3)O_2$																					
		Prt	Pseudorutile	$Fe_2(TiO_3)O_9$																					
Silicate	Silica	Qz	Quartz	SiO_2		◎	◎	◎	◎	◎	◎	◎	◎	◎	○	○		◎	◎	◎	◎	△	◎	◎	◎
	Clay	Chm	Chamosite	$(Fe,Al,Mg)_6(Si,Al)_4O_{10}(OH)_8$					△	△			△												
		Chl	Chlorite	$(Mg,Fe,Al)_{12}(Fe,Al,Si)_8O_{20}(OH)_{16}$											△	○									
		Dck	Dickite	$Al_2Si_2O_5(OH)_4$			○																○		
		Kal	Kaolinite	$Al_2Si_2O_5(OH)_4$	○				△						△	·							○	△	
		Nac	Nacrite	$Al_2Si_2O_5(OH)_4$																					
		Hal	Halloysite	$Al_2Si_2O_5(OH)_4\cdot 2H_2O$																					
		Pyr-Tc	Pyrophyllite-Talc	$Al\cdot MgSi_4O_{10}(OH)_2$						△								△							
		Mus	Muscovite	$K\cdot Al_2(Si_3Al)O_{10}(OH,F)_2$	△	△	△	△	△		○		△							△	·	○		○	
		Ilt	Illite	$K\cdot Al_2(Si_3Al)O_{10}(OH,F)_2$																					
		Mnt	Montmorillonite	$Na_{0.3}(Al,Mg)_2Si_4O_{10}(OH)_2\cdot xH_2O$																					
	Others	Olg	Oligoclase	$(Na,Ca)(Al,Si)_4O_8$											◎	◎		◎	◎						
		Ab	Albite	$(Na,Ca)(Al,Si)_4O_8$				◎	○	○		○	◎							◎	◎	◎			
		Or	Orthoclase	$(K,Na)(Al,Si)_4O_8$	△	△		△	△		△		△			△	·		○		△		△	△
		Mic	Microcline	$KAlSi_3O_8$	△		△																		
		Ho	Hornblende	$(Na,K)Ca_2(Fe,Mg)_5(Al,Si)_8O_{22}(OH)_2$														·							
		Di	Diposide	$CaMg(SiO_3)_2$																					
		Trm	Tremolite	$Ca_2(Mg)_5Si_8O_{22}(OH)_2$									△												
		Act	Actinolite	$Ca_2(Mg,Fe)_5Si_8O_{22}(OH)_2$														△							
		Rie	Riebeckite	$(Na,Ca)_2(Mg,Fe)_5Si_8O_{22}(OH)_2$																					
		Bt	Biotite	$K(Mg,Fe)_2Al[Si_3O_{10}(OH)_2]$																					
		Ep	Epidote	$Ca_2(Al,Fe)_3Si_3O_{12}(OH)$																					
	Zeolite	Hap	Hydroxyapophyllite	$KCa_4Si_8O_{20}(OH)\cdot 8H_2O$																					
		Gz	Gismondite	$CaAl_2Si_2O_8\cdot 4H_2O$																·					
		Mrd	Mordenite	$(Ca,Na_2,K_2)Al_2Si_{10}O_{24}\cdot 7H_2O$																					·
Sulfate		Alu	Alunite	$(K)Al_3(SO_4)_2(OH)_6$																					
		Na-Alu	Natroalunite	$(K,Na)Al_3(SO_4)_2(OH)_6$			○	○															△		○
		Btl	Butlerite	$Fe(OH)SO_4\cdot 2H_2O$																					
		Bld	Bloedite	$Na_2Mg(SO_4)_2\cdot 4H_2O$																					
		Gl	Glauberite	$Na_2Ca(SO_4)_2$																					
		Bas	Bassanite	$Ca(SO_4)_0.5H_2O$																					
		Anh	Anhydrite	$Ca(SO_4)$			△	○		△	△	◎	△	△						·				·	○
		Gyp	Gypsum	$Ca(SO_4)\cdot 2H_2O$							○		○										◎		·
Mn		Pr	Pyrolusite	MnO_2													△								
		Br	Braunite	Mn_7SiO_{12}													△								
		Crp	Cryptomelane	$K\cdot Mn_8O_{16}$																					
		Gro	Groutite	$MnO(OH)$																					
Carbonate		Cal	Calcite	$CaCO_3$											·	△				·	△				
		Dol	Dolmite	$CaMg(CO_3)_2$															△	△	△				
		Kut	Kutnohorite	$Ca(Mg,Mn)(CO_3)_2$																△					

Abundance: ◎ abundant ○ common △ minor · rare

TableII-1-8 Results of the powder X-ray diffraction (2)

Clasification		Abbr.	Mineral Name	Chemical Formulas	No.	21	22	23	24	25	26	27	28	29	30	31	32
					Drill hol Depth(m)	32.4	80.0	140.0	174.5	215.6	276.1	331.0	375.5	450.0	30.0	98.0	225.1
						MJCV-6									MJCV-9		
Cu	Sulphide	Tet	Tetrahedrite	Cu12Sb4S13													
		Cc	Chalcosine	Cu2S													
		Djr	Djurleite	Cu31S16													
		Ena	Enargite	Cu3AsS4													
		Cv	Covelline	CuS													
		Cp	Chalcopyrite	CuFeS2													
	Metal	Cu	Native copper	Cu													
	Sulfate	Cln	Chalcanthite	Cu(SO4)·5H2O											○		·
		Ant	Antrelite	Cu3(SO4)(OH)4													
		Brc	Brochanthite	Cu4(SO4)(OH)6													
	Carbonate	Az	Azurite	Cu3(CO3)2(OH)2													
		Mj	Malaquite	Cu2CO3(OH)2													
	Others	Atc	Atacamite	Cu2Cl(OH)3											○		
		Lam	Lammerite	Cu(AsO4)2													
		Clc	Clinoclase	Cu3(AsO4)(OH)3													
		Chm	Chmevixite	Cu2Fe2(AsO4)2(OH)2·H2O													
		Chr	Chrysocola	Cu2-xSi2O5(OH)3/xH2O													
Fe	Oxide & Hydrooxide	Ht	Hematite	Fe2O3		○	△	△	·				△			·	·
		Mgh	Magheamite	Fe2O3													
		Mt	Magnetite	Fe3O4					·								
		Akg	Akaganeite	FeO(OH)													
		Frx	Feroxyhyite	FeO(OH)													
		Goe	Goethite	FeO(OH)		·											
	Sulphide	Po	Pyrrhotite	Fe7S8													
		Apy	Arsenopyrite	FeAsS													
		Py	Pyrite	FeS2					·	○	○	○	○	○			
	Sulfate	Jar	Jarosite	(K)Fe3(SO4)2(OH)6											○	△	
		Na-Jar	Natrojarosite	(K,Na)Fe3(SO4)2(OH)6												○	·
		Btl	Butlerite	Fe(SO4)(OH)·2H2O													
		Prb	Parabutlerite	Fe(SO4)(OH)·2H2O													
		Krl	Kornelite	Fe(SO4)3·7H2O													
		Rzn	Rozenite	Fe(SO4)·4H2O													
		Sdr	Siderotil	Fe(SO4)·5H2O													
	Others	Scr	Scorodite	Fe(AsO4)·2H2O													
		Fml	Ferrimolybdit	Fe2(MoO4)3·nH2O													
		Pck	Pseudobrookite	Fe2(TiO3)O2													
		Prt	Pseudorutile	Fe2(TiO3)O9													
Silicate	Silica	Qz	Quartz	SiO2		◎	◎	◎	◎	◎	○	◎	◎	◎		○	◎
	Clay	Chm	Chamosite	(Fe,Al,Mg)6(Si,Al)4O10(OH)8													
		Chl	Chlorite	(Mg,Fe,Al)12(Fe,Al,Si)8O20(OH)16						△	△		△	○			△
		Dck	Dickite	Al2Si2O5(OH)4			○										
		Kal	Kaolinite	Al2Si2O5(OH)4										△	△		
		Nac	Nacrite	Al2Si2O5(OH)4													
		Hal	Halloysite	Al2Si2O5(OH)4·2H2O		·					·						
		Pyr-Tc	Pyrophyllite-Talc	Al·MgSi4O10(OH)2													
		Mus	Muscovite	K·Al2(Si3Al)O10(OH,F)2						△			○				○
		Ilt	Illite	K·Al2(Si3Al)O10(OH,F)2												·	
		Mnt	Montmorillonite	Na0.3(Al,Mg)2Si4O10(OH)2·xH2O				·		·							
	Others	Olg	Oligoclase	(Na,Ca)(Al,Si)4O8													
		Ab	Albite	(Na,Ca)(Al,Si)4O8					△	◎	◎	○	△	◎		◎	◎
		Or	Orthoclase	(K,Na)(Al,Si)4O8			△	△	△	○				△			△
		Mic	Microcline	KAlSi3O8		△											
		Hb	Hornblende	(Na,K)Ca2(Fe,Mg)5(Al,Si)8O22(OH)2													
		Di	Diposide	CaMg(SiO3)2												·	
		Trm	Tremolite	Ca2(Mg)5Si8O22(OH)2													
		Act	Actinolite	Ca2(Mg,Fe)5Si8O22(OH)2													
		Rie	Riebeckite	(Na,Ca)2(Mg,Fe)5Si8O22(OH)2													
		Bt	Biotite	K(Mg,Fe)2AlSi3O10(OH)2					·							·	
		Ep	Epidote	Ca2(Al,Fe)3Si3O12(OH)													
	Zeolite	Hap	Hydroxyapophyllite	KCa4Si8O20(OH)·8H2O													
		Gz	Gismondite	CaAl2Si2O8·4H2O													
		Mrd	Mordenite	(Ca,Na2,K2)Al2Si10O24·7H2O													
Sulfate		Alu	Alunite	(K)Al3(SO4)2(OH)6			○										
		Na-Alu	Natroalunite	(K,Na)Al3(SO4)2(OH)6		○											
		Btl	Butlerite	Fe(OH)SO4·2H2O													
		Bld	Bloedite	Na2Mg(SO4)2·H2O													
		Gl	Glauberite	Na2Ca(SO4)2													
		Bas	Bassanite	Ca(SO4)0.5H2O													
		Anh	Anhydrite	Ca(SO4)			·		△		△	○	○	○	◎		△
		Gyp	Gypsum	Ca(SO4)·2H2O		·		△	○			△	△				
Mn		Pr	Pyrolusite	MnO2													
		Br	Braunite	Mn7SiO12													
		Crp	Cryptomelane	K·Mn8O16													
		Gro	Groutite	MnO(OH)													
Carbonate		Cal	Calcite	CaCO3													
		Dol	Dolmite	CaMg(CO3)2													
		Kut	Kutnohorite	Ca(Mn,Mn)(CO3)2													

Abundance: ◎ : abundant ○ : common △ : minor · : rare

TableII-1-8 Results of the powder X-ray diffraction (3)

Clasification		Abbr.	Mineral Name	Chemical Formulas	No.	33	34	35	36	37	38	39	40	41	42	43	44	45	46	47	48
					Drill hol Depth(m)	29.5	64.6	150.0	189.0	234.0	293.0	10.7	49.0	72.4	158.1	192.5	205.1	232.0	245.8	266.5	300.0
						MJCV-10						MJCV-11									
Cu	Sulphide	Tet	Tetrahedrite	Cu12Sb4S13																·	
		Cc	Chalcosine	Cu2S																	
		Djr	Djurleite	Cu31S16																	
		Ens	Enargite	Cu3AsS4																	
		Cv	Coveline	CuS																	
		Cp	Chalcopyrite	CuFeS2														·		△	
	Metal	Cu°	Native copper	Cu																	
	Sulfate	Cln	Chalcanthite	Cu(SO4)·5H2O										·							
		Ant	Antrelite	Cu3(SO4)(OH)4																	
		Brc	Brochanthite	Cu4(SO4)(OH)6												·					
	Carbonate	Az	Azurite	Cu3(CO3)2(OH)2																	
		Mg	Malaquite	Cu2CO3(OH)2																	
	Others	Atc	Atacamite	Cu2Cl(OH)3																	
		Lam	Lammerite	Cu(AsO4)2																	
		Clc	Clinoclase	Cu3(AsO4)(OH)3																	
		Chn	Chnevixite	Cu2Fe2(AsO4)2(OH)2·H2O																	
		Chr	Chrysocola	Cu2-xSi2O5(OH)3/xH2O																	
Fe	Oxide & Hydrooxide	Ht	Hematite	Fe2O3					△								○	·	·		
		Mgh	Maghemite	Fe2O3												·	·				
		Mt	Magnetite	Fe3O4												·					
		Akg	Akaganeite	FeO(OH)																	
		Frx	Feroxyhyite	FeO(OH)											△						
		Goe	Goethite	FeO(OH)												·					
	Sulphide	Po	Pyrrhotite	Fe7S8																	
		Apy	Arsenopyrite	FeAsS																	
		Py	Pyrite	FeS2			○	○	○	○	○								△	○	○
	Sulfate	Jar	Jarosite	(K)Fe3(SO4)2(OH)6													△				
		Na-Jar	Natrojarosite	(K,Na)Fe3(SO4)2(OH)6								△	△	△	△	△					△
		Btl	Butlerite	Fe(SO4)(OH)·2H2O																	
		Prb	Parabutlerite	Fe(SO4)(OH)·2H2O																	
		Ccl	Kornelite	Fe(SO4)3·7H2O																	
		Rzn	Rozenite	Fe(SO4)·4H2O																	
		Sdr	Siderotil	Fe(SO4)·5H2O																	
	Others	Scr	Scorodite	Fe(AsO4)·2H2O																	
		Fml	Ferrimolybdit	Fe2(MoO4)3·nH2O																	
		Pbk	Pseudobrookite	Fe2(TiO3)O2																	
		Prt	Pseudorutile	Fe2(TiO3)O9																	
Silicate	Silica	Qz	Quartz	SiO2		◎	◎	◎	◎	◎	◎	◎	◎	◎	◎	◎	◎	◎	◎	◎	◎
	Clay	Cha	Chamosite	(Fe,Al,Mg)6(Si,Al)4O10(OH)8													○	△			
		Chl	Chlorite	(Mg,Fe,Al)12(Fe,Al,Si)8O20(OH)16					△		△										
		Dck	Dickite	Al2Si2O5(OH)4																	
		Kal	Kaolinite	Al2Si2O5(OH)4		○															
		Nac	Nacrite	Al2Si2O5(OH)4																	
		Hal	Halloysite	Al2Si2O5(OH)4·2H2O																	
		Pyr-Tc	Pyrophyllite-Talc	Al-MgSi4O10(OH)2		△															
		Mus	Muscovite	K-Al2(Si3Al)O10(OH,F)2		△	△	△		△	○			·		○		△	○		·
		Ilt	Illite	K-Al2(Si3Al)O10(OH,F)2																	
		Mnt	Montmorillonite	Na0.3(Al,Mg)2Si4O10(OH)2·xH2O								△									
	Others	Olg	Oligoclase	(Na,Ca)(Al,Si)4O8																	
		Ab	Albite	(Na,Ca)(Al,Si)4O8			◎	◎	◎	◎	◎	○	◎	◎	○	◎	◎	◎	◎	◎	◎
		Or	Orthoclase	(K,Na)(Al,Si)4O8	·	△				△	○	○		○	○		·	·	·	·	○
		Mic	Microcline	KAlSi3O8																	
		Ho	Hornblende	(Na,K)Ca2(Fe,Mg)5(Al,Si)8O22(OH)2																	
		Di	Diposide	CaMg(SiO3)2				·	·	·	·	·						·	·		·
		Trm	Tremolite	Ca2(Mg)5Si8O22(OH)2																	
		Act	Actinolite	Ca2(Mg,Fe)5Si8O22(OH)2																	
		Rie	Riebeckite	(Na,Ca)2(Mg,Fe)5Si8O22(OH)2																	
		Bt	Biotite	K(Mg,Fe)2Al(Si3O10(OH)2					△	△											
		Ep	Epidote	Ca2(Al,Fe)3Si3O12(OH)													△				
	Zeolite	Hap	Hydroxyapophyllite	KCa4Si8O20(OH)·8H2O																	
		Gz	Gismondite	CaAl2Si2O8·4H2O																	
		Mrd	Mordenite	(Ca,Na2,K2)Al2Si10O24·7H2O																	
Sulfate		Alu	Alunite	(K)Al3(SO4)2(OH)6										·							
		Na-Alu	Natroalunite	(K,Na)Al3(SO4)2(OH)6		○						△	○	△							
		Btl	Butlerite	Fe(OH)SO4·2H2O																	
		Bld	Bloedite	Na2Mg(SO4)2·4H2O																	
		Gl	Glauberite	Na2Ca(SO4)2																	
		Bas	Bassanite	Ca(SO4)0.5H2O														·		△	
		Anh	Anhydrite	Ca(SO4)						△		◎		○					○		·
		Gyp	Gypsum	Ca(SO4)·2H2O			·			○			·		△	·	○	△	△		
Mn		Pr	Pyrolusite	MnO2																	
		Br	Braunite	Mn7SiO12																	
		Crp	Cryptomelane	K-Mn8O16																	
		Gro	Groutite	MnO(OH)																	
Carbonate		Cal	Calcite	CaCO3								○								◎	
		Dol	Dolmite	CaMg(CO3)2																	
		Kut	Kutnohorite	Ca(Mg,Mn)(CO3)2																	

Abundance: ◎ : abundant ○ : common △ : minor · : rare

TableII--1--8 Results of the powder X-ray diffraction (4)

Clasification		Abbr.	Mineral Name	Chemical Formulas	No.	49	50	51	52	53	54	55	56	57	58	59	60	61	62	63	64	65	66	67	68	69	70	71
					Drill hol Depth (m)	8.0	14.5	35.0	48.0	72.0	89.4	101.4	129.0	145.5	194.5	4.5	12.0	13.0	78.5	79.0	104.8	137.1	141.0	142.1	200.2	205.0	230.6	250.5
						MuCV-12										MuCV-13												
Cu	Sulphide	Tet	Tetrahedrite	$Cu_{12}Sb_4S_{13}$																								
		Cc	Chalcosine	Cu_2S				·			·	·	·	·														
		Djr	Djurleite	$Cu_{31}S_{16}$																								
		Ena	Enargite	Cu_3AsS_4																								
		Cv	Coveline	CuS							·	·																
		Cp	Chalcopyrite	$CuFeS_2$				·						△											△		·	·
	Metal	Cu*	Native copper	Cu															△	◎	·	◎		·		·	·
	Sulfate	Cln	Chalcanthite	$Cu(SO_4)\cdot 5H_2O$						△	△	△		·														
		Ant	Antrelite	$Cu_3(SO_4)(OH)_4$																				·				
		Brc	Brochanthite	$Cu_4(SO_4)(OH)_6$			△	△					·				·		·					·				
	Carbonate	Az	Azurite	$Cu_3(CO_3)_2(OH)_2$																		·						
		Mg	Malaquite	$Cu_2CO_3(OH)_2$		·																						
	Others	Atc	Atacamite	$Cu_2Cl(OH)_3$												△	·	○										
		Lam	Lammerite	$Cu_3(AsO_4)_2$																								
		Clc	Clinoclase	$Cu_3(AsO_4)(OH)_3$																								
		Chn	Chenevixite	$Cu_2Fe_2(AsO_4)_2(OH)_2\cdot H_2O$																								
		Chr	Chrysocola	$Cu_{2-x}Si_2O_5(OH)_3/xH_2O$																								
Fe	Oxide & Hydrooxide	Ht	Hematite	Fe_2O_3				◎	○	○	·	·				△	·	·	·	◎	·	◎	○	○		◎	·	○
		Mgh	Maghemite	Fe_2O_3		·	△										·			·				·		◎		
		Mt	Magnetite	Fe_3O_4				△								·				○								
		Ahg	Akaganeite	$FeO(OH)$																								
		Frx	Feroxyhyite	$FeO(OH)$																								
		Goe	Goethite	$FeO(OH)$																								
	Sulphide	Po	Pyrrhotite	Fe_7S_8																								
		Apy	Arsenopyrite	FeAsS																								
		Py	Pyrite	FeS_2										·														
	Sulfate	Jar	Jarosite	$(K)Fe_3(SO_4)_2(OH)_6$			·										·							·				
		Na-Jar	Natrojarosite	$(K,Na)Fe_3(SO_4)_2(OH)_6$			·																					
		Btl	Butlerite	$Fe(SO_4)(OH)\cdot 2H_2O$																								
		Prb	Parabutlerite	$Fe(SO_4)(OH)\cdot 2H_2O$																								
		Crl	Kornelite	$Fe_2(SO_4)_3\cdot 7H_2O$																								
		Rzn	Rozenite	$Fe(SO_4)\cdot 4H_2O$																								
		Sdr	Siderotil	$Fe(SO_4)\cdot 5H_2O$																								
	Others	Scr	Scorodite	$Fe(AsO_4)\cdot 2H_2O$																								
		Fml	Ferrimolybdit	$Fe_2(MoO_4)_3\cdot nH_2O$																								
		Psb	Pseudobrookite	$Fe_2(TiO_3)O_2$																								
		Prt	Pseudorutile	$Fe_2(TiO_3)O_9$																								
Silicate	Silica	Qz	Quartz	SiO_2		○	○	◎	△	·		△		△		◎	◎	◎	◎		◎	◎	◎	◎	◎	△	○	◎
	Clay	Chm	Chamosite	$(Fe,Al,Mg)_6(Si,Al)_4O_{10}(OH)_8$																				△	○			
		Chl	Chlorite	$(Mg,Fe,Al)_{12}(Fe,Al,Si)_8O_{20}(OH)_{16}$				·	○	○	◎	○		◎						·	△	△	△			○	◎	○
		Dck	Dickite	$Al_2Si_2O_5(OH)_4$																								
		Kal	Kaolinite	$Al_2Si_2O_5(OH)_4$			△														△							
		Nac	Nacrite	$Al_2Si_2O_5(OH)_4$																								
		Hal	Halloysite	$Al_2Si_2O_5(OH)_4\cdot 2H_2O$																								
		Pyr-Tc	Pyrophyllite-Talc	$Al\text{-}MgSi_4O_{10}(OH)_2$																								
		Mus	Muscovite	$K\text{-}Al_2(Si_3Al)O_{10}(OH,F)_2$												○	·	△		○		·	·					
		Ilt	Illite	$K\text{-}Al_2(Si_3Al)O_{10}(OH,F)_2$																								
		Mnt	Montmorillonite	$Na_{0.3}(Al,Mg)_2Si_4O_{10}(OH)_2\cdot xH_2O$																								
	Others	Olg	Oligoclase	$(Na,Ca)(Al,Si)_4O_8$																								
		Ab	Albite	$(Na,Ca)(Al,Si)_4O_8$		◎		◎	◎	◎				◎		○	○	○	◎	◎	○	◎	◎	◎	◎	◎	◎	◎
		Or	Orthoclase	$(K,Na)(Al,Si)_4O_8$			△									△	·		△		·			·	·		△
		Mic	Microcline	$KAlSi_3O_8$		○				○	△	·	△													△		
		Ho	Hornblende	$(Na,K)Ca_2(Fe,Mg)_5(Al,Si)_8O_{22}(OH)_2$																								·
		Di	Diposide	$CaMg(SiO_3)_2$																								
		Trm	Tremolite	$Ca_2(Mg)_5Si_8O_{22}(OH)_2$		△			○															△	△			
		Act	Actinolite	$Ca_2(Mg,Fe)_5Si_8O_{22}(OH)_2$			·					·			○													
		Rie	Riebeckite	$(Na,Ca)_2(Mg,Fe)_5Si_8O_{22}(OH)_2$											◎													
		Bt	Biotite	$K(Mg,Fe)_2AlSi_3O_{10}(OH)_2$															○		○			△	△		△
		Ep	Epidote	$Ca_2(Al,Fe)_3Si_3O_{12}(OH)$		△					△	◎		○														
	Zeolite	Hap	Hydroxyapophyllite	$KCa_4Si_8O_{20}(OH)\cdot 8H_2O$																								
		Gz	Gismondite	$CaAl_2Si_2O_8\cdot 4H_2O$																								
		Mrd	Mordenite	$(Ca,Na_2,K_2)Al_2Si_{10}O_{24}\cdot 7H_2O$																								
Sulfate		Alu	Alunite	$(K)Al_3(SO_4)_2(OH)_6$																								
		Na-Alu	Natroalunite	$(K,Na)Al_3(SO_4)_2(OH)_6$																								
		Btl	Butlerite	$Fe(OH)SO_4\cdot 2H_2O$																								
		Bld	Bloedite	$Na_2Mg(SO_4)_2\cdot 4H_2O$																								
		Gl	Glauberite	$Na_2Ca(SO_4)_2$																								
		Bas	Bassanite	$Ca(SO_4)\cdot 0.5H_2O$																								
		Anh	Anhydrite	$Ca(SO_4)$															·		·					△		
		Gyp	Gypsum	$Ca(SO_4)\cdot 2H_2O$									△			◎	○		○		△	·		·	△			·
Mn		Pr	Pyrolusite	MnO_2																								
		Br	Braunite	Mn_7SiO_{12}																								
		Crp	Cryptomelane	$K\text{-}Mn_8O_{16}$																								
		Grg	Groutite	$MnO(OH)$																								
Carbonate		Cal	Calcite	$CaCO_3$		△	◎	·		○	○		·	○		·												
		Dol	Dolmite	$CaMg(CO_3)_2$																								
		Kut	Kutnohorite	$Ca(Mg,Mn)(CO_3)_2$																								

Abundance: ◎ abundant ○ common △ minor · rare

1-4 Considerations

1-4-1 Geology and Mineralizing Alteration

Using the data from the 8 holes, a total of 2,648.5m of boring carried out in this phase, drilling profiles and synthetic columns were drawn up, and these were used to study the connections between geological structure, mineralization and alteration effects.

1. Sierra Overa District

This district is made up of andesitic volcanic rocks with intrusive diorite-andesite porphyry, both of which have undergone intense hydrothermal alteration. The district has fractures running in a N-S and NW-SE direction, and it may be considered that these fractures acted as channels for the porphyry intrusion. In particular, the porphyry stock striking NW-SE and ranging in width from 100 to 200m is exposed on the northwest side of the foot of the Sierra Overa. In this district the surface stratum and along the above-mentioned fractures forms a leached zone 10 to 200 m thick made up of a strongly silicified zone, a quartz-sericitized zone and a siliceous argillized zone with strong concentrations of jarosite and reddish hematite. The lower part of the leached zone is divided into a siliceous argillized zone and a chloritized zone. The chloritized zone shows marked pyrite dissemination, and may be further divided from the top down into a siliceous argillized-chloritized zone, chloritized zone, silicified-chloritized zone and silicified-potassium feldspar-chloritized zone. From the mineral association in these zones, the first three may be considered to correspond to the phillic, and the last one to the potassic, zone of porphyry copper deposit alteration classification by Lowell and Guilbert (1970). In the northwestern hillside of the Sierra Overa, the aphanitic andesite and diorite porphyry are accompanied by mineralization containing copper oxides, native copper, chalcopyrite and small amounts of covelline, chalcocite and bornite. The mineralization relates to the alteration as shown below.

Depth	Cu mineral	Cu ave.	max.	Auppm	Alteration
0- 17m	atacamite/brochanthite	0.55%	1.24%	0.20	siliceous argillized-chloritized
17- 10m	atacamite/brochanthite	0.24	1.12	0.14	chloritized
10- 18m	atacamite/brochanthite	0.34	0.40	0.21	chloritized
18-149m	Cu'·atacamite·azurite	0.23	0.86	0.13	chloritized
149-180m	Cu'·atacamite·azurite	0.18	0.52	0.13	silicified-chloiritized-potash feldspar
180-198m	atacamite·azurite	0.14	0.21	0.09	silicified-chloiritized-potash feldspar
198-250m	chalcopyrite	0.11	0.26	<0.04	silicified-chloiritized-potash feldspar
250-300m	chalcopyrite	0.10	0.55	<0.04	silicified-chloiritized-potash feldspar

In the phillic zone 0-149m the T.Cu grade is >0.2% and the Au grade >0.1ppm, but below 149 m in the potassic zone the mineralization of both copper and gold tends to weaken. Native copper disseminate and film between 78-180.0m, and under microscopy small amounts of chalcopyrite and bornite are observable with native copper. In addition to the above-mentioned copper minerals, hematite and magnetite also occur throughout the hole. In places where native copper occurs hematite has not completely replaced magnetite, and the both associate together. In places where copper oxides are abundant, the replacement of magnetite by hematite is more advanced. From this, and from the stability relations of copper and iron compounds shown in Fig.II-1-4, native copper appears to have been formed as a secondary effect in an relative low Eh-high Ph environment in which there was no *soluble oxygen* when the primary copper sulfide minerals were resolved and dissolved; and that later, with the advance to an oxidizing environment copper oxides have been formed together with hematite and jarosite. If the environment had a somewhat lower Ph than that in which native copper has been formed, it is possible that covelline and chalcocite would be formed as secondary minerals.

As is shown in Fig.II-1-5, by MJCV-6 chalcopyrite dissemination was found in the potassic zone of the east of the Sierra Overa, and by MJCV-9 copper oxides dissemination was found in the leached zone of the north of the Sierra Overa, where the San Juan mine is located. Thus it may be expected that porphyry copper type deposits would be embedded under the leached zone that forms the Sierra Overa, and there is a need to continue further prospecting.

2. Cerro Veraguas District (MJCV-10,MJCV-11)

This area is made up of andesite volcanics with intrusive diorite-andesite porphyry, both of which as in the Sierra Overa district have undergone intense hydrothermal alteration. The district has fractures running in a NE-SW and NW-SE directions, and it may be considered that these fractures acted as channels for the porphyry intrusion. In the east of the Cerro Veraguas, the mineralization made up of covelline and chalcocite in width 2m, has been found in the porphyry assumed to have intruded controlled by the NW-SE fracture. Thus it may be expected that small porphyry copper type deposits would be embedded in the eastern part of the Cerro Veraguas. However, in the district from the center to the west of the Cerro Veraguas, although drilling in the first year and this year revealed some mineralization in the range of 0.7% to 0.2%, the poor continuity suggests that widespread mineralization is not to be expected.

3. Pampa District: the Plain east of the Cerro Veraguas (MJCV-12)

Quartz diorite stock, which NW-SE lineation is developed, is distributed over a range 2 x 2km. Copper oxide and chalcopyrite disseminate and film, accompanying hematite, chlorite, epidote, quartz and calcite in the quartz diorite. As shown in Fig.II-1-6, the mineralized zone is thought to be stockwork deposits controlled by the NW-SE structure.

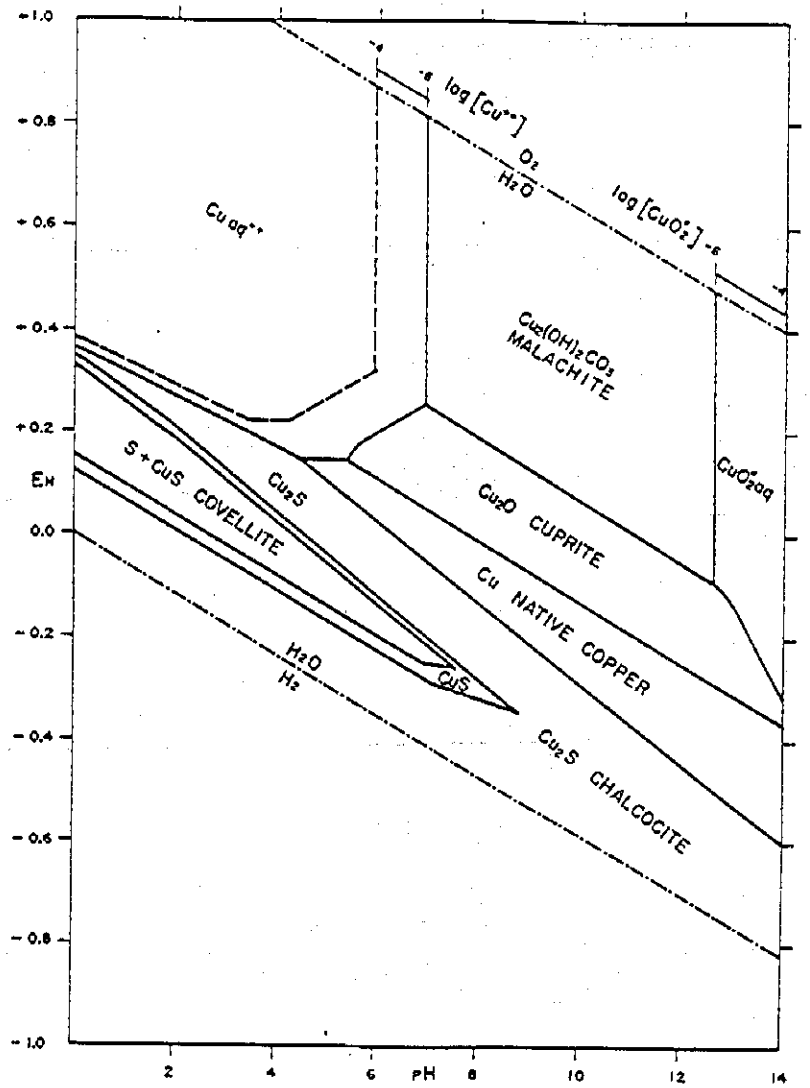

FIG. 7.27b. Stability relations among some copper compounds in the system $Cu-H_2O-O_2-S-CO_2$ at 25 °C and 1 atmosphere total pressure. $P_{CO_2} = 10^{-3.5}$, total dissolved sulfur species $= 10^{-1}$. [Courtesy J. Anderson.]

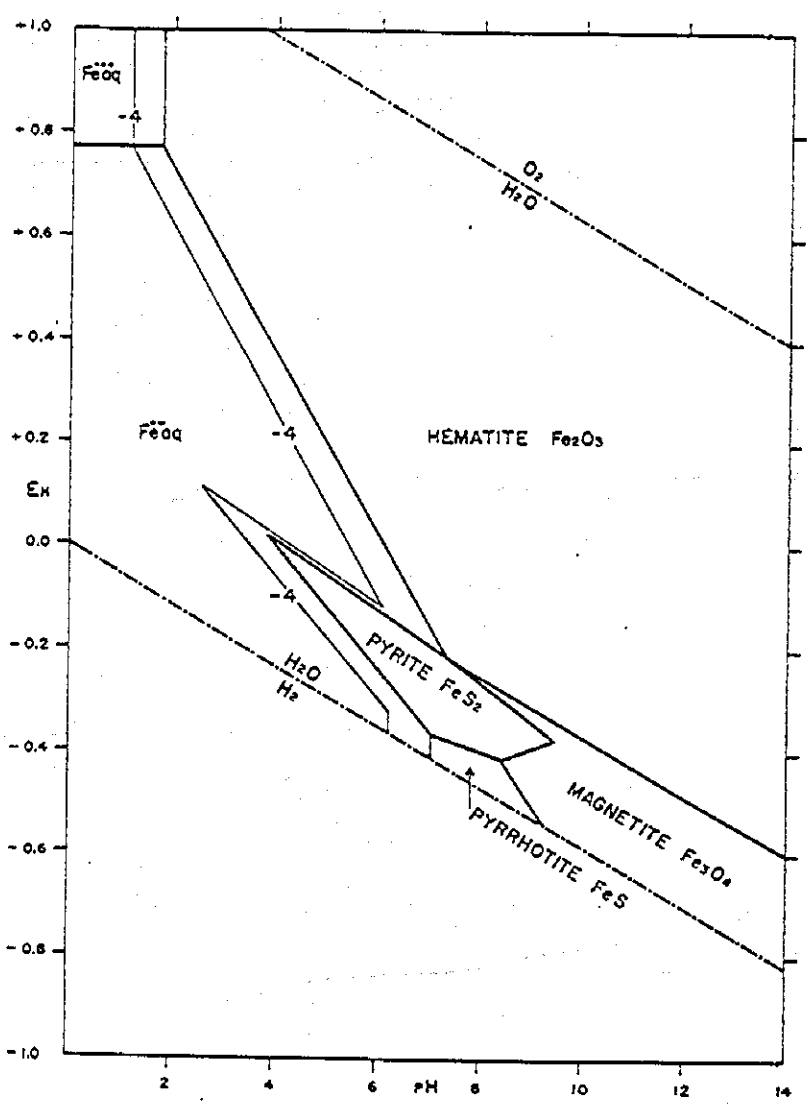

FIG. 7.20. Stability relations of iron oxides and sulfides in water at 25 °C and 1 atmosphere total pressure, when $\Sigma S = 10^{-6}$. Note shrinkage of sulfide boundaries and appearance of FeS as a stable phase at intermediate pH under strongly reducing conditions, as well as marked increase in the area of "acid solubility" over a wide range of Eh.

Fig.II—1—4 Stablity relations of copper and iron compounds [Garrels and Chirist,1965]

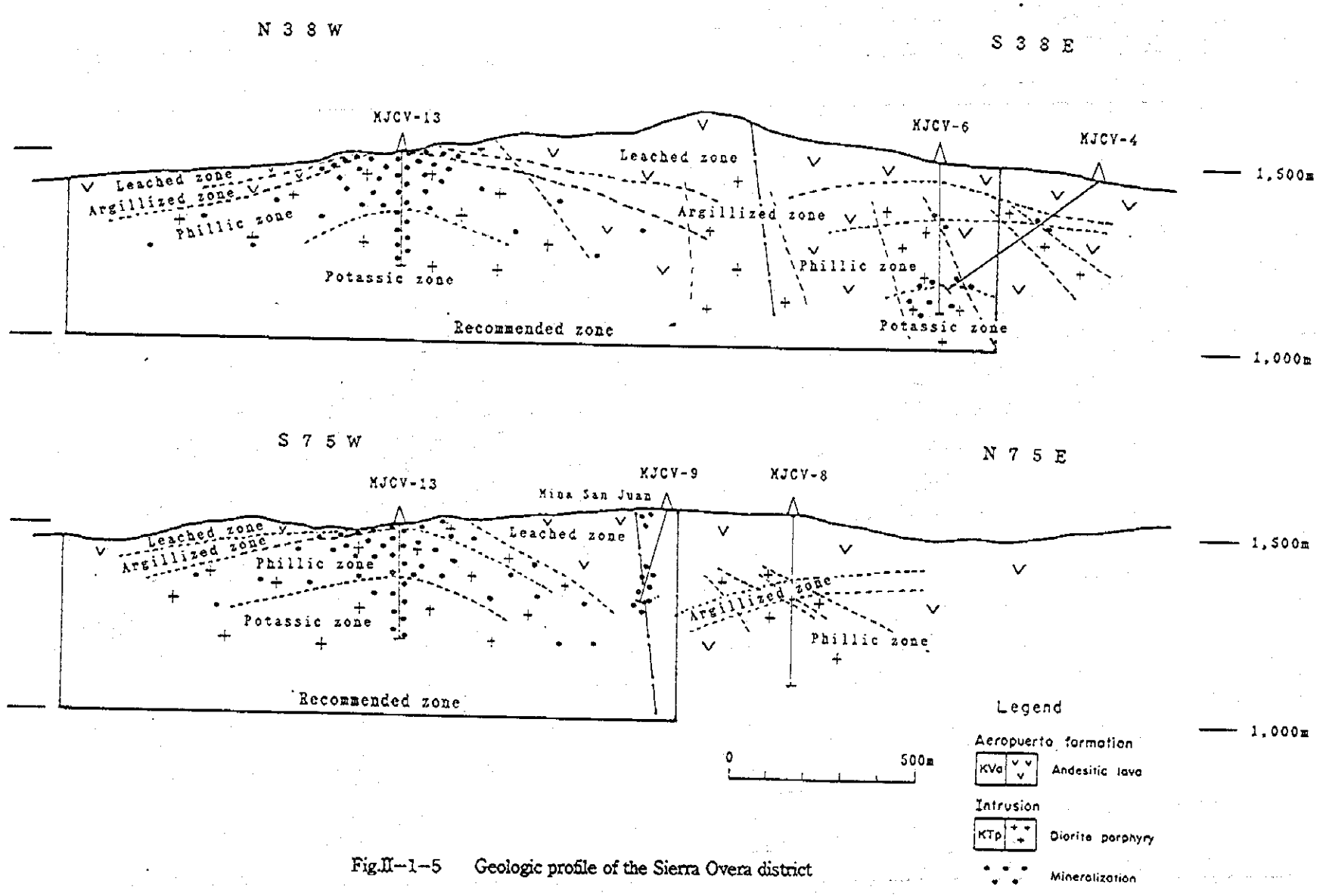

Fig.II-1-5 Geologic profile of the Sierra Overa district

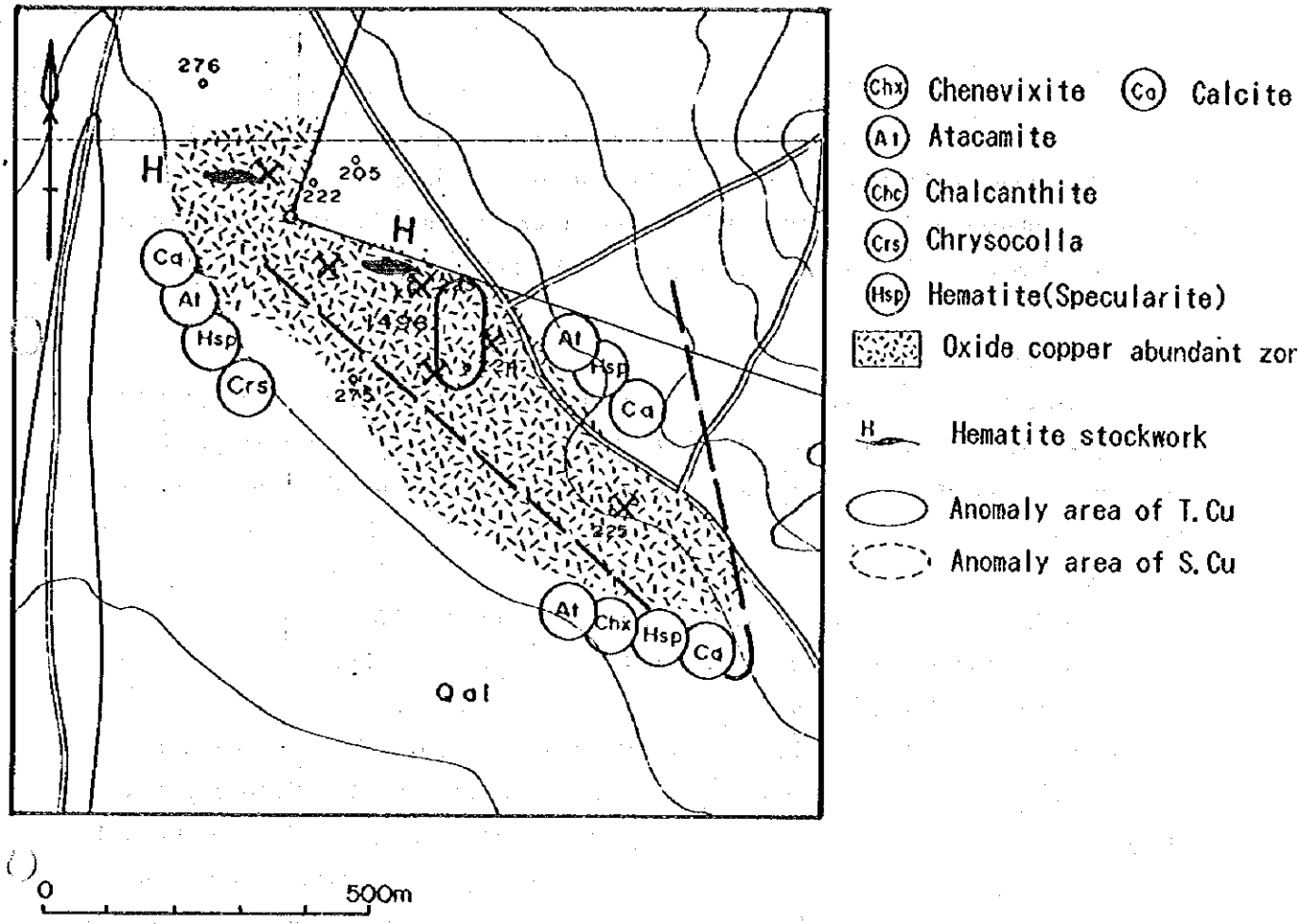

Fig.II-1-6 Geology of the Pampa district

The one or two kilometers between the Cerro Veraguas and the Pampa district are covered by alluviums and colluviums, and the border between the stock and the andesite volcanics of the Aeropuerto formation is not distinct. And the genetic relationship between the mineralization and the porphyry copper type mineralization is not apparent. These points should be further surveyed.

1-4-2 K-Ar Dating

K-Ar Dating was carried out on three core samples. As shown in Table I-1-9, the samples are of diorite porphyry and quartz diorite that had undergone hydrothermal alteration accompaning copper minerlization. It is thought that the K-Ar ages indicate the period in which the mineralization alteration occurred.

The results are as follows;

Diorite porphyry(Sierra Overa east district)	: 104.0±+2.0Ma
Diorite porphyry(Sierra Overa northwest district)	: 115.0±+4.0Ma
Quartz diorite(Pampa District)	: 93.8±+2.1Ma

1. K-Ar ages indicate them to be Cretaceous in age. The diorite porphyry of the Sierra Overa district has undergone either phillic and potassic alteration, which displays the alteration pattern of porphyry copper deposits, while the quartz diorite of the Pampa district is characterized by chlorite, epidote and calcite, which displays the typical alteration of vein and stockwork type deposits found widely in the coastal cordillera ; but there is little difference in the period in which both underwent mineralizing alteration.

2. Since the K-Ar ages of the Grupo Plutonico Cerro del Pingo,which have a wide distribution over the coastal cordillera, indicate 109-121Ma (Naronjo et. al., 1984), the period of the mineralizing alteration corresponds roughly to that of the activity of the granitic magma.

3. The K-Ar ages of the porphyry copper deposits embedding along the Domeyko Cordillera in northern Chile indicate 30-40Ma (Olson,1989), as shown in Fig.II-1-7.

Although the alteration pattern in the Sierra Overa district is similar to that of the porphyry copper deposits, the period in which the alteration has been formed differs from that of the porphyry copper deposits of the Domeyko Cordillera.

1-4-3 Microprobe Quantitative Analysis

Microprobe analyses of the native copper grains or films have been made on the TN-5400 of Tracer Northern attached to the JXA-733 of JEOL at 20kv with an effective specimen current of 2.50×10^{-10}A. Take off angle is 40, beam diameter 0.0001mm, counting time 100s. The standards are Cu, Fe, Au, Ag and Ni metals. The apparent concentration was on line ZAF corrected, and normalized to the total=100%.

As shown in Table II-1-10, the samples are the native copper grains or films from the native copper

Table II-1-9 Results of the K-Ar dating

Sample Locality	Rock Type	Alteration / Mineralization	POTASSIUM (K wt%)	Rad.40Ar (10-8cc/g)	K-Ar AGE (Ma)	AIR CONT. (%)	Average of K-Ar Age (Ma)
Sierra overa east district							
MJCV-6 342.0-342.5m	diorite porphyry	qz-kf-ch / py-cp dis. T.Cu 1430 ppm, S.Cu 24 ppm, Au <0.04 ppm, Ag 0.6 ppm, Mo 18 ppm	3.78±0.08	1583±17 1549±17	105±2.0 103±2.0	3.9 4.1	104±2.0
Sierra overa northwest district							
MJCV-13 143.5-144.0m	diorite porphyry	ch-qz-ab-bt-se-gp cu°-mt-hm T.Cu 3000 ppm, S.Cu 610 ppm, Au 0.04 ppm, Ag <0.4 ppm, Mo 96 ppm	1.15±0.03	536±12	117±4	48.8	115±4
Pampa district							
MJCV-12 145.0-145.5m	quartz diorite	ch-ep-qz-ab-cal py-cp-hm-ge T.Cu 3890 ppm, S.Cu 210 ppm, Au <0.04 ppm, Ag <0.4 ppm, Mo 5 ppm	7.92±0.16	2983±32 2936±32	94.5±2.1 93.1±2.1	4.3 4.4	93.8±2.1

* Dating was done on bulk samples by Mitsubishi Material Co.,Ltd. Central Laboratory.
* Decay Constant(after Steiger and Jaeger,1977):

$$\lambda e = 0.581 \times 10^{-10}/yr$$

$$\lambda \beta = 4.962 \times 10^{-10}/yr$$

* ^{40}K content in K : $^{40}K/K = 0.01167$ atom %
* Error estimation was done after Nagao et al.(1984)
* Mineral names qz:quartz kf:k-feldspar ab:albite se:sericite bt:biotite ch:chlorite ep:epidote cal:calcite gp:gypsum
  py:pyrite cp:chalcopyrite cu°:native copper mt:magnetite hm:hematite ge:geothite

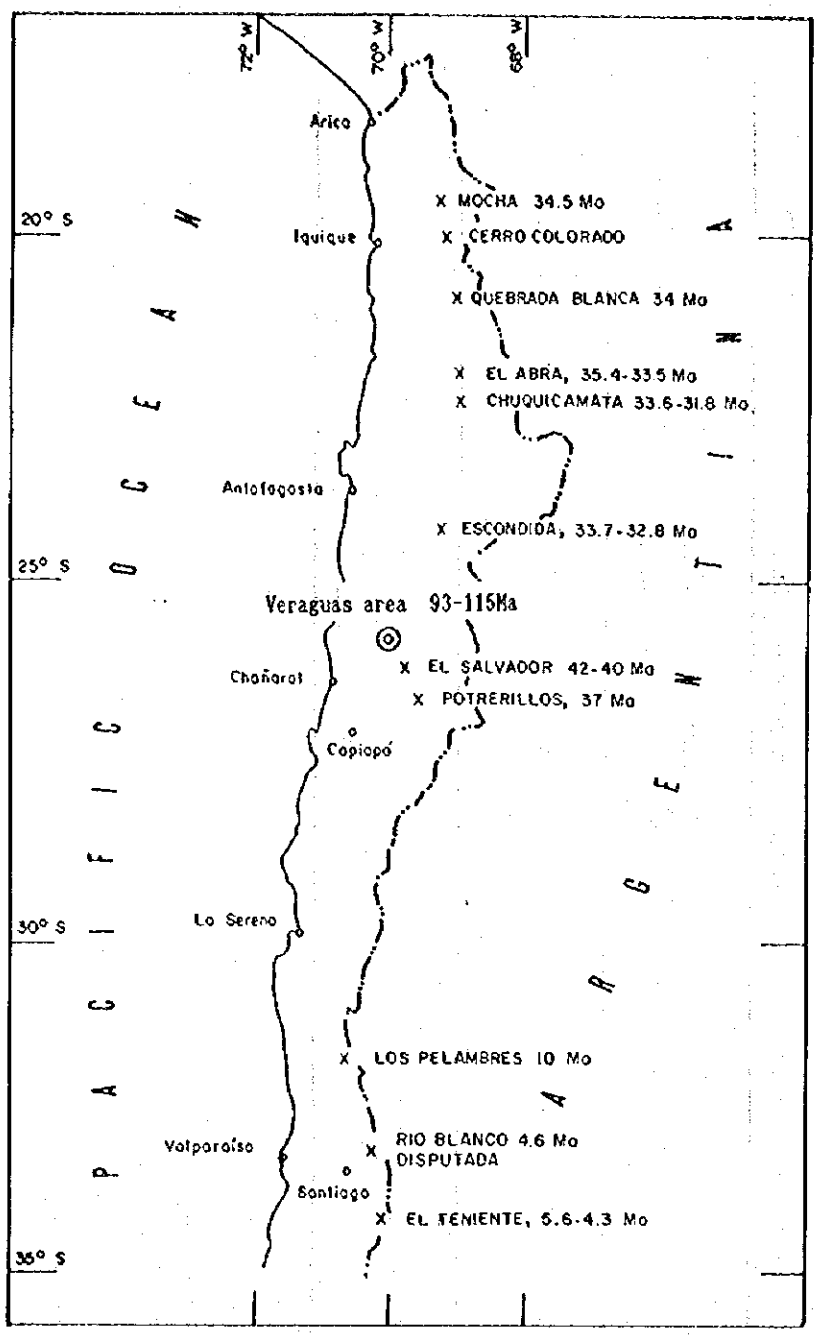

Fig.II-1-7 Location and K-Ar ages of major porphyry copper deposits in northern Chile. Ages of porphyry copper deposits from Quirt *et al.* (1971; Mocha, Los Pelambres, Río Blanco, and El Teniente), Gustafson and Hunt (1975; El Salvador), Olson (1984; Potrerillos), Internal report, CODELCO-Chile, División Chuquicamata (no date: Chuquicamata), Ambrus (1977; El Abra), C. Alpers and G. Brimhall (written commun.; Escondida), and Hunt *et al.* (1983; Quebrada Blanca).

[Olson, 1989]

TableII-1-10 Microprobe analyses of native copper

	13-78.4m	13-78.4m	13-78.4m	13-126.6m	13-126.6m	13-126.6m
WT.%						
Cu	100.74	100.58	100.36	100.31	98.77	100.65
Fe	0.00	0.00	0.00	0.66	0.69	0.36
Au	0.00	0.00	0.00	0.00	0.00	0.00
Ag	0.00	0.00	0.00	0.36	0.00	0.00
Total	100.74	100.58	100.36	101.32	99.46	101.01
ATM.%						
Cu	100.00	100.00	100.00	99.05	99.21	99.59
Fe	0.00	0.00	0.00	0.74	0.79	0.41
Au	0.00	0.00	0.00	0.00	0.00	0.00
Ag	0.00	0.00	0.00	0.21	0.00	0.00
	13-134.1m	13-134.1m	13-134.1m	13-147.0m	13-147.0m	13-147.0m
WT.%						
Cu	99.31	100.47	100.81	98.63	99.52	99.82
Fe	0.00	0.08	0.00	0.11	0.00	0.33
Au	0.00	0.00	0.00	0.00	0.00	0.00
Ag	0.40	0.00	0.00	0.00	0.00	0.00
Total	99.71	100.55	100.81	98.74	99.52	100.15
ATM.%						
Cu	99.76	99.91	100.00	99.87	100.00	99.62
Fe	0.00	0.09	0.00	0.13	0.00	0.38
Au	0.00	0.00	0.00	0.00	0.00	0.00
Ag	0.24	0.00	0.00	0.00	0.00	0.00
	13-152.0m	13-152.0m	13-152.0m			
WT.%						
Cu	98.84	100.56	99.38			
Fe	0.33	0.30	0.88			
Au	0.00	0.00	0.00			
Ag	0.00	0.00	0.00			
Total	99.18	100.86	100.26			
ATM.%						
Cu	99.62	99.66	99.00			
Fe	0.38	0.34	1.00			
Au	0.00	0.00	0.00			
Ag	0.00	0.00	0.00			

dissemination zone between 78-180m in MJCV-13 at the five places,78.4m,126.6m, 134.1m, 147.0m, 152.0m, at which microscopic observation was carried out.

The results are as follows:

1.All native copper grains or films have a Cu content of 98atm% or higher, and the native copper at 78.4m in particular had a Cu content of 100%.

2. Impurities included <1.0atm% of Fe and <0.2atm% of Ag.

1-4-4 Resistivity and Polarizability Measurement

Resistivity and polarizability were measured on a total of 59 cores, 33 samples taken in Phase 1 of the drilling survey, and 26 samples taken in Phase 2. Lengths of core about 10cm long were split in half with a cutter to form semicylindrical samples. These were submerged in distilled water for one week, drained for one hour and then submerged in distilled water for one more week before being measured. A Phoenix Geophysics Limited IP and Resistivity Core Tester CT-1 was used for the measuring. Because of the special qualities of the measuring equipment, frequencies of 0.3Hz and 0.5Hz were used to measure the polarizability.

The results, together with the mode of production and chemical analysis values, are shown in Fig.I-1-11.

Samples were classified into the following 5 types, on the basis of the differences in alteration and original rock.

Alteration zone	Original rock	RES(Ω)			PFE(%)			T.Cu(ppm)			S.Cu(ppm)		
		Max.	Min.	Ave.	Max.	Min.	Ave.	Max.	Min.	Ave.	Max.	Min.	Ave.
1. silicified zone	andesite	1,402	131	828	0.4	0.2	0.3	80	5	22	<10	<10	<10
2. siliceous argillized zone	andesite	1,950	27	300	16.0	0.2	2.5	616	5	126	138	<10	18
3. siliceous argillized zone	andesite	439	30	118	8.8	0.4	2.5	8,600	10	1,038	6,100	<10	622
4. chloritized zone	porphyrite	2,809	1	617	17.5	2.5	9.0	13,800	28	2,381	3,850	<10	644
5. chloritized zone	porphyrite/diorite	5,892	1	1,243	24.0	2.0	7.2	7,000	23	1,387	2,340	<10	500

The following tendencies may be observed between resistivity/polarizability and alteration/original rock/copper grades.

Resistivity

1. Resistivity The fact that the strongly silicified zone gives an average resistivity value of 828 ohm/m, higher than the resistivity value for the siliceous argillized zone, indicates that the area of high resistivity at the surface measured by CSAMT corresponds to the strongly silicified zone.

2. Sulphide minerals such as pyrite generally give a low resistivity value. However, as shown above the siliceous argillized zone has a lower resistivity value than the chlorite zone accompanied by pyrite dissemination.

3. Pyrite dissemination is most marked in the chlorite zone with porphyry/diorite as the original rock, and the resistivity value is the highest with an average value of 1,243ohm/m.

Chlorite zones with original rock of porphyry/diorite display medium to high resistivity values; the sample from MJCV-12, with copper oxide and chalcopyrite dissemination, gives an average reading of 285ohm/m, while the sample from MJCV-13, with copper oxide and natural copper dissemination, gives an average reading of 2993ohm/m

4. With regard to abave mensioned, it may be considered that the low resistivity values are due to the influence of argillization rather than to pyrite dissemination or copper prospects.

Porlarization

1. The average reading for the strongly silicified zone was 0.3, and for the argillized zone, 2.5: argillization displays a higher value than strong silicification.

2. Differences in original rock were not seen to affect the readings in either the siliceous argillized or chlorite zones.

3. The chloritized zone accompanied by pyrite dissemination displayed the highest values, at 7.2 to 9.0. The average reading of the sample from MJCV-12, with copper oxide and chalcopyrite dissemination, was 4.8, and from MJCV-13,with native copper dissemination, the average reading was 4.3. Thus it may be considered that pyrite dissemination has a greater effect than copper mineralization in showing high polarizability values.

TableII-1-11 Results of the resistivity and polarization measurement

No.	Drill hole	meter	Mineralisation	Alteration		Alteration zone	Original rock	RES(Ωm)	PFE(%)	T.Cu	S.Cu	Mo	Au	Ag	T.Fe
1	MJCV-01	11.7	hs>lm dis	sil wk		silicified zone	andesite	1,402.6	0.2	6	<10	18	<0.04	<0.4	5.63
2	MJCV-01	28.2	hm dis wk	sil>kal				1,388.7	0.3	5	<10	12	<0.04	<0.4	3.30
3	MJCV-03	31.5	hm vwk	sil vwk				196.6	0.4	16	<10	12	<0.04	<0.4	0.70
4	MJCV-04	16.0	hm fla	sil-kal				131.7	0.4	80	<10	10	<0.04	<0.4	2.20
5	MJCV-05	16.2	hm dis	sil wk				1,082.9	0.2	14	<10	6	<0.04	0.4	0.67
6	MJCV-05	138.9	hm-lm crm	sil>kal				765.8	0.3	11	<10	6	<0.04	<0.4	1.10
							average	828.1	0.3	22	<10	11	<0.04	<0.3	
7	MJCV-01	106.0	hm fla	sil<kal		argillized zone	andesite	495.7	0.2	5	<10	<5	<0.04	<0.4	5
8	MJCV-01	316.3	hm - jar wk	kal>chl	phillic zone			67.0	1.2	72	33	7	<0.04	<0.4	7
9	MJCV-02	138.0	hm dis	kal wk				57.5	1.1	174	40	<5	<0.04	<0.4	5
10	MJCV-03	241.0		kal wk				66.7	0.6	67	26	10	<0.04	<0.4	4
11	MJCV-03	361.8	hm wk	kal wk				80.9	0.5	98	<10	26	<0.04	<0.4	2
12	MJCV-04	186.9	hm-lm	kal vwk				44.8	0.8	58	<10	18	<0.04	<0.4	3
13	MJCV-04	322.8	py dis wk	kal-chl	phillic zone			165.7	16.0	42	<10	18	<0.04	<0.4	5
14	MJCV-05	283.6	hm-lm	kal wk				27.0	1.4	816	138	<5	<0.04	<0.4	5
15	MJCV-05	307.8	hm-lm	kal vwk				42.0	1.8	104	<10	<5	<0.04	<0.4	5
16	MJCV-11	49.0		kal wk				1,950.7	2.0	23	<10	4	<0.04	<0.4	
							average	299.8	2.5	126	18	6	<0.04	<0.4	
17	MJCV-01	242.6	py dis wk	kal>chl	phillic zone	argillized zone	diorite porphyry	51.5	4.2	187	<10	6	<0.04	<0.4	3
18	MJCV-02	158.5	py dis	kal>chl	phillic zone			62.3	4.0	190	30	<5	<0.04	<0.4	4
19	MJCV-02	167.5	py dis	kal	phillic zone			30.8	2.8	404	75	<5	<0.04	0.6	5
20	MJCV-02	247.0	hm-jar st	kal st				59.5	0.6	180	25	6	<0.04	<0.4	15
21	MJCV-03	140.9	hm flm wk	kal vwk				34.7	1.8	10	<10	6	<0.04	<0.4	2
22	MJCV-03	203.5	hm-lm dis	kal vwk				71.2	0.6	19	<10	6	<0.04	<0.4	4
23	MJCV-05	319.0	hm jar py	kal>chl st				253.9	0.4	105	30	76	<0.04	<0.4	3
24	MJCV-04	221.6	py dis vwk	kal-chl	phillic zone			68.0	1.0	48	<10	14	<0.04	<0.4	4
25	MJCV-05	350.9	hm dis	kal st				194.6	0.4	60	<10	<5	<0.04	<0.4	4
26	MJCV-05	364.2	py dis st	kal-chl	phillic zone			30.3	8.8	1,620	638	8	<0.04	<0.4	5
27	MJCV-13	12.0	cuoxd-hm	kal				438.8	2.7	M,600	6,100	11	0.70	<0.4	
							average	117.6	2.5	1,038	620	11	0.03	<0.3	
28	MJCV-04	335.4	py dis wk	chl	phillic zone	chloritized zone	andesite	144.6	11.8	36	<10	10	<0.04	<0.4	4
29	MJCV-04	374.2	py dis wk	kf sil chl	potassic zone			588.9	7.5	76	<10	18	<0.04	<0.4	3
30	MJCV-04	406.0	py dis wk	chl	phillic zone			37.2	17.5	154	17	12	<0.04	0.8	8
31	MJCV-06	149.6	py dis m	chl	phillic zone			1.4	7.7	13,800	3,850	19	<0.04	3.8	
32	MJCV-07	55.0	hm dis	chl				123.5	2.5	28	10	4	<0.04	<0.4	
33	MJCV-11	232.0	py dis	chl st	phillic zone			2,808.7	7.2	193	10	11	<0.04	<0.4	
							average	617.4	9.0	2,361	645	12	<0.04	0.5	
34	MJCV-01	266.1	py flm dis	kf kal chl	phillic zone	chloritized zone	diorite porphyry	55.5	3.6	73	18	<5	<0.04	<0.4	5
35	MJCV-03	368.1	py cp	kal-chl st	phillic zone			11.8	12.0	7,000	1,260	24	<0.04	<0.4	7
36	MJCV-03	371.1	py dis	kal-chl st	phillic zone			85.4	4.8	84	24	16	<0.04	<0.4	8
37	MJCV-04	469.2	py dis wk	kf chl	potassic zone			274.4	5.1	294	16	16	<0.04	<0.4	4
38	MJCV-04	485.0		kf chl	potassic zone			414.9	2.0	94	<10	18	<0.04	<0.4	4
39	MJCV-06	250.0	py dis st	chl	phillic zone			186.6	6.3	23	10	9	<0.04	<0.4	
40	MJCV-06	357.9	py>cp dis st	chl	potassic zone			417.9	11.2	1,260	21	32	<0.04	3.2	
41	MJCV-06	369.5	cp dis	chl	potassic zone			868.4	11.8	1,340	25	40	<0.04	<0.4	
42	MJCV-06	394.4	py dis m	chl	potassic zone			612.5	10.7	1,470	20	120	<0.04	<0.4	
43	MJCV-08	215.6	py dis st	kal-chl	phillic zone			104.5	11.2	74	7	15	<0.04	0.4	
44	MJCV-11	246.8	py dis	chl-sil	phillic zone			879.9	12.0	50	10	26	<0.04	0.6	
45	MJCV-11	266.5	py-cv-cc dis	chl-cal-sil	phillic zone			0.7	14.6	124	20	33	<0.04	4.4	
46	MJCV-11	300.0	py dis	chl-sil	phillic zone			336.1	24.0	50	<10	14	<0.04	0.4	
47	MJCV-12	46.2	cuoxd-hm	chl-ep		chloritized zone	quartz diorite	244.3	2.9	550	310	4	<0.04	<0.4	
48	MJCV-12	72.0	cuoxd-hm	chl-ep				231.4	3.6	1,450	1,200	24	0.04	<0.4	
49	MJCV-12	129.0	cuoxd-hm	chl-ep				158.7	4.4	3,500	2,200	25	<0.04	<0.4	
50	MJCV-12	153.0	cp-hm	chl-ep				507.2	8.1	1,240	90	4	<0.04	<0.4	
51	MJCV-13	78.5	ntcu	chl	phillic zone	chloritized zone	diorite porphyry	5,104.9	3.7	2,100	980	18	0.22	1.2	
52	MJCV-13	83.9	cuoxd-hm	chl	phillic zone			5,892.4	3.1	2,900	2,340	40	0.28	<0.4	
53	MJCV-13	104.8	cuoxd-ntcu	chl	phillic zone			5,217.7	2.6	2,700	1,920	54	0.12	<0.4	
54	MJCV-13	142.1	cuoxd-ntcu	chl	phillic zone			1,298.1	3.0	2,600	770	60	0.12	<0.4	
55	MJCV-13	164.7	cuoxd-ntcu	chl	potassic zone			509.8	2.3	1,100	540	19	0.10	<0.4	
56	MJCV-13	200.2	py-cp dis	chl	potassic zone			2,688.1	4.4	1,400	310	23	0.10	<0.4	
57	MJCV-13	209.0	py-cp dis	chl	potassic zone			80.9	9.3	1,200	320	29	0.06	<0.4	
58	MJCV-13	220.6	py-cu oxd-hm	chl	potassic zone			1,495.2	5.1	2,100	260	22	0.06	<0.4	
59	MJCV-13	250.5	ntcu	chl	potassic zone			3,651.4	5.4	1,300	360	17	<0.04	<0.4	
							average	1,243.3	7.2	1,388	501	27	0.02	0.1	

CHAPTER 2 TRENCH SURVEY IN THE VERAGUAS AREA

2-1 Purpose of survey

The purpose of this survey was to ascertain the existence of mineralization corresponding to the Cu geochemical anomalies by the Phase I survey in the northwestern hillside of the Sierra Overa.

2-2 Operating conditions

On-site trench survey work was carried out during the period 1st November 1994 to 31st November 1994. Trenches 5m in width were dug using a bulldozer.

Three lines, each 500m long, were dug, a total of 1,500m.

2-3 Results of survey

The results of the trench survey are shown in Fig.II-2-1. After the trenches were dug, detailed geological survey was carried out. The sketch of the trenches was drawn to a scale of 1,000:1 overall, and 50:1 for areas with mineral prospects. At the time of the trench observation, samples of mineral and rock have been taken where considered necessary, and subjected to polished thin-section observation, powder X-ray diffraction and chemical analysis. The results of these are shown in Table II-2-1, 2 & 3 respectively.

2-3-1 Line 1

This line is located in the geochemical anomalous zone of Phase 1 survey. Throughout the whole length of the line is covered by the leached zone with strong concentrations of pulverized reddish hematite, jarosite and natrojarosite with siliceous argillization. The original rock is a aphanitic andesite that has undergone chloritization, but because of the strong degree of alteration there are many places where the primary texture is indistinct. The T.Cu grade is 0.004-0.021%, and mineralization have not found along this line.

2-3-2 Line 2

A length of 120m on the eastern side is composed of aphanitic andesite that has undergone chloritization. Phenocrysts of plagioclase may be observed in the rock, but the primary mineral has altered into chlorite,secondary quartz, albite, biotite, sericite, epidote, etc. In the surface area, caliche formed of bassanite, zeolite, etc., is developed in network form. Chalcanthite and other copper oxides are found with gypsum film. Observation under the microscope also reveals the sulfide minerals chalcopyrite, bornite and chalcocite as well as the iron oxides magnetite, hematite and goethite. The T.Cu grade is 0.16-

0.53%, with an average of 0.28%.

In the line west of that described above, the aphanitic andesite is covered by a leached zone which, like Line 1, has undergone siliceous argillization having strong concentrations of pulverized reddish hematite, jarosite and natrojarosite. The T.Cu grade here is 0.018-0.11%.

2-3-3 Line 3

This line is made up of aphanitic andesite and medium grained diorite porphyry.

A length of 330m on the eastern side is made up of fine grained andesite that has undergone silicification and siliceous argillization; the T.Cu grade is 0.03-0.25%.

A length 140m on the central is made up of medium grained diorite porphyry that has undergone siliceous argillization and is accompanied by pulverized reddish hematite, jarosite and natrojarosite. The T.Cu grade here is 0.079-0.19%, and small amounts of copper oxides is observable.

A length of approximately 180m on the western side is made up of aphanitic andesite that has undergone chloritization, similar to Sampling Line 2. Phenocrysts of plagioclase may be observed in the rock, but much of the primary minerals have altered into chlorite, secondary quartz, albite, kaolin, sericite etc. In the surface, caliche formed of gypsum, anhydrite gypsum, bassanite, graubelite, zeolite etc., is developed in network form. Chalcanthite and other copper oxides are found throughout the rock, permeating the veins of gypsum. Observation under the microscope also reveals the iron oxides hematite and goethite. The T.Cu grade in the 180m in which the rock is found is 0.051-0.84%, with an average of 0.33%.

2-3-4 Test Pits

Pit survey has been carried out in four places approximately 80-100m southwest of the Line 2. The results are shown Fig.II-2-2. From this spot to the central part of the Line 2 mentioned above, diorite porphyry distributes over a width of 100-200m in a NW-SE direction. The rock is comprised of primary minerals of plagioclase and hornblende which altered to secondary quartz, albite, sericite, biotite, chlorite, epidote, calcite, etc. In the pits, the surface is covered with a caliche formed of quartz, gypsum, anhydrite gypsum, bassanite, albite etc. Below the caliche zone, chalcanthite, atacamite and other copper oxides disseminate and film. Observation under the microscope also reveals chalcocite, magnetite, hematite and goethite. The T.Cu grade in and around the pits is 0.6-3.66%, with an average of 1.91%.

2-3-5 Consolidation of survey results

The survey district is made up of aphanitic andesite of the Cretaceous Aeropuerto formation and intrusive diorite porphyry that have undergone hydrothermal alteration. It is thought that the diorite porphyry is in stock form in a NW-SE direction, across a width of 100-200m. The district may be classi-

fied into three alteration zones, from the top.

(1) Silicified/siliceous argillized zone: The eastern part of the Line 3, on the mountain side of the Sierra Overa.

(2) Leached zone with strong concentrations of pulverized reddish hematite, jarosite and natro-jarosite, accompanying siliceous argillization : The central part of the Line 3, and Lines 1 and 2 at the foot of the Sierra Overa.

(3) Chlorite zone: Western part of the Line 3 and the eastern part of the Line 2.

The aphanitic andesite and diorite porphyry belonging to the chloritized zone are accompanied by film and dissemination of copper oxides such as chalcanthite and atacamite. Observation under the microscope also reveals the sulfides such as chalcopyrite, bornite and chalcocite, and the iron oxides such as magnetite, hematite and goethite.

2-4 Considerations

The survey district is made up of aphanitic andesite of the Cretaceous Aeropuerto formation and diorite porphyry that have undergone hydrothermal alteration. It is thought that the diorite porphyry is in stock form in a NW-SE direction, across a width of 100-200m.

The surface is covered by the leached zone with strong concentrations of jarosite and reddish hematite. In the chloritized zone below the leached zone, copper oxides occur and under the microscope chalcopyrite, bornite and chalcocite are observable. Statistical processing has been carried out using the chemical analysis data from the 64 samples taken in this survey.

The basic statistical values for each element, and the results of the analysis of the principal components, are shown in Table II-2-4. The results of the principal components analysis are as follows:

(1) First principal component: T.Cu, S.Cu, I.Cu, Au display identical behavior.

(2) Second principal component: Mo shows independent behavior.

(3) Third principal component: Au and I.Cu interact.

Judging from the occurrence and the behavior of the components described above, the copper oxides have been formed as secondary minerals after the primary copper sulfide minerals oxidized. It is thought that gold has been a secondary concentration with the same behavior as copper oxide.

It is therefore necessary to continue prospecting, in order to ascertain the spread of the secondary oxidation zone in the environs and the existence of primary mineral deposits in the deeper zone.

Sample No.	T.Cu PPM	S.Cu PPB	Mo PPB	Au PPB	Ag PPB
P1	25200	25000	19	2.50	-0.4
P2	8000	5200	15	0.49	-0.4
P3	36600	35400	16	0.28	-0.4
P4	23000	22600	22	2.00	-0.4
1	590	210	18	0.05	-0.4
2	2500	2060	11	0.05	-0.4
3	190	90	25	-0.04	-0.4
4	30	10	39	-0.04	-0.4
5	1100	610	29	0.04	-0.4
6	3000	270	17	0.07	-0.4
7	790	260	18	0.49	-0.4
8	1100	250	16	-0.04	-0.4
9	1900	850	16	2.30	-0.4
10	2200	1500	21	-0.04	-0.4
11	2500	2200	32	-0.04	-0.4
12	7100	6700	29	-0.04	-0.4
13	2700	2400	24	-0.04	-0.4
14	2200	1800	31	0.07	-0.4
15	4300	3900	28	0.23	-0.4
16	2200	1830	22	0.05	-0.4
17	3900	3800	20	0.23	-0.4
18	2590	2300	20	0.07	-0.4
19	8400	8700	17	-0.04	-0.4
20	2600	2300	30	0.07	-0.4
21	510	340	70	-0.04	-0.4
22	1600	1300	30	0.07	-0.4
23	2200	1760	22	-0.04	-0.4
24	1600	650	19	0.16	-0.4
25	2400	1900	33	0.07	-0.4
26	2400	1960	34	-0.04	-0.4
27	2950	2700	21	0.12	-0.4
28	3500	3300	27	0.26	-0.4
29	2400	2200	26	-0.04	-0.4
30	2900	2700	26	-0.04	-0.4
31	2200	2000	20	-0.04	-0.4
32	5500	5300	33	0.28	-0.4
33	5200	5700	18	0.49	-0.4
34	9500	9400	14	0.21	-0.4
35	18200	17600	16	0.30	-0.4
36	14000	13200	16	1.70	-0.4
37	26400	25400	13	1.20	-0.4
38	27400	26500	20	1.69	-0.4
39	17500	17200	20	0.16	-0.4
40	5300	4300	23	0.56	-0.4
41	1100	270	93	0.05	-0.4
42	550	440	25	0.12	-0.4
43	720	490	40	0.23	-0.4
44	630	380	28	-0.04	-0.4
45	450	180	31	-0.04	-0.4
46	260	70	21	0.07	-0.4
47	360	70	19	0.05	-0.4
48	180	30	31	-0.04	-0.4
49	250	50	42	-0.04	-0.4
50	130	20	20	-0.04	-0.4
51	100	20	24	-0.04	-0.4
52	70	30	28	-0.04	-0.4
53	60	20	26	-0.04	-0.4
54	50	10	18	-0.04	-0.4
55	40	10	20	-0.04	-0.4
56	60	10	32	-0.04	-0.4
57	70	10	24	-0.04	-0.4
58	40	10	20	-0.04	-0.4
59	90	20	11	-0.04	-0.4
60	210	60	19	-0.04	-0.4

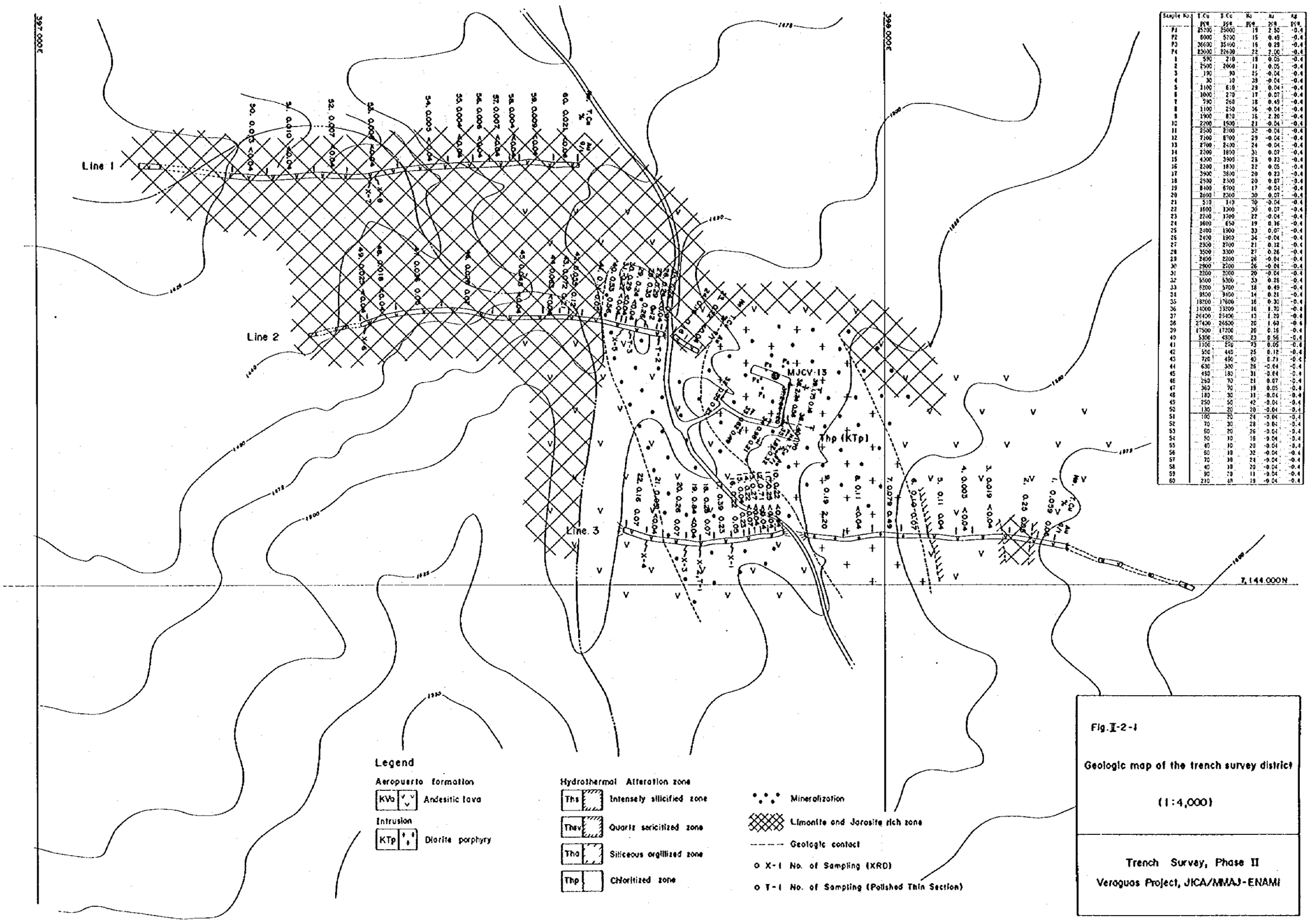

Fig.II-2-1

Geologic map of the trench survey district

(1:4,000)

Trench Survey, Phase II

Veroguas Project, JICA/MMAJ-ENAMI

Pit-1 ←NW30°

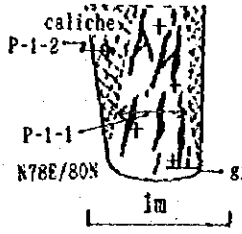

P-1-1 0.5m channel sampling
cuoxd dis. with gypsum network in meta diorite porphyry
XRD:gypsum,quartz,anhydrite

T.Cu(%)	S.Cu(%)	Mo(ppm)	Au(ppm)	Ag(ppm)
2.52	2.50	19	2.5	<0.4

P-1-2 spot sampling, caliche zone
XRD:gypsum,anhydrite,gismondite(zeolite)

Pit-2 ←NW75°

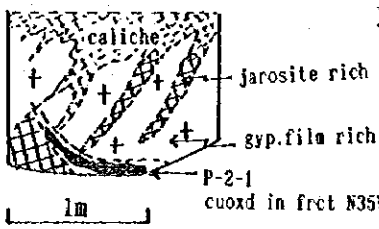

P-2-1 spot sampling, cuoxd film in meta diorite porphyry
XRD:quartz,albite,muscovite,gypsum,natrojarosite

T.Cu(%)	S.Cu(%)	Mo(ppm)	Au(ppm)	Ag(ppm)
0.60	0.52	15	0.49	<0.4

Pit-3

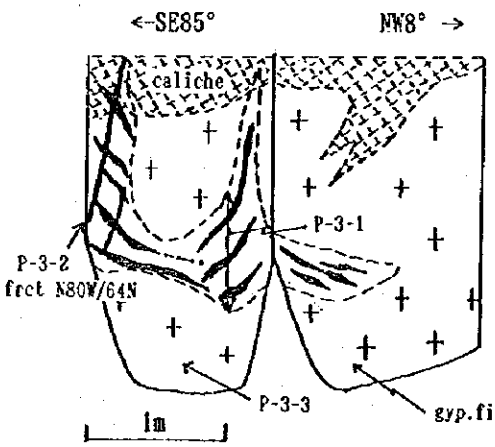

P-3-1 0.8m channel sampling
cuoxd film rich in meta diorite porphyry
XRD:quartz,albite,muscovite,atacamite

T.Cu(%)	S.Cu(%)	Mo(ppm)	Au(ppm)	Ag(ppm)
3.66	3.54	16	0.29	<0.4

P-3-2 spot sampling, cu oxd film with gypsum network
XRD:quartz,gypsum,bassanite,atacamite,anhydrite,albite

P-3-3 spot sampling, cu oxd dis. wk with gypsum network
XRD:gypsum,quartz,albite,anhydrite,muscovite

Pit-4

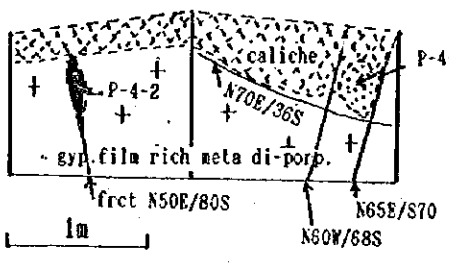

P-4-1 spot sampling, cu oxd dis. with caliche zone
XRD:quartz,albite,microcline

P-4-2 spot sampling, cu oxd film with fracture
XRD:gypsum,gismondite(zeolite),albite,orthoclase,
anhydrite,bassanite,atacamite

T.Cu(%)	S.Cu(%)	Mo(ppm)	Au(ppm)	Ag(ppm)
2.30	2.26	22	2.00	<0.4

Fig.II-2-2 Sketch of the test pits (1:50)

Table II-2-1 Results of the microscopic observation (Polished thin section)

Samples					Primary minerals						Original texture of igneous rock	Alteration Minerals												Opaque minerals												Remarks
No.	Drill Hole	Depth (m)	Original Rock	Alt. Zone	Qz	Pl	Px	Hb	Bt			degree of alt.	Qz	Ab	Kf	Bt	Se	Ch	Ep	Ah	Gp	Ca		Py	Po	Cu	Cp	Cv	Cc	Cu	Sp	Mt	Hm	Ge	
1	Trench	T-1	Andesite			○					porphyritic	◆	◎	○		?	○	○															◎	△	Mt→Ht, Ch→Bt?
2	Trench	T-2	Andesite								porphyritic	◆	○	◎		○	○	○	△	△	○						△		·			○	○	△	Mt→Ht(Maghemite?)
3	Trench	T-3	Andesite			○					holocrystalline	◆	◎	◎		◎	○	○			△						△					○	○	△	dioritic, Bo:△
4	Trench	P-3	Di-Porphyry		?	△						◆	◎	○		?	○	△	△								·						◎	○	Silicified porphyrite?
5	Trench	P-4	Di-Porphyry		?	◎			△			◆	◎	○	○		○	○	△								·					○	○	○	Silicified porphyrite?
6	Trench	Platform	Di-Porphyry		?	◎		○	△			◆	◎				△	○	△				△				△					○	△	△	Silicified porphyrite?

* Di-Porphyry: Diorite Porphyry

[abandance]
◎:abandant
○:common
△:minor
·:rare

[degree of alteration]
◆:completely altered
◇:partlly altered
:fresh or not altered

[Mineral names]
Qz:quartz
Pl:plagioclase
Px:pyroxene
Hb:hornblende
Ab:albite
Kf:K-feldspar
Se:sericite
Ch:chlorite
Gp:gypsum
Ca:carbonate
Py:pyrite
Po:pyrrhotite
Cu*:oxidized copper
Cp:chalcopyrite
Cu:native copper
Sp:sphalerite
Mt:magnetite
Hm:hematite
Am:amphibole group
Se:sphene
Ka:kaolinite
Sm:smectite

Tablell-2-2 Results of the powder X-ray diffraction

Clasification		Abbr.	Mineral Name	Chemical Formulas	No.	1	2	3	4	5	6	7	8	9	10	11	12	13	14	15	16
					Sample No.	X-1 Line3	X-2 Line3	X-3 Line3	X-4 Line3	X-5 Line2	X-6 Line2	X-7 Line1	X-8 Line1	P-1-1	P-1-2	P-2-1	P-3-1	P-3-2	P-3-3	P-4-1	P-4-2
Cu	Sulphide	Tet	Tetrahedrite	Cu12Sb4S13																	
		Cc	Chalcosine	Cu2S										△		△					
		Djr	Djurleite	Cu31S16																	
		Ena	Enargite	Cu3AsS4										·			·				
		Cv	Coveline	CuS																	
		Cp	Chalcopyrite	CuFeS2																	
	Metal	Cu	Native copper	Cu																	
	Sulfate	Cln	Chalcanthite	Cu(SO4)·5H2O																	
		Ant	Antrelite	Cu3(SO4)(OH)4																	
		Brc	Brochanthite	Cu4(SO4)(OH)6																	
	Carbonate	Az	Azurite	Cu3(CO3)2(OH)2																	
		Mg	Malaquite	Cu2CO3(OH)2																	
	Others	Atc	Atacamite	Cu2Cl(OH)3													△	○			△
		Lam	Lamnerite	Cu(AsO4)2										△							·
		Cic	Clinoclase	Cu3(AsO4)(OH)3																	
		Chn	Chnevixite	Cu2Fe2(AsO4)2(OH)2·H2O																	
		Chr	Chrysocola	Cu2-xSi2O5(OH)3/xH2O																	
Fe	Oxide & Hydroxide	Ht	Hematite	Fe2O3				·													
		Mgh	Maghemite	Fe2O3																	
		Mt	Magnetite	Fe3O4																	
		Akg	Akaganeite	FeO(OH)																	
		Frx	Feroxyhyte	FeO(OH)																	
		Goe	Goethite	FeO(OH)																	
	Sulphide	Po	Pyrrhotite	Fe7S8																	
		Apy	Arsenopyrite	FeAsS																	
		Py	Pyrite	FeS2																	
	Sulfate	Jar	Jarosite	(K)Fe3(SO4)2(OH)6																	
		Na-Jar	Natrojarosite	(K,Na)Fe3(SO4)2(OH)6								△	△			△					
		Btl	Butlerite	Fe(SO4)(OH)·2H2O																	
		Prb	Parabutlerite	Fe(SO4)(OH)·2H2O																	
		Crl	Kornelite	Fe(SO4)3·7H2O																	
		Rzn	Rozenite	Fe(SO4)·4H2O																	
		Sdr	Siderotil	Fe(SO4)·5H2O																	
	Others	Scr	Scorodite	Fe(AsO4)·2H2O																	
		Fml	Ferrimolybdit	Fe2(MoO4)3·nH2O																	
		Ptk	Pseudobrookite	Fe2(TiO3)O2																	
		Prt	Pseudorutile	Fe2(TiO3)O9																	
	Silica	Qz	Quartz	SiO2			◎	◎				◎	◎	◎		◎	◎	◎	◎	◎	
Silicate	Clay	Chm	Chamosite	(Fe,Al,Mg)6(Si,Al)4O10(OH)8																	
		Chl	Chlorite	(Mg,Fe,Al)12(Fe,Al,Si)8O20(OH)16				△	△												
		Dck	Dickite	Al2Si2O5(OH)4																	
		Kal	Kaolinite	Al2Si2O5(OH)4				△													
		Nac	Nacrite	Al2Si2O5(OH)4																	
		Hal	Halloysite	Al2Si2O5(OH)4·2H2O																	
		Pyr-Tc	Pyrophyllite-Talc	Al-MgSi4O10(OH)2								◎									
		Mus	Muscovite	K·Al2(Si3Al)O10(OH,F)2				○	○			△	○			○	△		○		
		Ilt	Illiite	K-Al2(Si3Al)O10(OH,F)2																	
		Mnt	Montmorillonite	Na0.3(Al,Mg)2Si4O10(OH)2·xH2O																	
	Others	Olg	Oligoclase	(Na,Ca)(Al,Si)4O8																	
		Ab	Albite	(Na,Ca)(Al,Si)4O8				◎			·					○	○	△	○	○	△
		Or	Orthoclase	(K,Na)(Al,Si)4O8										·			△			△
		Mic	Microcline	KAlSi3O8															△		
		Ho	Hornblende	(Na,K)Ca2(Fe,Mg)5(Al,Si)8O22(OH)2																	
		Di	Diposide	CaMg(SiO3)2																	
		Tre	Tremolite	Ca2(Mg)5Si8O22(OH)2																	
		Act	Actinolite	Ca2(Mg,Fe)5Si8O22(OH)2																	
		Rie	Riebeckite	(Na,Ca)2(Mg,Fe)5Si8O22(OH)2																	
		Bt	Biotite	K(Mg,Fe)2AlSi3O10(OH)2																	
		Ep	Epidote	Ca2(Al,Fe)3Si3O12(OH)																	
	Zeolite	Hap	Hydroxyapophyllite	KCa4Si8O20(OH)·8H2O								○									
		Gz	Gismondite	CaAl2Si2O8·4H2O		○				○	·				△						○
		Mrd	Mordenite	(Ca,Na2,K2)Al2Si10O24·7H2O																	
Sulfate		Alu	Alunite	(K)Al3(SO4)2(OH)6																	
		Na-Alu	Natroalunite	(K,Na)Al3(SO4)2(OH)6									△								
		Btl	Butlerite	Fe(OH)SO4·2H2O				△													
		Bld	Bloedite	Na2Mg(SO4)2·H2O								○									
		Gl	Glauberite	Na2Ca(SO4)2	△																
		Bas	Bassanite	Ca(SO4)0.5H2O	○				○								○				△
		Anh	Anhydrite	Ca(SO4)			△					◎	○	△			△	△	△	-	△
		Gyp	Gypsum	Ca(SO4)·2H2O	◎	◎		◎	◎	◎			◎	◎	△		◎	◎			◎
Mn		Pr	Pyrolusite	MnO2																	
		Br	Braunite	Mn7SiO12																	
		Crp	Cryptomelane	K·Mn8O16																	
		Gro	Groutite	MnO(OH)																	
Carbonate		Cal	Calcite	CaCO3																	
		Dol	Dolmite	CaMg(CO3)2																	
		Kut	Kutnohorite	Ca(Mn,Mn)(CO3)2																	

Abundance: ◎ : abundant ○ : common △ : minor · : rare

TableII−2−3 Results of chemical analysis

Sample No.	T.Cu	S.Cu	Mo	Au	Ag
	ppm	ppm	ppm	ppm	ppm
P1	25200	25000	19	2.50	-0.4
P2	6000	5200	15	0.49	-0.4
P3	36600	35400	16	0.29	-0.4
P4	23000	22600	22	2.00	-0.4
1	590	210	19	0.05	-0.4
2	2500	2000	11	0.05	-0.4
3	190	90	25	-0.04	-0.4
4	30	10	39	-0.04	-0.4
5	1100	610	29	0.04	-0.4
6	1000	270	17	0.07	-0.4
7	790	260	18	0.49	-0.4
8	1100	250	16	-0.04	-0.4
9	1900	820	18	2.20	-0.4
10	2200	1900	21	-0.04	-0.4
11	2500	2200	32	-0.04	-0.4
12	7100	6700	29	-0.04	-0.4
13	2700	2400	24	-0.04	-0.4
14	2200	1800	31	0.07	-0.4
15	4000	3900	28	0.23	-0.4
16	2200	1800	22	0.05	-0.4
17	3900	3800	20	0.23	-0.4
18	2800	2300	20	0.07	-0.4
19	8400	6700	17	-0.04	-0.4
20	2600	2300	30	0.07	-0.4
21	510	140	70	-0.04	-0.4
22	1600	1300	30	0.07	-0.4
23	2200	1700	22	-0.04	-0.4
24	1600	650	19	0.16	-0.4
25	2400	1900	33	0.07	-0.4
26	2400	1900	34	-0.04	-0.4
27	2900	2700	21	0.12	-0.4
28	3500	3300	27	0.26	-0.4
29	2400	2200	26	-0.04	-0.4
30	2900	2700	26	-0.04	-0.4
31	2200	2000	20	-0.04	-0.4
32	5500	5300	33	0.28	-0.4
33	6200	5700	18	0.49	-0.4
34	9800	9400	14	0.21	-0.4
35	18200	17600	16	0.30	-0.4
36	14000	13200	16	1.70	-0.4
37	26400	25400	13	1.20	-0.4
38	27400	26600	20	1.60	-0.4
39	17500	17200	20	0.16	-0.4
40	5300	4800	23	0.56	-0.4
41	1100	270	73	0.05	-0.4
42	550	440	25	0.12	-0.4
43	720	490	40	0.21	-0.4
44	630	300	26	-0.04	-0.4
45	480	180	31	-0.04	-0.4
46	260	70	21	0.07	-0.4
47	360	70	19	0.05	-0.4
48	180	30	11	-0.04	-0.4
49	250	50	42	-0.04	-0.4
50	130	20	20	-0.04	-0.4
51	100	20	24	-0.04	-0.4
52	70	30	28	-0.04	-0.4
53	60	20	26	-0.04	-0.4
54	50	10	16	-0.04	-0.4
55	40	10	20	-0.04	-0.4
56	60	10	32	-0.04	-0.4
57	70	10	24	-0.04	-0.4
58	40	10	20	-0.04	-0.4
59	90	20	11	-0.04	-0.4
60	210	40	19	-0.04	-0.4

TableII-2-4 Results of statstics

Original data infomation

number of samples : 64

Elements	unit	max value	min value	average	standerd deviation
T.Cu	%	3.6602	0.0030	0.1354	6.4983
S.Cu	%	3.5400	0.0010	0.0666	11.2590
I.Cu	%	0.6001	0.0020	0.0280	3.1117
Mo	ppm	72.9962	11.0002	22.7562	1.4408
Au	ppm	2.4998	0.0200	0.0720	4.4147

covariance matrix	T.Cu	S.Cu	I.Cu	Mo	Au
T.Cu	0.6606	0.8261	0.2926	-0.0198	0.3312
S.Cu	0.8261	1.1057	0.3026	-0.0247	0.4373
I.Cu	0.2926	0.3026	0.2431	-0.0062	0.1046
Mo	-0.0198	-0.0247	-0.0062	0.0251	-0.0264
Au	0.3312	0.4373	0.1046	-0.0264	0.4160

correlation matrix	T.Cu	S.Cu	I.Cu	Mo	Au
T.Cu	1.0	0.9666	0.7302	-0.1538	0.6319
S.Cu	0.9666	1.0	0.5836	-0.1484	0.6448
I.Cu	0.7302	0.5836	1.0	-0.0798	0.3289
Mo	-0.1538	-0.1484	-0.0798	1.0	-0.2582
Au	0.6319	0.6448	0.3289	-0.2582	1.0

Principal component analysis

No.	Eig_value	Eig_pct	Eig_sum
Z-01	3.0313	60.6265	60.6265
Z-02	1.0052	20.1045	80.7310
Z-03	0.6319	12.6376	93.3686
Z-04	0.3181	6.3612	99.7299
Z-05	0.0135	0.2701	100.0000

Fact_ld	Z-01	Z-02	Z-03	Z-04	Z-05
CuT	0.9717	0.1340	-0.0286	-0.1706	0.0883
CuS	0.9378	0.0945	0.1129	-0.3061	-0.0722
Au	0.7557	-0.2379	0.5159	0.3259	-0.0019
CuI	0.7516	0.2754	-0.5220	0.2937	-0.0220
Mo	-0.2677	0.9197	0.2823	0.0527	0.0006

Eig_vec	Z-01	Z-02	Z-03	Z-04	Z-05
CuT	0.5581	0.1337	-0.0360	-0.3026	0.7601
CuS	0.5386	0.0943	0.1420	-0.5428	-0.6214
Au	0.4340	-0.2373	0.6490	0.5778	-0.0162
CuI	0.4317	0.2747	-0.6566	0.5208	-0.1891
Mo	-0.1537	0.9173	0.3552	0.0934	0.0055

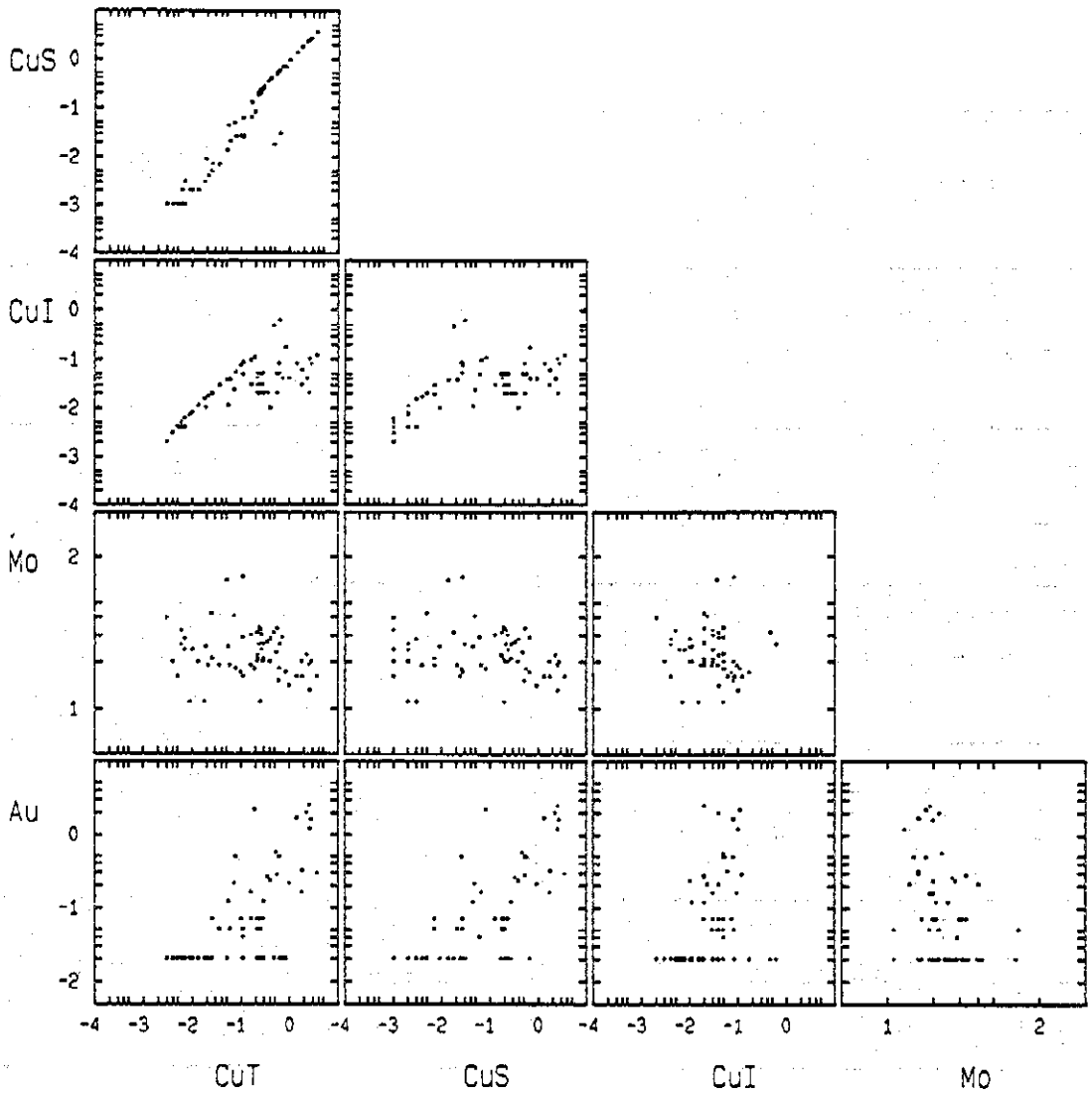

Fig.II−2−3 Correlation coefficients diagram

CHAPTER 3 GEOPHYSICS SURVEY OF THE PROGRESO AREA

3-1 Purpose and Method of Survey

3-1-1 Purpose of Survey

A boing survey conducted in the area in 1993 confirmed that the Punta del Cobre formation which is a horizon for Manto-type ore deposits is distributed at a depth of around 470m underground in DDH-6A in the south of the survey area. Occurrence of skarn was also ascertained in the limestone of the Abundancia formation above. As a result of an airborne magnetic, new magnetic anomalies were confirmed in the northeast of the survey area, and from the results of a core analysis in DDH-1A in the north of the area, weak copper anomalies (around 200ppm) were extracted from a depth of 182m over a distance of 222m.

In order to clarify the distribution of the Punta del Cobre formation in the survey area, the resistivity structure of the deep zone is clarified by AMT (Audio-frequency Magneto-Telluric Method) . In addition to extracting the Manto-type ore deposits and the occurrence of skarn in the Abundancia formation limestone using the IP (Induced Polarization) method. The correspondence between the geophysical anomalies and mineral occurrence is clarified by measuring the resistivity value and polarizability of core samples. The survey also purpose to check the extent of the occurrence of copper which was confirmed by core analysis in DDH-1A using PEM (Pulse Electromagnetic Method).

3-1-2 Contents of survey

The map showing the location of the profiles is shown in Fig.II-3-1, the survey method and list of quantities are shown in Table II-3-1, and the list of equipment used is shown in Table II-3-2.

3-1-3 Survey method

1. AMT method

Several surveys already carried out in this area by CSAMT method, SIP method, etc. , and the rough distribution of the resistivity has been obtained. Nevertheless, as stated earlier, distribution of the Punta del Cobre formation is about 470m underground, it would be difficult to say that the resistivity structure of the depths has been adequately obtained by CSAMT which is affected by near field. For this reason, the AMT method which enables surveying up to a depth of about 1000m underground was used in this area. The AMT method works on the same measuring principle as CSAMT, but it differs in that it measures the phenomena of induction, corresponding to the subterranean resistivity structure, which produced natural world phenomena of electromagnetic induction as signals, such as lightning. As the natural world electromagnetic field differs to the electromagnetic field produced by artificial signals, the conditions for plane waves are effected even in low frequency zones. Therefore the problem of near field in the low frequency domain which occurs with the CSAMT method does not arise and an adequate depth of investigation is possible.

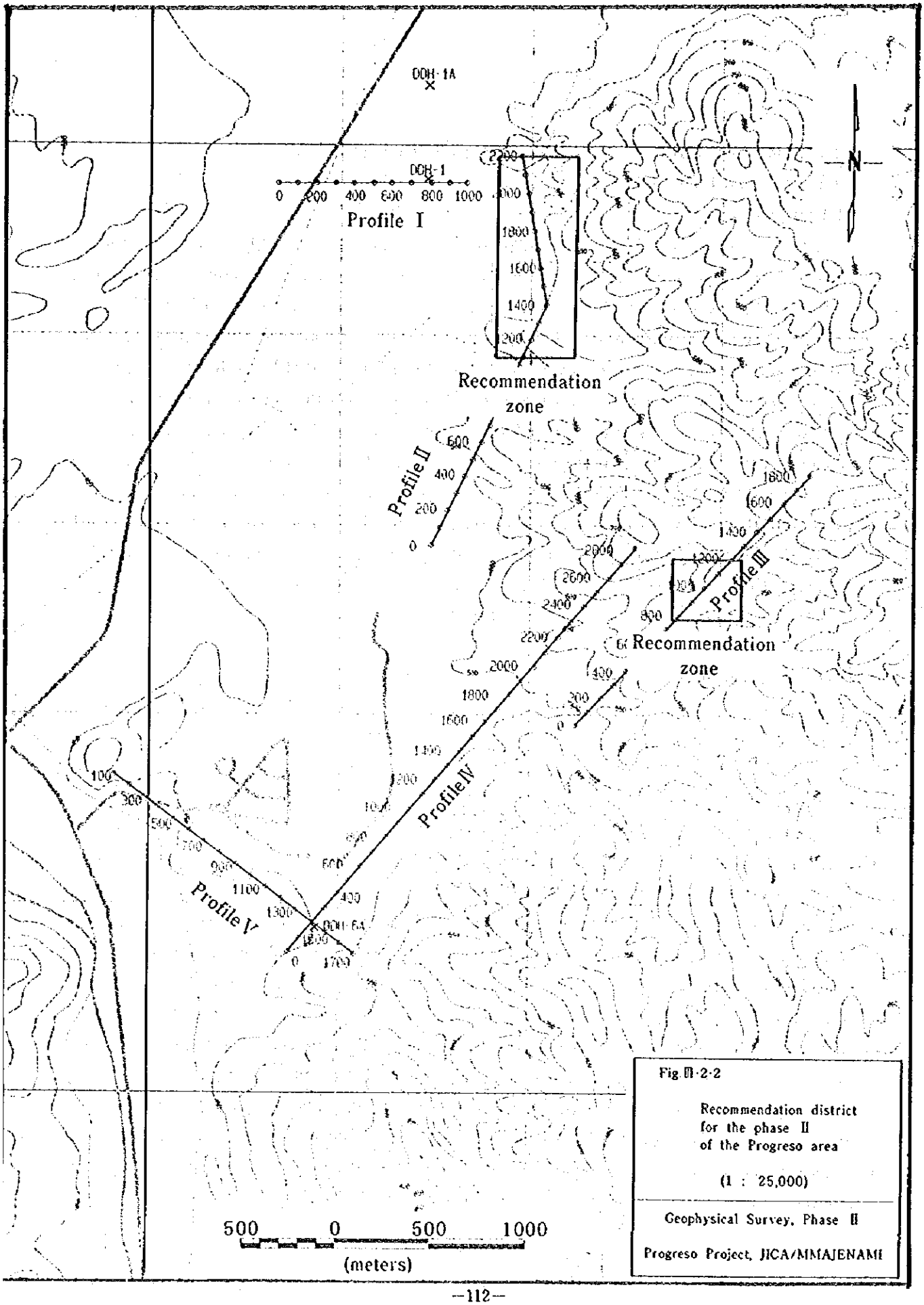

Fig. II-2-2

Recommendation district for the phase II of the Progreso area

(1 : 25,000)

Geophysical Survey, Phase II

Progreso Project, JICA/MMAJENAMI

Table II-3-1 Contents of Geophysical Survey

	Profile length	AMT measuring points	IP measuring length	Electrode spacing
Profile I	1,000m	4	1,000m	100m
ProfileII	2,200m	10	2,200m	100m
ProfileIII	1,800m	9	1,800m	100m
ProfileIV	2,800m	14	2,800m	100m
ProfileV	1,600m	8	1,600m	100m
Total	9,400m	45	9,400m	
PEM	1 hole DDH-1A (mesuring depth from 10m to 278m) 2 horizontal and 1 vertical components 5 transmission loops(250m × 250m)			
Core Sample	Measurements of resistivity and polarization 30pcs			

The AMT investigation theory is explained briefly below.

When the subterranean resistivity structure is a homogeneous or horizontally multi-layered structure, the following relation between the horizontal electric field and the horizontal magnetic field which crosses it perpendicularly is effected. (Cagniard, 1953)

$$Ex(\omega) = Z(\omega)Hy(\omega) \qquad \cdots\cdots\cdots (1)$$

where Z can be expressed by $Z_{XY} = (1+i)\sqrt{\frac{\rho\omega\mu}{2}}$

$$\rho_{XY} = \frac{1}{\mu\omega}\left|\frac{E_X}{H_Y}\right|^2$$

is obtained and apparent resistivity ρxy as a function of the frequency can be found. Where μ is the free air magnetic permeability ($4\pi \times 10^{-7}$ H/m), and ω is the angular frequency. As electromagnetic waves are generally better transmitted to the subterranean depths at lower frequencies, it is possible to measure changes in the apparent resistivity in the direction of the deep zone by measuring various frequencies.

When the earth is a two-dimensional structure, the following linear relationship is effected between the electric field and the magnetic field which cross each other perpendicularly (Cantwell, 1960).

$$Ex = ZxxHx + ZxyHy \quad \text{..... (2)}$$

$$Ey = ZyxHx + ZyyHy \quad \text{..... (3)}$$

Where each variable is a function of the frequency. This equation generally uses a determinant and is expressed as

$$\begin{bmatrix} E_X \\ E_Y \end{bmatrix} = \begin{bmatrix} Z_{XX} & Z_{XY} \\ Z_{YX} & Z_{YY} \end{bmatrix} \begin{bmatrix} H_X \\ H_Y \end{bmatrix} \quad \text{.....(4)}$$

or $$E = ZH \quad \text{..... (5)}$$

Where Z is a complex impedance tensor. When the subterranean structure is a homogeneous layer structure or horizontally multi-layered structure,

$$Zxx = Zyy = 0, \quad Zxy = Zyx$$

is effected and equation (1) is obtained.

Also, when the subterranean structure forms a two-dimensional structure and either the x or y direction runs along the strike direction, it becomes

$$Zxx = Zyy = 0, \quad |Zxy| \neq |Zyx|$$

and

$$\rho_{XY} = \frac{1}{\mu\omega}\left|\frac{E_X}{H_Y}\right|^2 \quad \text{.....(6)}$$

$$\rho_{YX} = \frac{1}{\mu\omega}\left|\frac{E_Y}{H_X}\right|^2 \quad \text{.....(7)}$$

are obtained. With the ATM method, four components, the horizontal electric fields (Ex, Ey) which cross each other perpendicularly and the horizontal magnetic fields (Hx, Hy) which run parallel to them, are measured simultaneously at each measurement point and the resistivity structure in the two directions mentioned above is measured.

The AMT measurement conceptual diagram is shown in Fig.II-3-3. From the fact that the depth of penetration of electromagnetic waves underground depends on the frequency, the subterranean resistivity distribution can be obtained from the above equations by measuring the electromagnetic wave signals over a broad range of frequencies. 28 frequencies from 10,000Hz to 1.0Hz were measured. The frequency table for ATM measurement is shown in Table II-3-2.

Table II-3-2 Frequency table for AMT measurment

No.	freq.(Hz)	No.	freq.(Hz)	No.	freq.(Hz)	No.	freq.(Hz)
1	10,000.0	8	960.0	15	80.0	22	7.500
2	7,500.0	9	640.0	16	60.0	23	5.000
3	5,000.0	10	480.0	17	40.0	24	3.750
4	3,750.0	11	320.0	18	30.0	25	2.500
5	2,560.0	12	240.0	19	20.0	26	1.875
6	1,920.0	13	160.0	20	15.0	27	1.250
7	1,280.0	14	120.0	21	10.0	28	0.9375

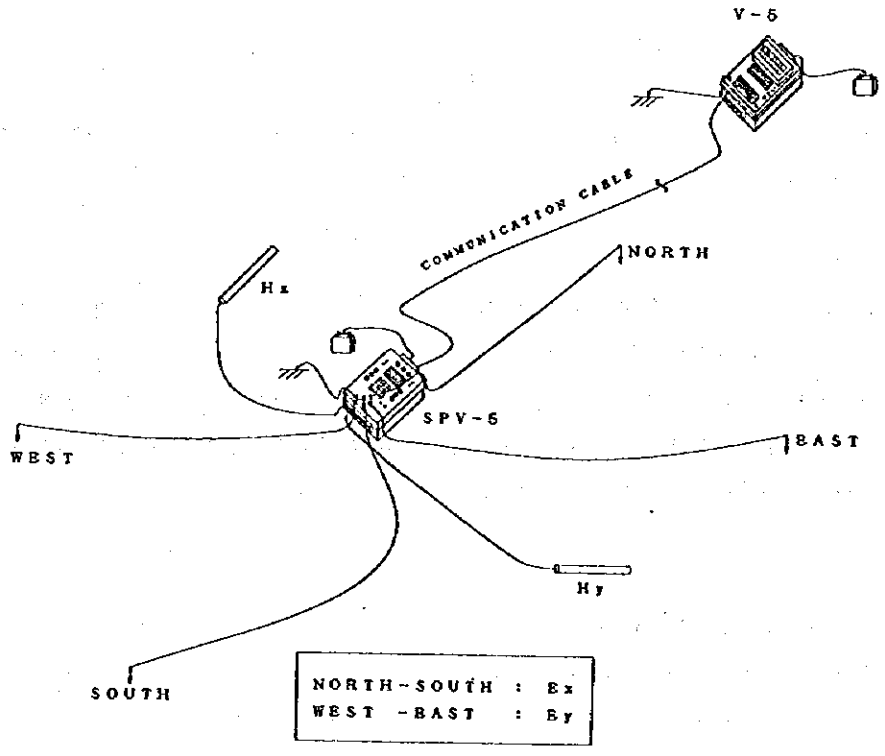

Fig. II-3-2 Field layout of AMT survey.

2. IP Method

If metal deposits, etc. are distributed in the earth and a direct current is applied, the electric charge is stored in the surface of the metal deposits, and if the direct current is then turned off, the electric charge that has been stored is gradually released. By measuring this phenomenon (polarization effect, induced polarization effect) together with the resistivity value, subterranean metal deposits that could not be detected by the changes in resistivity alone, can be investigated. In order to detect the induced polarization effect, measurements were taken in the time domain. The current is induced into the ground for a fixed time, and the ratio of the potential time integral value of 100msec-1sec after the current turned off is taken as an indicator of the size of the induced polarization effect (chargeability). The electrodes are arranged in dipole-dipole electrode arrangement, and as for the apparent resistivity, a 0.25Hz frequency (duty cycle 50%) current (I) is supplied to the current electrodes (C1, C2) shown in Fig.II-3-3(a) and the electric potential (Vp) is measured by potential electrodes (P1, P2). The apparent resistivity value of the earth (ρa) is expressed as

$$\rho_a = K\frac{V_P}{I} \quad \cdots\cdots\cdots\cdots(8)$$

Where K is called the electrode separation index and is expressed by the following equation.

$$K = \frac{2\pi}{1/C_1P_1 - 1/C_1P_2 - 1/C_2P_1 - 1/C_2P_2} \quad \cdots\cdots\cdots\cdots(9)$$

Generally when the distance between the current electrodes and the potential electrodes is N times the distance between the electrodes, it becomes

$$K = \frac{\pi}{2}n(n+1)(n+2) \quad \cdots\cdots\cdots\cdots\cdots \quad (10)$$

The chargeability(M) is obtained by the sum of the transients of the electric potential (secondary electric potential) during the current off time (t1-t2) shown in Fig.II-3-3(b) and normalized by primary electric potential Vp. In this survey the secondary electric potential measuring time is 1sec. For pseudosection, the apparent resistivity and chargeability obtained are shown at the vertex of a right-angled isosceles triangle whose base is a straight line joining the middle points of each electrode series.

3. PEM Method

A primary magnetic field created by the electric current flowing along the transmission loop set up around the borehole on the surface of the earth. When the primary field is broken, an induced magnetic field (secondary magnetic field) is produced by conductors such as subterranean mineral deposits. It is possible to detect the existence of low resistivity zones, such as mineral deposits, using a magnetic field sensor for three components, the vertical direction inside the borehole and the two directions crossing it perpendicularly, by continuously measuring inside the borehole. Furthermore, by placing transmission loops of the same size as the transmission loop around the borehole in four places on the north, south, east and

west of the borehole and taking the same measurements, it is possible to discover from variations in the magnetic field of each transmitting loop, the extension direction in the case of the borehole reaching the mineral deposit, or the direction of the mineral deposit in the case of there being one in the vicinity of the borehole. Measurements were taken using a 20.00ms time base (1 cycle/120.0ms) and dividing the off-time of 30.0ms into 20 windows. The size of the transmission loops was 200m x 200m, and measuring was carried out with a 20A electric current, using the loop around the borehole and loops of the same size in 4 places on the north, south, east and west of the borehole. The schematic illustration of the PEM survey is shown in Fig.II-3-4. A list of the equipment used in the survey is given in Table II-3-3.

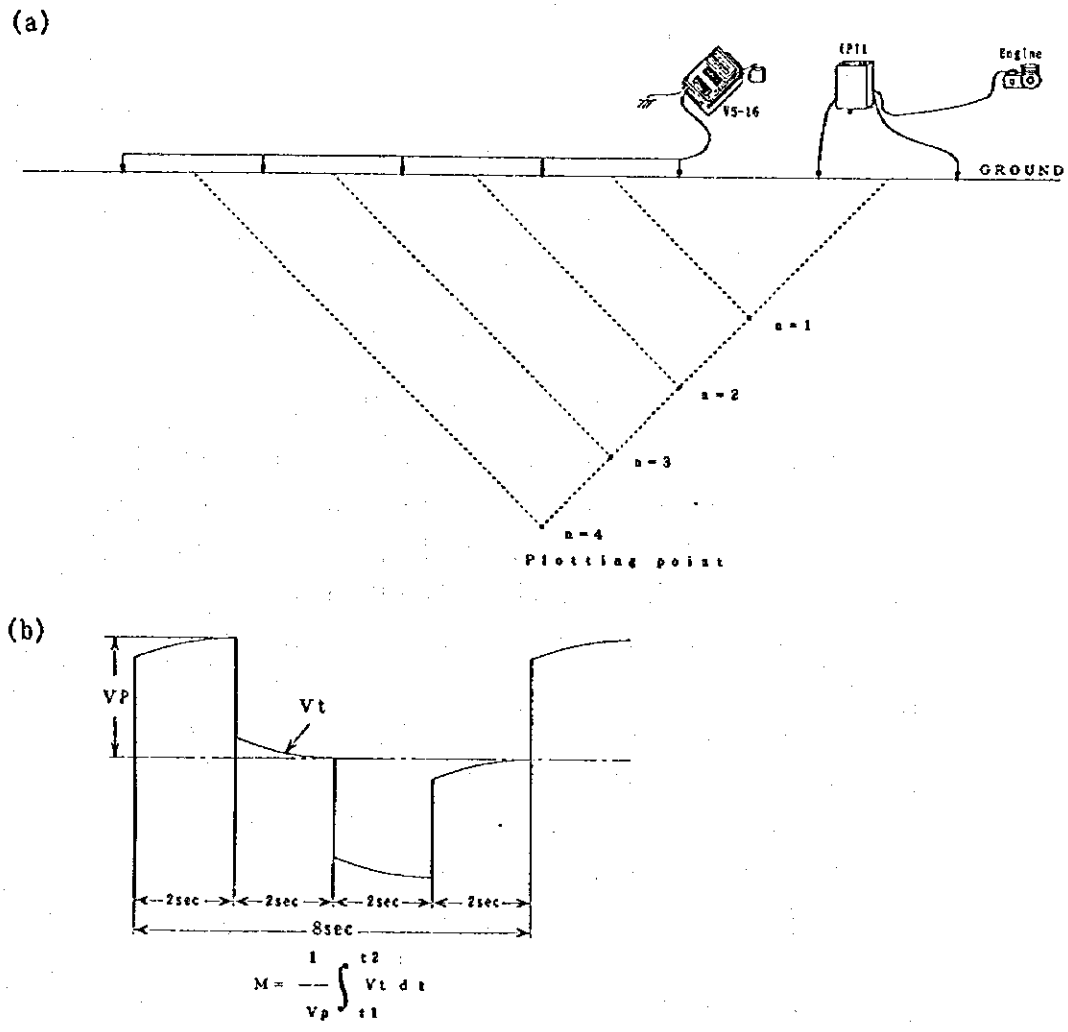

Fig. II-3-3 Field setup of IP survey(a) and Typical Time Domain measurment(b)

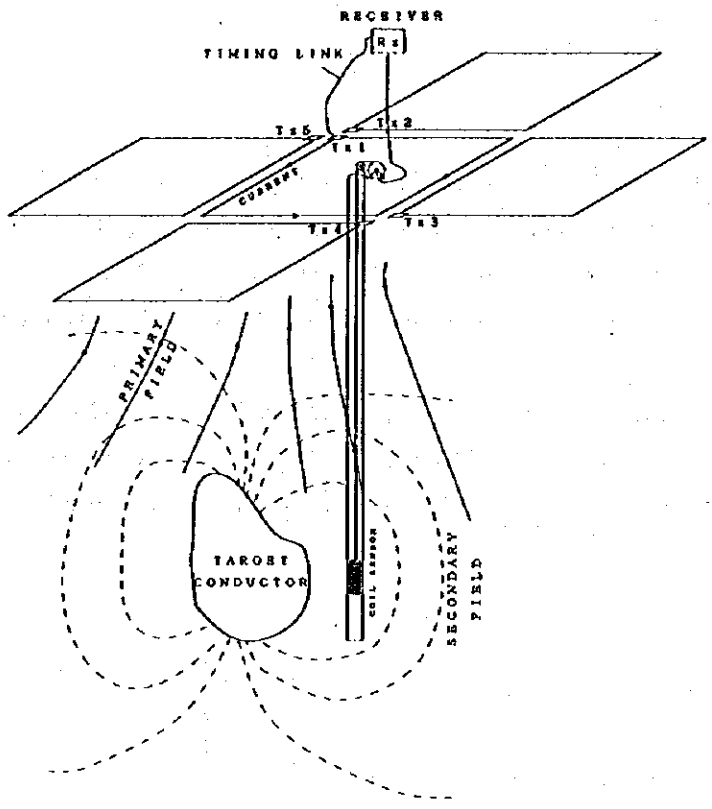

Fig. II-3-4 Schematic illustration of PEM survey.

Table II-3-3 List of equipments

AMT method	QTY	Specification
Multipurpose receiver V-5 Phoenix Geophysics	1	Sensitivity 0.2μV
Signal processor SPV-5 Phoenix Geophysics	2	Noise level 16nV/$\sqrt{Hz}$
Induction coil AMT-25 Phoenix Geophysics	4	Sensitivity 100nV/nT
Porus Pb-$PbCl_2$ electrode Phoenix Geophysics	30	Noise level 100nV
IP method	**QTY**	**Specification**
Multipurpose receiver V-5 Phoenix Geophysics	1	Sensitivity 0.2μV
Porus Pb-$PbCl_2$ electrode Phoenix Geophysics	30	Noise level 100nV
IP transmitter IPT-1 Phoenix Geophysics	1	2 kVA 10A max.
Engine Generator EX3000 HONDA	1	2.2kVA 50Hz
PEM method	**QTY**	**Specification**
Digital PEM Receiver Crone Geophysics	1	
Borehole PEM z-axis receiver probe	1	
Borehole X-Y probe Noranda Exploration	1	
PEM transmitter Crone Geophysics	1	2.0kVA 5A, 20A
Computer	**QTY**	
Laptop computer	1	16bit 386CPU,40Mbyte

3-2 Interpretation Method

3-2-1 AMT Method

Topographic and static effects are included in the apparent resistivity values measured by the AMT method. As they influence all the electric field data from the shallow zone to the deep zone, they must be adequately evaluated.

With regard to topographic effects, the current flow in the direction of the electric field being measured is affected by topography in that direction, and as the variations in measured potential show in Fig.II-3-5. The electric current density is dense in valley terrain. As a result, the density of the equipotential line is high and the disparity in measured potential is high. In other words, it forms a high apparent resistivity anomaly. Conversely, in mountainous terrain the electric current density is thin, forming a low apparent resistivity anomaly. Also, by the variations in topography, a low apparent resistivity anomaly is formed in convex terrain, and a high apparent resistivity anomaly in concave terrain. Such topographical effects are extremely great in AMT surveys.

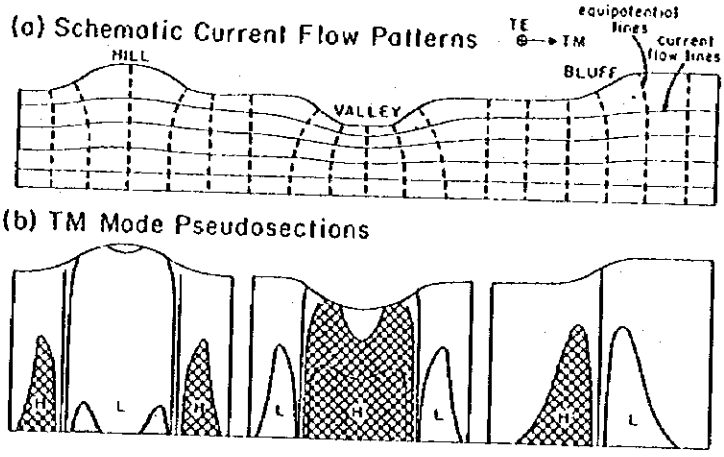

Fig. II-3-5(1) Schematic illustration of topographic effects on E-field mesurments.
(a)Distortion of current flow patterns over topographic features. (b)TM mode resistivity pseudosections resultant from topographic features.
H = high resistivity, L = low resistivity. (After Zonge and Hughes)

With regard to static effects, as shown in Fig.II-3-6, when the measurement points are located in a local resistivity anomaly zone, the apparent resistivity curve shifts to horizontal on the high resistivity or low resistivity side, corresponding to the local anomaly, so no true apparent resistivity curve is seen. Static

effects create a problem in surveying methods which aim to find the apparent resistivity structure by measuring the electric field, including direct current electric investigations. In direct current electric investigations, as the distance between the electrodes is gradually extended to obtain deeper data, in general not all of the measurement data are affected by static effects. But with surveying methods which obtain deeper information by changing the frequency without moving the potential electrodes, such as the electromagnetic method, all the data from high frequencies to low frequencies are influenced by static effects.

Unless combined with an investigation method which surveys the subterranean resistivity structure by only the magnetic field without measuring the electric field, an objective evaluation cannot be obtained. As this phenomenon is a problem which only affects the apparent resistivity and not the phase difference, the influence can be assessed from phase difference section. Also, by establishing measurement points continuously along the profiles, a relative assessment can be obtained by comparing the measurement results of adjacent measurement points. Furthermore, interpretation that includes the static effects can be carried out by conducting two-dimensional interpretation along the profiles.

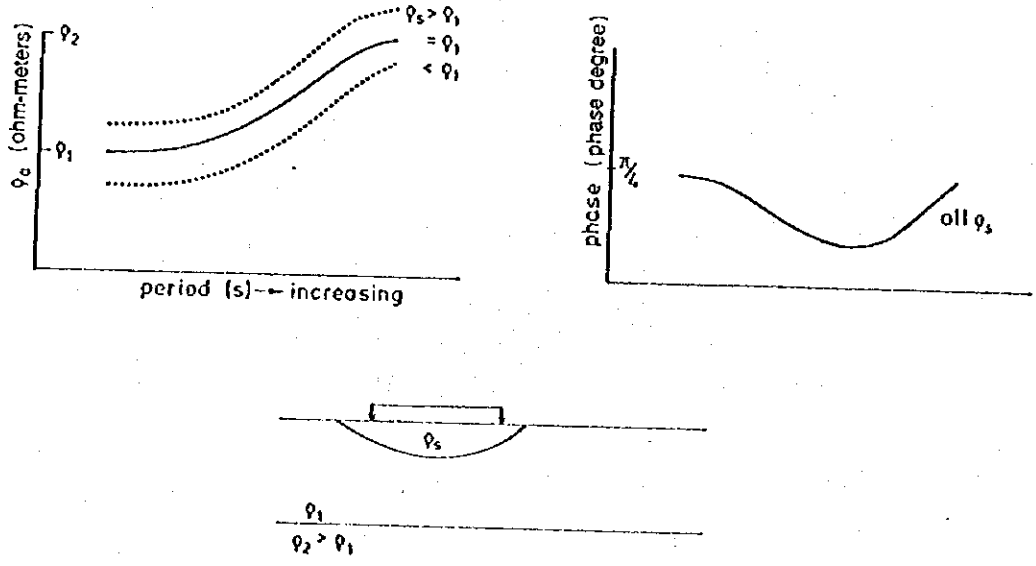

Fig. II-3-5(2) Sketch of model used to explain static effects. The middle apparent resistivity curve is that which would be observed if the inlier had the same resistivity as the layer containing it. (After Sternberg et al.,1985)

3-2-2 IP Method

Like the AMT method, the IP method apparent resistivity values are affected by the topography, but conversely to the AMT method, in mountainous terrain the electric current density is high and a high resistivity anomaly is formed, while in valley terrain the electric current density is thin and a low resistivity anomaly is formed. The terrain correction coefficients were calculated by the two-dimensional finite element method considering a point current sorce. With the IP method which uses the dipole-dipole arrangement as mentioned earlier, as the electric potential is measured by changing the distance between the electrodes, the probability of the occurrence of a local resistivity anomaly is low and the resistivity sections in the direction of the profile which can virtually be read from the pseudosection correspond to the actual resistivity structure, but the correct structure is not shown in the depth direction. Furthermore, chargeability is not affected by the topography, but this does not mean that the points indicated on the pseudosection necessarily show the anomaly points. Also, as anomalies in the shallow zone are accumulated the deeper the chargeability, in many cases they appear as large anomalies. A qualitative interpretation using the pseudosections obtained by the dipole-dipole method explained earlier is the limit. Therefore, in order to carry out a quantitative interpretation, it is necessary to conduct two-dimensional inversion interpretation that takes the topography into account.

3-2-3 Two-dimensional Inversion Interpretation

Two-dimensional inversion interpretation is a repetitive interpretation method that combines forward modeling by the finite element method with automatic interpretation by the method of nonlinear least squares. When the subterranean structure cannot be approximated a horizontally multi-layered structure, it is impossible to conduct adequately interpretation by using such as one-dimensional interpretation which cannot take into account the effects of resistivity changes in the profile direction. Therefore it is necessary to use two-dimensional interpretation which can include the effects of resistivity discontinuous boundaries in the profile direction.

Two directions data of apparent resistivity and phase difference which cross each other perpendicularly are measured in AMT method. One of the data(ρxy) is generally rotated in the strike direction of the subterranean structure and the other(ρyx) is rotated in the direction crossing it perpendicularly in accordance with equation (2) or (3), and these are called the TE mode and TM mode respectively. If the subterranean structure is a homogeneous structure or a horizontally multi-layered structure, ρxy = ρyx holds good, but in the case of a two-dimensional structure, in the TE mode, there is no resistivity discontinuous boundary in the measuring direction and approximation is possible as a horizontally multi-layered structure. However, in the TM mode, as the resistivity discontinuous boundary exists in the measuring direction and approximation to a horizontally multi-layered structure is impossible. As the geophysical survey profiles are generally set in the direction running perpendicular to the strike, it is

necessary to carry out two-dimensional interpretation of the measurement data in the profile direction. Even using the IP method with dipole-dipole electrode arrangement, as the electrodes are placed in the direction of the profile, it is desirable to apply two-dimensional interpretation because of the influence of the resistivity discontinuous boundaries in the direction of the profile.

In two-dimensional interpretation, the subterranean structure is divided at resistivity blocks. In the past, a resistivity model was made which applied the presumed resistivity block values, and a comparison was made of the theoretical values calculated from the resistivity model and the actual measured values. Forward modeling was attempted in which a model showing the results nearest to the measured values was assembled by trial and error. But this method had problems, such as the inclusion of the arbitrariness of the interpreter in the interpretation results. The two-dimensional inversion interpretation method used in our interpretation enables objective interpretation results to be obtained without regard for the arbitrariness of the interpreter, by using an automatic repetitive interpretation method where the resistivity values applied to each block are assumed by the method of nonlinear least squares.

In the ATM method, a resistivity block boundaries were established at each measurement point and quadrilateral resistivity blocks were prepared in which the blocks were divided so that they were thin in the shallow zone, gradually becoming thicker towards the deep zone. They were deformed in conformity with the topography of the surface of the earth, forming resistivity blocks whose shape was parallel to the topography in a horizontal direction. When resistivity values are applied to each of these resistivity blocks, the apparent resistivity and phase difference curves at each measurement point are obtained as the surface response corresponding to the subterranean resistivity structure by forward modeling according to the finite element method. To minimize any remaining difference between the surface responses and the measured values, the values of the resistivity blocks were found by automatic repetitive interpretation according to the method of nonlinear least squares. The resistivity block values from the first repetitive interpretation (initial guesses) were taken to show a subterranean homogeneous structure with the same resistivity values and the influence of the initial values on the interpretation results was eliminated.

In the IP method, a resistivity block boundaries were established for each electrode (however, as the measurement data density becomes less at either end of the profile, two electrodes were set up on one block), and after the quadrilateral blocks had been prepared, thinner in the shallow zone and gradually becoming thicker towards the deep zone, interpretation was conducted following the same routine as for AMT inversion interpretation explained earlier.

3-2-4 Two-Dimensional Joint Inversion Interpretation

This is an interpretation method based on two-dimensional inversion interpretation to find the subterranean resistivity structure which most closely approximates at the same time both the measurement data obtained by the dipole-dipole method and the measurement data obtained by the AMT method.